Some Aspects of Reliability of Offshore Structures

Sigurdsson, Gudfinnur

Publication date:
1989

Document Version
Publisher's PDF, also known as Version of record

INSTITUTTET FOR BYGNINGSTEKNIK

INSTITUTE OF BUILDING TECHNOLOGY AND STRUCTURAL ENGINEERING

AALBORG UNIVERSITETSCENTER · AUC · AALBORG · DANMARK

STRUCTURAL RELIABILITY THEORY
PAPER NO. 55

Ph.D.-Thesis defended publicly at the University of Aalborg
April 19, 1989

GUDFINNUR SIGURDSSON

SOME ASPECTS OF RELIABILITY OF OFFSHORE STRUCTURES

JUNE 1989 ISSN 0902-7513 R8909

The STRUCTURAL RELIABILITY THEORY papers are issued for early dissemination of research results from the Structural Reliability Group at the Institute of Building Technology and Structural Engineering, University of Aalborg. These papers are generally submitted to scientific meerings, conferences or journals and should therefore not be widely distributed. Whenever possible, reference should be given to the final publications (proceedings, journals, etc.) and not to the Structural Reliability Theory papers.

INSTITUTTET FOR BYGNINGSTEKNIK
INSTITUTE OF BUILDING TECHNOLOGY AND STRUCTURAL ENGINEERING
AALBORG UNIVERSITETSCENTER · AUC · AALBORG · DANMARK

STRUCTURAL RELIABILITY THEORY
PAPER NO. 55

Ph.D.-Thesis defended publicly at the University of Aalborg
April 19, 1989

GUDFINNUR SIGURDSSON
SOME ASPECTS OF RELIABILITY OF OFFSHORE STRUCTURES
JUNE 1989
ISSN 0902-7513 R8909

ACKNOWLEDGEMENTS

The present thesis is made under the supervision of Prof. P. Thoft-Christensen to whom I am very grateful for a good cooperation. Furthermore, I would like to thank Dr. J. D. Sørensen for fruitful discussions.

I am very grateful to technical assistant N. Hornung for her careful preparations of the figures for the thesis, and to secretary K. Aakjær for her skilful proofreading of the manuscript.

The work presented has been partly financed by the Danish Ministry of Energy.

Aalborg, March 1989

Gudfinnur Sigurdsson

RESUMÉ

Inden for de sidste år er det blevet mere og mere udbredt at anvende pålidelighedsteori til at modellere usikkerheder ved design af offshorekonstruktioner. Usikkerhederne relaterer til fysiske størrelser, såsom materialegenskaber, og til usikkerheder i forbindelse med matematisk modellering af konstruktioners opførsel. De mest anvendte metoder inden for systempålidelighed er baseret på den antagelse, at en konstruktion er et system af såkaldte svigtelementer. Et svigtelement er defineret som et lokalt svigt i konstruktionen. Som eksempler på svigtelementer kan nævnes:

1) træk/tryk svigtelement (flydning)

2) bøjnings svigtelement (flydning)

3) kombineret virkning af flere snitkræfter (flydning)

4) udmattelses svigtelement

5) instabilitets svigtelement

6) folnings svigtelement

Formålet med denne afhandling er at beskrive nogle praktisk anvendelige metoder til at estimere offshorekonstruktioners pålidelighed. To forskellige metoder betragtes:

I Metode til estimering af pålidelighed af ramme- og gitterkonstruktioner med hensyn til flydemekanisme (kollaps), hvori svigtelementer 1), 2) og 3) medtages. Metoden, der er baseret på øvreværdisætningen fra plasticitetsteorien, er beskrevet i kapitel 3. I afsnit 3.2 er generel plasticitetsteori for ramme- og gitterkonstruktioner beskrevet. Afsnit 3.3 omhandler anvendelse af pålidelighedsteori i forbindelse med estimering af pålidelighed med hensyn til kollaps, og i afsnit 3.4 er beskrevet en metode til identifikation af de mest signifikante kollapsformer. I forbindelse hermed er udarbejdet et computerprogram "COLLAPSE". Programmet er kort beskrevet og illustreret med to eksempler i afsnit 3.5.

II Metode til estimering af pålidelighed af jacket-konstruktioner med hensyn til udmattelse, d.v.s. svigtelement 4) er benyttet. Konstruktionen antages at svigte, når et enkelt svigtelement svigter. Kun bølgebelastning betragtes. Korttids- og langtids-modellering af bølgetilstande er beskrevet i afsnit 4.2. I afsnit 4.3 er beskrevet en sansynlighedsmodel af bølgebelastningen. Morisons formel benyttes ved estimering af bølgelaster på konstruktionselementer. I afsnit 4.4 er beskrevet hvordan kryds-spektral tætheder for spændingerne i et svigtelement kan estimeres. To forskellige metoder til at estimere fordelinger af spændingsvariationer i svigtelementer for en given kryds-spektral tæthed, er beskrevet, nemlig

rain-flow-counting metoden og range-counting metoden. I afsnit 4.5 er betragtet tre forskellige modeller til estimering af den akkumulerede udmattelsesskade i svigtelementer, nemlig Miners regel, en brudmekanisk model og den såkaldte B-model. I forbindelse hermed, er udarbejdet et computerprogram "SAOFF" (Stochastic Analysis Of Fatigue Failure). Programmet er kort beskrevet og illustreret med et enkelt eksempel i afsnit 4.6.

LIST OF CONTENTS

1. INTRODUCTION

The use of modern structural reliability theory for modelling uncertainties in offshore engineering has gained widespread support. The uncertainties may relate to both physical quantities, e.g. material quantities and loads, and uncertainties in the mathematical modelling of the structural system. Most systems reliability methods are based on the concept of failure elements. A failure element is defined as a local failure mode for a structure. In Thoft-Christensen^p 1987[1] †, some examples of different failure elements used in structural systems reliability theory are discussed, namely

1) Tension/compression failure elements (yielding)
2) Bending failure elements (yielding)
3) Combined load effect failure elements (yielding)
4) Strain softening failure elements
5) Instability failure elements
6) Buckling failure elements
7) Global instability failure elements
8) Fatigue failure elements
9) Punching failure elements
10) Slab failure elements.

It is of great importance when estimating the reliability of an offshore structure to include all failure elements in the analysis. However, the number of failure elements will often be very high, so from a computational point of view it is therefore necessary to exclude insignificant failure elements.
Reliability of a single failure element can be estimated sufficiently accurately by the reliability methods available to-day. However, estimation of the reliability of a structural system is much more complicated. Even such an important and difficult question how to define systems failure is still being discussed, Thoft-Christensen^p 1987[2].

The scope of this thesis is the development of some applicable methods for evaluating the reliability of offshore structures.

Two different definitions of system failure modes are used, namely a failure mode due to formation of a mechanism (collapse), and a failure mode due to fatigue failure.

In chapter 2 a short introduction on the reliability theory relevant in this thesis on

† In the following, references are made as: author(s)^c year^i, where the code ^{c} indicates in which part of the reference list the reference is located. The following codes are used: b = books, t = thesis and p = papers. If the author(s) has more than one publication in the same year, index ^{i} indicates which of these the reference signifies.

structural reliability analysis is given.

Chapter 3 contains an applicable method for evaluating the reliability of jacket type offshore structures with respect to plastic collapse, where failure elements 1), 2) and 3) are used. The method is based on the upper-bound theorem of plasticity (kinematic theorem of mechanisms). To make this method applicable a new program package "COLLAPSE" has been made. Failure elements 1), 2) and 3) have been included for plane structures, but for space structures only failure elements 1) and 2) have been included so far. The program package is briefly described in section 3.5, and is illustrated by two examples. Problems connected with modelling of the loading on a jacket structure are not treated in the chapter.

In chapter 4 an applicable method for evaluating the reliability of jacket type offshore structures with respect to fatigue failure, i.e. failure element 8) is used. The structure is considered to be in a state of failure when a single failure element fails. Only wave loading is considered. In section 4.2. a probabilistic model of the sea states is considered, where for a short-term period (a few hours) the sea surface is assumed to be a zero-mean ergodic Gaussian process. The long-term probability of the sea states is estimated from wave observations in the ocean area concerned. Section 4.3 contains a probabilistic modelling of the wave loading. Morison's equation is applied to estimate the force on the structural elements. In section 4.4 the structural response in considered. A modal analysis is applied. Section 4.5 contains a stochastic modelling of fatigue failure. Two different methods to estimate the distribution of stress amplitudes for a given sea state is described, namely the rain-flow-counting method and the range-counting method. The probability of fatigue failure is estimated using three different damage accumulation models, namely 1) Miner's rule combined with the so-called S-N approach, 2) a crack growth model, and 3) model introduced by Bogdanoff et al.[p] 1978[1,2,3], 1980, called the B-model.
To make this method applicable a new program package "SAOFF" (Stochastic Analysis Of Fatigue Failure) has been made. The program package is briefly described in section 4.6, and is illustrated by a single example.

At last, chapter 5 offers some general conclusions.

In connection with this thesis a number of computer programs have been made, containing approx. 15000 source lines written in FORTRAN77. Some of the programs, e.g. simulation programs used in sections 4.5.2.1-4.5.2.3, are not described in the present thesis.

2. STRUCTURAL RELIABILITY THEORY

2.1. Introduction

In this chapter a short introduction to the reliability theory relevant in this thesis is given.

A large number of books and papers of structural reliability theory has been written in the last few years. It is beyond the scope of this thesis to give a thorough description of this theory. The reader is referred to e.g. Melchers[b] 1987, Madsen, Krenk & Lind[b] 1986, Thoft-Christensen & Murotsu[b] 1986, Augusti, Baratta & Casciati[b] 1984, Sørensen[t] 1984, Bjerager[t] 1984 and Thoft-Christensen & Baker[b] 1982.

Most systems reliability methods are based on the concept of a failure element. A failure element is defined as a local failure mode for a structure. In section 2.2 it is described how the reliability of a failure element can be estimated using the first-order second-moment reliability index. When the reliability of the structure is considered the reliability of every failure element must be evaluated. This can be estimated using a systems approach. In section 2.3 it is described how the reliability of a structure is estimated on the basis of a series system, i.e. the structure is defined in failure when a single failure element fails.

2.2. Reliability of a Failure Element

In this section an estimation of the reliability of a failure element is briefly described using the first-order reliability index.

The stochastic variables $\overline{X} = (X_1, \ldots, X_n)$ used to model the uncertainties of a structure are called basic variables and are defined by the joint distribution function $p_{\overline{X}}$. In general, these variables model physical quantities e.g. material quantities and loads, but model uncertainty variables are also included in $\overline{X}$. For a given failure element it is assumed that there is a deterministic failure function $f(\overline{x})$, defined in such a way that it divides the n-dimensional basic variable space ω into two regions, namely a safe region ω_s, where $f(\overline{x}) > 0$, and an unsafe region ω_f where $f(\overline{x}) \leq 0$. The stochastic variable

$$M = f(\overline{X}) \tag{2.2.1}$$

is called the safety margin of the failure element.

The probability of failure P_f of the failure element is defined by

$$P_f = P[M \leq 0] = \int_{\omega_f} p_{\overline{X}}(\overline{x})\, d\overline{x} \tag{2.2.2}$$

In general, the safety margin M in eq.(2.2.1) is a function of correlated non-Gaussian distributed basic variables. However, by a suitable transformation, e.g. Rosenblatt

transformation, Sørensen[t] 1984, the correlated and non-Gaussian distributed basic variables $\overline{X}$ are transformed into uncorrelated and standardised Gaussian distributed variables $\overline{Z}$. By this transformation the failure surface $\partial\omega$ is given by $f^*(\overline{z}) = 0$ in the corresponding z-space. In the n-dimensional z-space the reliability index β is defined as the shortest distance from the origin to the failure surface, i.e.

$$\beta = \min_{\overline{z}\in\partial\omega} \left(\sum_{i=1}^{n} z_i^2 \right)^{\frac{1}{2}} \tag{2.2.3}$$

In many situations the probability of failure in eq.(2.2.2) can be determined with good approximation from

$$P_f \approx \Phi(-\beta) \tag{2.2.4}$$

where $\Phi(\cdot)$ is the standard Gaussian distribution function.

2.3. Reliability of a Structural System

In section 2.2 the probability of failure for a single failure element has been considered. When the probability of failure of the whole structure is considered, the probability of failure for every failure element must be evaluated. If the largest of these probabilities is used as a measure of the probability of failure of the structure it is called reliability modelling at level 0. A more satisfactory estimate of the probability of failure of the structure P_f^s is based on a systems approach, Thoft-Christensen & Murotsu[b] 1986. A simple definition of systems failure is failure in a single failure element, i.e. the structure is considered to be in a state of failure when a single failure element fails. The system probability of failure can be estimated as

$$P_f^s \approx 1 - \Phi_n(\overline{\beta};\overline{\overline{\rho}}) \tag{2.3.1}$$

where n is the number of failure elements in the structure, Φ_n is the n-dimensional Gaussian distribution function, $\overline{\beta} = (\beta_1,\ldots,\beta_n)$ are the reliability indices for the failure elements and $\overline{\overline{\rho}}$ is the correlation coefficient matrix for the safety margins. In real structures the number of failure elements n is often very large, but usually a large number of the failure elements are not significant for the systems reliability, which means that the evaluation of the systems probability of failure in eq.(2.3.1) becomes much less complicated. A number of approximate evaluations of eq.(2.3.1) can be found in the literature. It is beyond the scope of this thesis to deal with these approximate evaluations. The reader is referred to the references given is section 2.1.

3. RELIABILITY ANALYSIS OF A DISCRETIZED IDEAL PLASTIC STRUCTURAL SYSTEM

3.1. Introduction

This chapter focuses on time-invariant system reliability analysis with respect to plastic collapse of truss and frame structures of ideal rigid plastic materials.
It is assumed that the points of possible yield hinge formation (failure elements) have fixed positions in the structure and that the number of such points is finite. The external load is represented as a finite set of random forces/moments. Furthermore, the yield stress is assumed to be random.
The reliability analysis of ideal-plastic structures is usually based on the lower-bound theorem of plasticity theory (static theorem of admissible stress fields) or the upper-bound theorem (kinematic theorem of mechanisms). Application of the lower-bound theorem leads to lower bounds on the reliability, and is more relevant for engineering decision than the upper-bound theorem which leads to upper bounds of the reliability. However, analysis based on the lower-bound theorem is in general quite difficult and often the best lower bounds known in deterministic theory are not nearly as close to the exact result as the upper bound results, Ditlevsen & Bjerager[p] 1984.
In this thesis the analysis is carried out using the upper-bound theorem. The number of potential failure modes is usually very large. However, in most cases the majority of these are not significant, i.e. they have negligible influence on the failure probability of the structure.
In section 3.2 the general theory of plasticity for frame and truss structures is described. This description is mainly based on Hodge[b] 1959, Neal[b] 1970, Lange-Hansen[p] 1983 and Thoft-Christensen, Sigurdsson & Sørensen[p] 1986. In section 3.3 a reliability theory of ideal plastic frame and truss structures is described. In section 3.4 a method to identify the most significant plastic collapse mechanisms is described. In section 3.5 a new computer package "COLLAPSE" is introduced. The program, which is based on the methods and assumptions described in sections 3.2 - 3.4, is illustrated by two examples.

3.2. General Theory of Plasticity

Traditionally the estimate of the load-bearing capacity of a structural system is based on either the theory of elasticity or the theory of plasticity.
If the theory of plasticity is used then it is assumed that the material behaviour is elasto-plastic. This assumption is in general reasonable for steel frame structures, e.g. offshore jacket structures, considered in this chapter. Further, it is assumed that the definition of structural failure is formation of a collapse mechanism (mechanism level).

In this section $\overline{\sigma} = (\sigma_1, \sigma_2, \ldots, \sigma_n)^T$ and $\overline{\epsilon} = (\epsilon_1, \epsilon_2, \ldots, \epsilon_n)^T$ denote generalised stresses and strains, see Hodge[b] 1959 or Neal[b] 1970. The yield capacity of the material is described by the yield condition $f(\overline{\sigma}) = 0$, where the generalised stresses $\overline{\sigma}$ are functions of material properties, e.g. the yield stress Y in pure tension. The yield surface in the n-dimensional $\overline{\sigma}$-space is defined by the yield condition and it is assumed to be convex. States of the stress where $f(\overline{\sigma}) < 0$ are elastic, states where $f(\overline{\sigma}) = 0$ are plastic and states where $f(\overline{\sigma}) > 0$ are impossible.
In the following it is assumed that the elastic strains are zero, i.e. the material is a rigid-plastic material and $\overline{\epsilon}$ denotes the plastic strains. The ultimate strength of the structure can then be estimated using the upper- and lower-bound theorems of plasticity.
The rate of internal work $\dot{A}^i$ at a given point on the yield surface can be written as

$$\dot{A}^i = \dot{\overline{\epsilon}}^T \overline{\sigma} \tag{3.2.1}$$

where $\overline{\sigma}$ is the state of stress at which the plastic strain velocities $\dot{\overline{\epsilon}}$ occur. The strain velocities $\dot{\overline{\epsilon}} = (\dot{\epsilon}_1, \dot{\epsilon}_2, \ldots, \dot{\epsilon}_n)$ are determined by the so-called associated flow rule (normality condition) which at a regular point on the yield surface can be written as

$$\dot{\epsilon}_i = \lambda \frac{\partial f(\overline{\sigma})}{\partial \sigma_i} \quad , \quad i = 1, 2, \ldots, n \tag{3.2.2}$$

where $\lambda \geq 0$ is a constant.

As mentioned above the elastic strains are neglected. This implies that the static and geometric equilibrium equations at the moment of initiation of yield failure can be formulated in the undeformed state.
Approximate determination of the collapse load using the theory of plasticity can be performed using the lower-bound theorem of plasticity or the upper-bound of plasticity.

The lower-bound theorem of plasticity states that a structure will be able to carry a set of loads if it is possible to find a stress distribution which is safe and statically admissible.

A stress distribution is safe if the stresses $\overline{\sigma}$ at any point in the structure satisfy the condition $f(\overline{\sigma}) \leq 0$. A stress distribution is statically admissible if static equilibrium is obtained at all points in the structure.

The upper-bound theorem of plasticity states that a structure will not be able to carry a set of loads if there exists a kinematically possible displacement rate field and a corresponding strain rate field, for which the rate of work of the external loads exceeds the total internal dissipation (rate of internal work) in the structure.

A displacement rate field is kinematically possible if it fulfils the boundary conditions and if the rate of external work is positive.

The upper- and lower-bound theorems can be used to estimate upper and lower values of the load-bearing capacity of a structure. If some of the quantities are modelled as random variables these theorems can be used to estimate lower and upper values of the probability of failure of the structure.

For structures modelled by plane beam elements and/or truss elements, the generalised stresses and strains are related to the cross-sectional stress effects and the yield capacities. The effect of the shear forces is neglected in this thesis and it is assumed that the structural material has the same yield stress in compression and tension.

The structure is modelled by straight elements with constant cross-section and the loading is assumed to consist of concentrated forces. The plastic deformations take place in a number of discrete points called yield hinges or failure elements. The possible yield hinges are placed at the end points of the structural elements or below the concentrated forces. The following generalised stresses are used ($n = 2$)

$$(\sigma_1, \sigma_2) = \left(\frac{N}{N_F}, \frac{M}{M_F}\right) \tag{3.2.3}$$

where

N is the axial force in a yield hinge

N_F is the corresponding axial strength capacity

M is the bending moment in a yield hinge

M_F is the corresponding yield moment capacity

The associated generalised strains are

$$(\epsilon_1, \epsilon_2) = (N_F u_1, M_F u_2) \tag{3.2.4}$$

where

u_1 is the mutual axial deformation in a yield hinge

u_2 is the mutual rotation deformation in a yield hinge

The rate of internal work in a yield hinge is then

$$\dot{A}^i = \frac{N}{N_F} N_F \dot{u}_1 + \frac{M}{M_F} M_F \dot{u}_2 \tag{3.2.5}$$

The yield condition is

$$f(\frac{N}{N_F}, \frac{M}{M_F}) \; = \; 0 \tag{3.2.6}$$

and the flow rule (eq.(3.2.2)) gives

$$N_F \dot{u}_1 = \lambda \frac{\partial f(\frac{N}{N_F}, \frac{M}{M_F})}{\partial(\frac{N}{N_F})} \tag{3.2.7}$$

$$M_F \dot{u}_2 = \lambda \frac{\partial f(\frac{N}{N_F}, \frac{M}{M_F})}{\partial(\frac{M}{M_F})} \tag{3.2.8}$$

Combining eq.(3.2.7) and eq.(3.2.8) gives

$$\frac{N_F \dot{u}_1}{M_F \dot{u}_2} = \frac{\partial f(\frac{N}{N_F}, \frac{M}{M_F})}{\partial(\frac{N}{N_F})} \left(\frac{\partial f(\frac{N}{N_F}, \frac{M}{M_F})}{\partial(\frac{M}{M_F})} \right)^{-1} \tag{3.2.9}$$

From eq.(3.2.9) it is seen that if the ratio between the generalised stresses in a yield hinge is known then the ratio between the generalised strains can be determined. However, this fact is not valid at singular points. In figure 3.2.1 a), b) and c), the singular points appear where the yield surface intersects the N/N_F-axis.
On the other hand, when the ratio between the generalised strains is known the ratio between the generalised stresses can be determined uniquely, except where the yield surface is linear, see figure 3.2.1 d) and e).

The yield condition in generalised stresses for a general cross-section will depend on the material as well as the geometry of the cross-section. In the example 3.2.1 below the yield condition for four different cross-sections are shown.

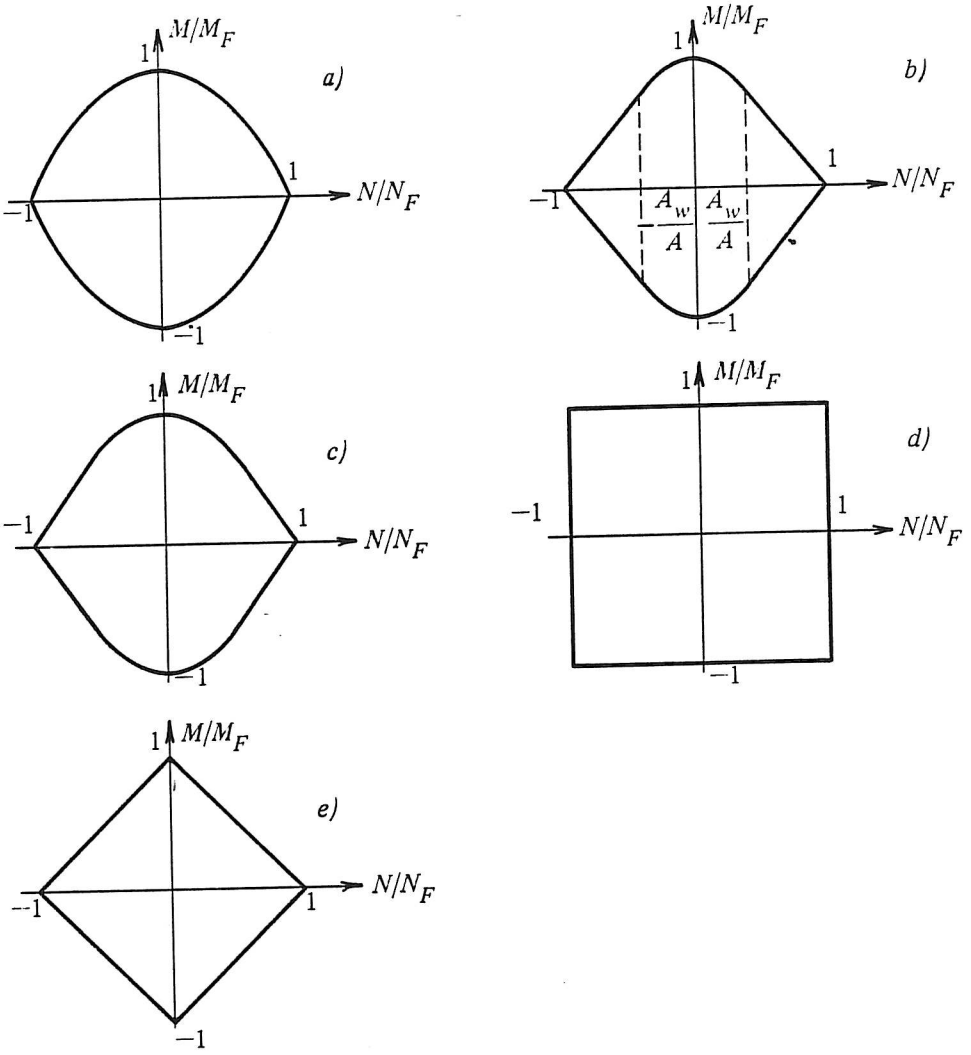

Figure 3.2.1. Yield surfaces (plastic axial/moment interaction curves) for
a) rectangular cross-section, b) I- and box sections, c) thin-walled
tubular section, d) interaction not taken into account, and
e) linear yield surface.

Example 3.2.1

In this example the yield conditions for four different double-symmetric cross-sections, namely rectangular-, I-, box- and thin-walled tubular sections are stated. A detailed derivation is given in appendix A. The surfaces are shown in figure 3.2.1.

Rectangular cross-section

$$f(\frac{N}{N_F}, \frac{M}{M_F}) = \left(\frac{N}{N_F}\right)^2 + |\frac{M}{M_F}| - 1 = 0 \tag{3.2.10}$$

I- and box-sections

$$f(\frac{N}{N_F},\frac{M}{M_F}) = \begin{cases} a\left(\frac{N}{N_F}\right)^2 + |\frac{M}{M_F}| - 1 = 0 & |\frac{N}{N_F}| \leq \frac{A_w}{A} \\ |\frac{N}{N_F}| + b|\frac{M}{M_F}| - 1 = 0 & |\frac{N}{N_F}| > \frac{A_w}{A} \end{cases} \tag{3.2.11}$$

where

$$a = \left(2\frac{A_w}{A} - \left(\frac{A_w}{A}\right)^2 + \frac{t_1}{d}\left(\frac{A-A_w}{A}\right)^2\right)^{-1} \tag{3.2.12}$$

$$b = 1 - \frac{A_w}{2A} \tag{3.2.13}$$

and where A is the total cross-sectional area, A_w is the web area, t_1 is the web thickness and d is the flange width, see appendix A.

Thin-walled tubular cross-section

$$f(\frac{N}{N_F},\frac{M}{M_F}) = |\frac{M}{M_F}| - cos\left(\frac{\pi}{2}\frac{N}{N_F}\right) = 0 \tag{3.2.14}$$

Interaction not taken into account

$$f(\frac{N}{N_F},\frac{M}{M_F}) = \begin{cases} |\frac{N}{N_F}| - 1 = 0 \\ \text{or} \\ |\frac{M}{M_F}| - 1 = 0 \end{cases} \tag{3.2.15}$$

Linear yield surface

$$f(\frac{N}{N_F},\frac{M}{M_F}) = |\frac{N}{N_F}| + |\frac{M}{M_F}| - 1 = 0 \tag{3.2.16}$$

3.3. Reliability Theory of Ideal Plastic Frame and Truss Structures

Calculation of collapse probabilities for truss and frame structures may be based on a variety of different idealisations of the load and the structural models. Considering a structure subjected to a time dependent random load, the possible collapse events become dependent on the entire load history during the service life and on the material properties in a complicated way. The best that can be done at present is to perform computer simulation studies by which the behaviour of a sample of the structure is followed step by step through each sample load path, Ditlevsen & Bjerager[p] 1987. This way to obtain collapse probability estimates of reasonable confidence is in general very costly in terms of computer time, even for simple structures. Therefore, a complete analysis based on simulation is far too complicated for practical applications.

In this thesis the load and the structural models are defined in the following way

- The external loads are assumed to be time independent and are represented by a finite set of random forces and moments.
- The structure is discretized (lumped) into a finite set Ω of r points of potential yield hinges. In a yield hinge i the strain rate is $\overline{\dot{\epsilon}}_i = (\dot{\epsilon}_{i1}, \dot{\epsilon}_{i2}, \ldots, \dot{\epsilon}_{in})^T$, where n is the number of degrees of freedom in the yield hinge i. This implies that the structural elements joining these points are infinitely rigid and strong.
- A yield condition

$$f(\overline{\sigma}) = 0 \tag{3.3.1}$$

  is associated with each of the points of Ω. The yield condition for a given point i in Ω is given solely in terms of generalised stresses $\overline{\sigma}_i = (\sigma_{i1}, \sigma_{i2}, \ldots, \sigma_{in})^T$, $i = 1, 2, \ldots, r$, and the stochastic properties does not change during the lifetime of the structure.
- The yield surface is assumed to be convex and the plastic strain rates are derivable from the yield function through the associated flow rule (the normality condition).
- The geometrical quantities of the structure are assumed to be deterministic, and changes in geometry at plastic collapse are assumed to be insignificant.
- The collapse probability of the structure is estimated by using the upper-bound theorem of plasticity.

In the following, a frame and truss structure of n_r degrees of redundancy subjected to n_p concentrated external random loads, $\overline{P} = (P_1, P_2, \ldots, P_{n_p})^T$, is considered. The number of points of potential yield hinge formations is r and by neglecting the

effect of the shear forces and the torsion moments the yield conditions depend on two internal forces, namely the bending moments $\overline{M} = (M_1, M_2, \ldots, M_r)^T$ and the axial forces $\overline{N} = (N_1, N_2, \ldots, N_r)^T$. Then the yield conditions for the r critical sections become two-dimensional (i.e. $n = 2$). Further, plastic deformations of the structure are described by the set of generalised strain rates

$$\dot{\overline{\overline{\epsilon}}} = \begin{bmatrix} \dot{\epsilon}_{11} & \dot{\epsilon}_{12} \\ \vdots & \vdots \\ \dot{\epsilon}_{r1} & \dot{\epsilon}_{r2} \end{bmatrix} \tag{3.3.2}$$

where $\dot{\epsilon}_{i1}$ is the strain rates corresponding to axial deformation rates and $\dot{\epsilon}_{i2}$ is the strain rates corresponding to rotational deformation rates in the yield hinge i.

Let $\Omega_{\dot{\epsilon}} \subseteq R^r$ be the set of plastic strain rates derived from the complete set of kinematically admissible velocity fields, which depend only on the geometry of the structure.
For a given plastic mechanism with strain rates $\dot{\overline{\overline{\epsilon}}} \in \Omega_{\dot{\epsilon}}$, an upper-bound safety margin M^* can, by the principle of the virtual work, be written as

$$M^* = \sum_{k=1}^{r} \dot{A}_k^i - \sum_{l=1}^{n_p} \dot{A}_l^e \tag{3.3.3}$$

where

$\dot{A}_k^i$ is the internal work rate for yield hinge no. k

$\dot{A}_l^e$ is the external work rate performed by the concentrated load no. l

r is the number of potential yield hinges

n_p is the number of concentrated loads.

The internal work rate $\dot{A}_k^i$ for yield hinge no. k can be written as

$$\dot{A}_k^i = \frac{|\dot{\epsilon}_{k1}|}{N_{F_k}} N_k + \frac{|\dot{\epsilon}_{k2}|}{M_{F_k}} M_k \tag{3.3.4}$$

where

$\frac{|\dot{\epsilon}_{k1}|}{N_{F_k}}$ is the mutual axial deformation rate $\dot{u}_{k1}$ in yield hinge no. k

$\frac{|\dot{\epsilon}_{k2}|}{M_{F_k}}$ is the mutual rotational deformation rate $\dot{u}_{k2}$ in yield hinge no. k

N_k is the axial force in yield hinge no. k

N_{F_k} is the corresponding axial strength capacity in yield hinge no. k

M_k is the bending moment in yield hinge no. k

M_{F_k} is the corresponding bending moment capacity in yield hinge no. k

The axial strength capacity N_{F_k} and the yield moment capacity M_{F_k} in the yield hinge no. k can be written

$$N_{F_k} = A_k Y_k$$

$$M_{F_k} = W_{p_k} Y_k$$

where A_k is the cross-sectional area, W_{p_k} is the plastic modulus and Y_k is the yield stress in yield hinge k.
Using the yield condition and the flow rule (see eq.(3.2.6)-eq.(3.2.9)) the internal work rate $\dot{A}_k^i$ can be rewritten as

$$\dot{A}_k^i = c_k Y_k \tag{3.3.5}$$

where c_k only depends on $\dot{\epsilon}_{k1}$ and $\dot{\epsilon}_{k2}$ in the yield hinge and the type of cross-section.
The external work rate $\dot{A}_l^e$ for the concentrated load l can be written as

$$\dot{A}_l^e = v_l P_l \tag{3.3.6}$$

where v_l is the virtual displacement/rotation rate for load l and P_l is the magnitude of load l.
Using eq.(3.3.5) and eq.(3.3.6) the eq.(3.3.3) can be rewritten as

$$M^* = \sum_{k=1}^{r} c_k Y_k - \sum_{l=1}^{n_p} v_l P_l \tag{3.3.7}$$

The failure probability P_f with respect to plastic collapse is, according to the upper-bound theorem of plasticity, determined by

$$P_f = P\left\{ \bigcup_{all\ \dot{\bar{\epsilon}}} \left\{ \left(\dot{\bar{\epsilon}} \in \Omega_{\dot{\epsilon}} \right) \cap M^*(\dot{\bar{\epsilon}}) \leq 0 \right\} \right\} \tag{3.3.8}$$

The set $\Omega_{\dot{\epsilon}}$, which may be determined by a set of geometrical conditions, is a set of infinity numbers of plastic strain rates $\dot{\bar{\epsilon}}$. However, P_f can be approximately estimated by a finite number of plastic strain rates $\dot{\bar{\epsilon}}_1, \dot{\bar{\epsilon}}_2, \ldots, \dot{\bar{\epsilon}}_m \in \Omega_{\dot{\epsilon}}$. An upper bound of the reliability is then given by

$$1 - P_f \leq 1 - P\left\{ \bigcup_{i=1}^{m} \left\{ M^*(\dot{\bar{\epsilon}}_i) \leq 0 \right\} \right\} \tag{3.3.9}$$

For the sake of simplicity the yield stresses Y_k, $k = 1,\ldots,r$ and the concentrated loads P_l, $l = 1,\ldots,n_p$ are modelled as Gaussian distributed random variables. All the remaining parameters (e.g. geometrical quantities) are assumed deterministic. Generally, the assumption of Gaussian distribution of the loading is an unsatisfactory approximation. In some cases a more logical assumption will be to use an extreme-value distribution. In such a case the non-Gaussian distributed stochastic variables are transformed into Gaussian distributed stochastic variables by e.g. the Rosenblatt transformation, Sørensen[t] 1984.

For a structure of the discrete type the number of plastic mechanisms of one-degree-of-freedom (ODOF) is finite. For such a structure the equality sign in eq.(3.3.9) is valid if m is taken as the total number of possible ODOF-mechanisms, and the safety margin in eq.(3.3.7) for all mechanisms (strain rates) becomes linear. However, even for relatively simple structures the number may be very large. Instead, a subset of significant plastic mechanisms can be applied in order to obtain a close upper bound of the reliability.
When each yield hinge in the structure only has one possible strain rate e.g. rotation, the multi-degrees-of-freedom (MDOF) -mechanisms will not become significant for estimation of the reliability. However, when yield hinges have more that one possible strain rate, e.g. axial elongation and rotation, some of the MDOF-mechanisms can become significant, and the safety margin in eq.(3.3.7) becomes nonlinear for this kind of mechanisms. Such MDOF-mechanisms can be divided into a finite number of ODOF-mechanisms, and all possible strain rates for the MDOF-mechanism can be described as a linear combination of the ODOF-mechanisms. The most significant strain rates, which become dependent on the yield condition in the yield hinge, can be found e.g. by using optimisation.
The corresponding reliability index β corresponding to the linear safety margin M^* in eq.(3.3.7) can be estimated by

$$\beta = \min_{\underline{\dot{\epsilon}} \in \Omega_{\dot{\epsilon}}} \left(\frac{\mu_{M^*}}{\sigma_{M^*}} \right) \tag{3.3.10}$$

where

$$\mu_{M^*} = \sum_{k=1}^{r} c_k \mu_{Y_k} - \sum_{l=1}^{n_p} v_l \mu_{P_l} \tag{3.3.11}$$

$$\sigma_{M^*} = \left(\sum_{k=1}^{r} \sum_{n=1}^{r} c_k c_n \sigma_{Y_k} \sigma_{Y_n} \rho_{Y_k Y_n} + \sum_{l=1}^{n_p} \sum_{m=1}^{n_p} v_l v_m \sigma_{P_l} \sigma_{P_m} \right)^{\frac{1}{2}} \tag{3.3.12}$$

and where μ, σ and ρ is the mean value, the standard deviation, and the coefficient

of correlation, respectively. For given strain rates $\overline{\overline{\dot{\epsilon}}} \in \Omega_{\dot{\epsilon}}$, c_k, $k = 1, \ldots, r$ and v_l, $l = 1, \ldots, n_p$ can be calculated from the relevant yield condition and the corresponding flow rule.

Example 3.3.1

The plane steel frame shown in figure 3.3.1 and the MDOF-mechanism in figure 3.3.2 is considered. The mechanism can be divided into the 9 independent ODOF-mechanisms shown in figure 3.3.3. The deformation rates $\overline{\overline{\dot{u}}}$ in the failure elements and the rotation/displacement rates for the external loads and the reliability indices for the ODOF-mechanisms are shown in table 3.3.3.
All geometrical quantities are assumed to be deterministic.The yield stress for each failure element Y_i, and the external loads P_i, are modelled as Gaussian distributed stochastic variables. The expected values $E[\cdot]$ and the coefficient of variation $V[\cdot]$ for the stochastic variables are shown in table 3.3.1. The yield stresses for all failure elements are assumed to be fully correlated, i.e. $\rho_{Y_iY_j} = 1$, $i, j = 1, 2, \ldots, 6$ and the correlation between the external loads is assumed to be 0.3, except for $\rho_{P_1P_2} = 1$, and $\rho_{P_3P_4} = 1$.

Stochastic variables	Expected values $E[\cdot]$	coefficient of variation $V[\cdot]$
$Y_i, i = 1, \ldots, 6$	$2.4 \cdot 10^5 \mathrm{kN/m^2}$	0.15
P_1	50 kN	0.25
P_2	50 kN	0.25
P_3	250 kN	0.25
P_4	50 kN	0.25
P_5	50 kNm	0.25

Table 3.3.1. Expected values and coefficient of variation for the stochastic variables.

The following abbreviations will be used

- $\times$ failure element (potential location of yield hinge)
- $\blacklozenge$ failure element fails with rotational displacement
- $+$ failure element fails with axial displacement
- $\blacklozenge$ failure element fails with a combination of axial and rotational displacement
- β^I the reliability index of a mechanism, using the yield condition for I-cross-sections
- β° the reliability index of a mechanism, using the yield condition for thin-walled tubular sections

$\beta^{\triangle}$ the reliability index of a mechanism, using the linear yield condition

$\beta^{\square}$ the reliability index of a mechanism, when the interaction between the axial force and bending moment is not taken into account

N_{F_i} axial strength capacity for failure element no. i

M_{F_i} yield moment capacity for failure element no. i

$\dot{u}_{i1}$ the mutual axial deformation rate in the failure element no. i, which is defined positive if it gives prolongation

$\dot{u}_{i2}$ the mutual rotational deformation rate in failure element no. i, which is defined to be positive if it gives tension in the lower side of the element

v_i the virtual displacement/rotational rate for load no. i

Failure element i	Cross-section area A_i (m^2)	Plastic section modulus W_{P_i} (m^3)
1,2,3	$3.34 \cdot 10^{-3}$	$2.85 \cdot 10^{-4}$
4,5,6	$3.91 \cdot 10^{-3}$	$3.66 \cdot 10^{-4}$

Failure element i	Type of cross-section	Web area A_{W_i} (m^2)	Web thickness t_1 (m)	Flange width d (m)
1,2,3	IPE-220	$1.31\ 10^{-3}$	0.0059	0.11
4,5,6	IPE-240	$1.56\ 10^{-3}$	0.0062	0.12

Table 3.3.2. Cross-sectional data for failure elements.

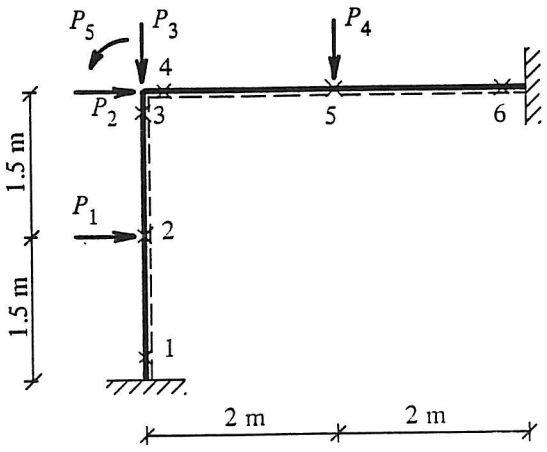

Figure 3.3.1. Geometry, loading and potential failure elements.

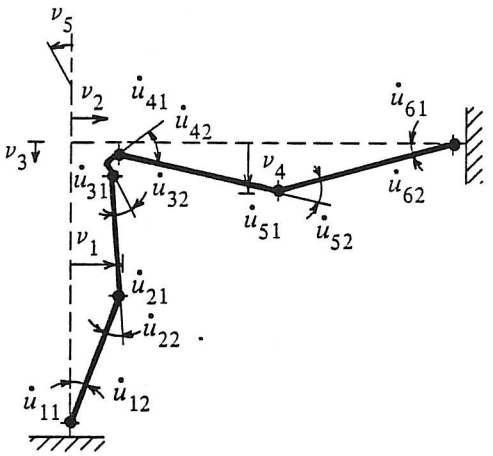

Figure 3.3.2. MDOF-mechanism.

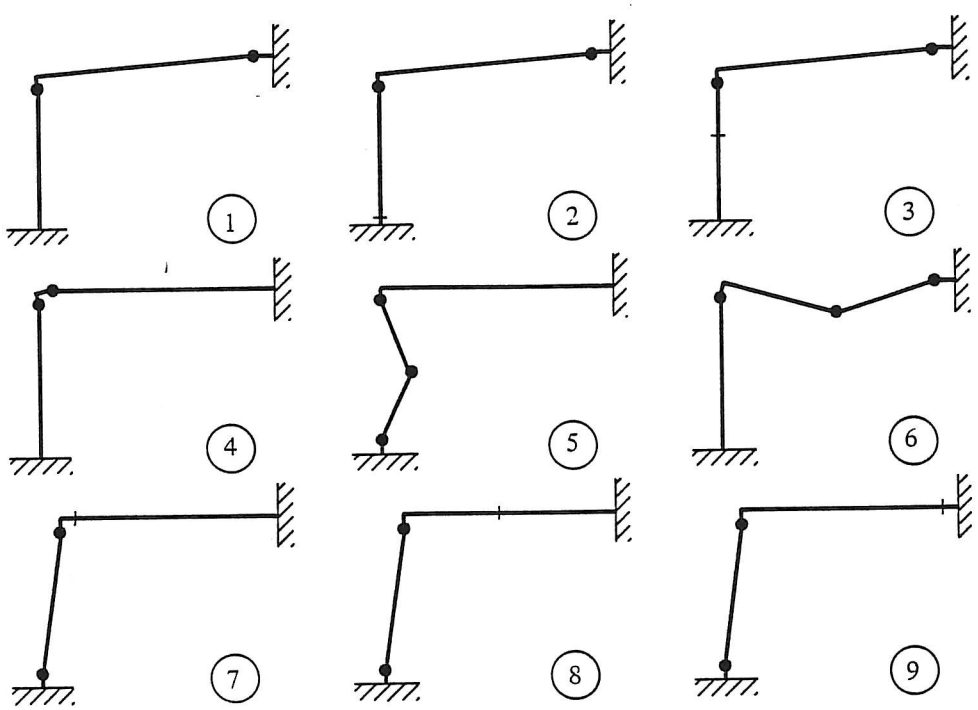

Figure 3.3.3. ODOF-mechanisms

All possible mutual axial and rotational deformation rates in the yield hinges for the mechanisms shown in figure 3.3.2 can now be expressed as a linear combination of the mutual axial and rotational deformation rates in the yield hinges in the ODOF-mechanisms given in table 3.3.3 as

$$\overline{\overline{\dot{u}}} = \begin{bmatrix} \dot{u}_{11} & \dot{u}_{12} \\ \vdots & \vdots \\ \dot{u}_{61} & \dot{u}_{62} \end{bmatrix} = \sum_{i=1}^{9} \alpha_i \, \overline{\overline{\dot{u}}}_i \tag{3.3.13}$$

$$\overline{v} = \begin{bmatrix} v_1 \\ \vdots \\ v_5 \end{bmatrix} = \sum_{i=1}^{9} \alpha_i \, \overline{v}_i \tag{3.3.14}$$

where α_i, $i = 1,\ldots,9$ are arbitrary real numbers, $\overline{\overline{\dot{u}}}_i$ are the mutual axial and rotational deformation rates and $\overline{v}_i$ are the virtual rotation/displacement rates in the ODOF-mechanism no. i, see table 3.3.3.

Mechanism no.	1	2	3	4	5	6	7	8	9
$\dot{u}_{11}$		4							
$\dot{u}_{12}$					-1		-1	-1	-1
$\dot{u}_{21}$			4						
$\dot{u}_{22}$					2				
$\dot{u}_{31}$	4								
$\dot{u}_{32}$	1	1	1	1	-1	-1	1	1	1
$\dot{u}_{41}$				-1			3		
$\dot{u}_{42}$									
$\dot{u}_{51}$								3	
$\dot{u}_{52}$						2			
$\dot{u}_{61}$									3
$\dot{u}_{62}$	-1	-1	-1			-1			
rot./disp. rate:									
v_1					1.5		1.5	1.5	1.5
v_2							3	3	3
v_3	4	4	4						
v_4	0.4	0.4	0.4			0.4			
v_5	1	1	1	1		-1			
reliability indices:									
β^I	3.78	3.84	3.84	4.00	4.40	4.48	6.11	6.11	6.11
β°	3.78	3.84	3.84	4.00	4.40	4.48	6.11	6.11	6.11
$\beta^\triangle$	3.78	3.84	3.84	4.00	4.40	4.48	6.11	6.11	6.11
$\beta^\square$	3.84	3.84	3.84	4.00	4.40	4.48	6.11	6.11	6.11

Table 3.3.3. Mutual axial and rotational deformation rates, rotation/displacement rates and reliability indices for the ODOF-mechanisms

The choice of α_is which gives the most significant mutual axial and rotational deformation rates can be estimated by using optimisation. The optimisation problem is formulated as

$$\begin{aligned} \min \quad & \beta(\overline{\alpha}) \\ \text{s.t.} \quad & \overline{\overline{\dot{\epsilon}}} \in \Omega_{\dot{\epsilon}} \\ & (\alpha_1,\ldots,\alpha_9) \neq (0,\ldots,0) \end{aligned}$$

Here the so-called "Nelder&Mead" algorithm is used, Kuester & Mize[b] 1973. The results of the optimisation are shown in table 3.3.4.

α_1	$1.288\ 10^{-3}$	$7.520\ 10^{-4}$	0
α_2	$2.789\ 10^{-2}$	$2.239\ 10^{-2}$	0
α_3	$5.534\ 10^{-2}$	$4.443\ 10^{-2}$	0
α_4	$9.987\ 10^{-1}$	$9.997\ 10^{-1}$	1
α_5	1.043	1.041	1
α_6	$4.241\ 10^{-4}$	$-1.101\ 10^{-3}$	0
α_7	$7.625\ 10^{-3}$	$5.991\ 10^{-3}$	0
α_8	$1.606\ 10^{-5}$	$6.872\ 10^{-5}$	0
α_9	$7.164\ 10^{-4}$	$2.065\ 10^{-3}$	0
β^I	2.02*	2.16	3.31
β°	2.23*	2.28	3.31
$\beta^\triangle$	2.01	1.71*	3.31
$\beta^\square$	3.79	3.78	3.31*

Table 3.3.4. The most significant combination of ODOF-mechanisms for the four yield conditions, * denote optimum value for a cross-section.

It follows from table 3.3.4 that the reliability index for given mechanism as expected depends significantly on the cross-section. It is also interesting to note that the most significant strain rates also depend on the cross-section and that the difference between the upper bound (interaction not taken into account) and the lower bound (linear yield surface) is large.

3.4. Method for Identifying Plastic Collapse Mechanisms

A great variety of methods and techniques for identifying failure modes defined as formation of plastic collapse mechanisms, for structural reliability assessment has been developed in the literature in the last decade. These methods can be classified in two categories, namely methods based on incremental methods, see e.g. Thoft-Christensen & Murotsu[b] 1986, and methods based on a plastic limit analysis, i.e. methods based on the lower-bound theorem of plasticity (static theorem of admissible stress fields) which leads to lower reliability bounds, and methods based on the upper-bound theorem of plasticity theory (kinematic theorem of mechanisms) which leads to upper reliability bounds, see e.g. Ditlevsen & Bjerager[p] 1984 or Bjerager[t] 1984.

Methods in the first category use a number of elastic analysis of the structure. However, these methods are not very suitable if the structure is highly redundant. The reason is that mechanisms are formed after formation of a large number of plastic hinges and it can therefore be difficult and expensive to identify the most significant failure modes.

A central problem for methods based on the plastic limit theory is to find lower reliability bounds, which are reasonably close to the upper reliability bounds. Experience seems to show that the upper bound calculated from only a few significant mechanisms is often quite close to the exact mathematical reliability calculated using the total set of possible mechanisms, Ditlevsen & Bjerager[p] 1987. This experience only concerns a certain type of the ideal plastic models, i.e. examples of simple structures where the yield conditions in each yield hinge only depend on the internal force, e.g. the bending moment or the axial force. On the other hand, even for simple structures, it turns out to be difficult by systematic analysis methods to find lower reliability bounds which are close to the exact result, Bjerager[t] 1984.

In this section a technique for identifying the most significant upper-bound failure modes for ideal plastic frame and truss structures is presented. It is assumed that the single members of the structure fail by plastic yielding (yield hinge model). It is well known that any plastic mechanism for a structure can be described as a linear combination of a set of independent mechanisms called fundamental mechanisms. Let n be the number of internal degrees of freedom of the structure, i.e. the number of potential yield hinges multiplied by the degree of freedom in each yield hinge. Further, let r be the degree of redundancy of the structure. Then the number of fundamental mechanisms is

$$m = n - r \tag{3.4.1}$$

Each fundamental mechanism fulfils the compatibility conditions, but does not necessarily have positive external work. A set of fundamental mechanisms can be automatically generated by a method proposed by Watwood[p] 1979, describing a method for automatic generation of fundamental mechanisms for plane frame structures with potential yield hinges of ODOF, namely rotation. This method can easily be extended

to spatial frame and truss structures and to yield hinges of MDOF. The presentation of this method here is based on Watwood[P] 1979 and Sørensen, Thoft-Christensen & Sigurdsson[P] 1985.

Basically the geometry of the structure determines the set of fundamental mechanisms, but in addition it is necessary to make judgements regarding the locations and the number of degrees of freedom of the potential plastic yield hinges. It is well known that the problem of hinge location can be handled, if the loading can be approximated in the form of concentrated loads and moments, since possible hinges can be placed at all such load points as well as at member intersections. The net result is that the structure is modelled as an assembly of beam elements, with potential hinges only at the ends of these elements and where the concentrated loads are acting. In the following presentation only the mutual rotations and the mutual axial displacements in each yield hinge are taken into account (shear deformation and torsion are neglected).

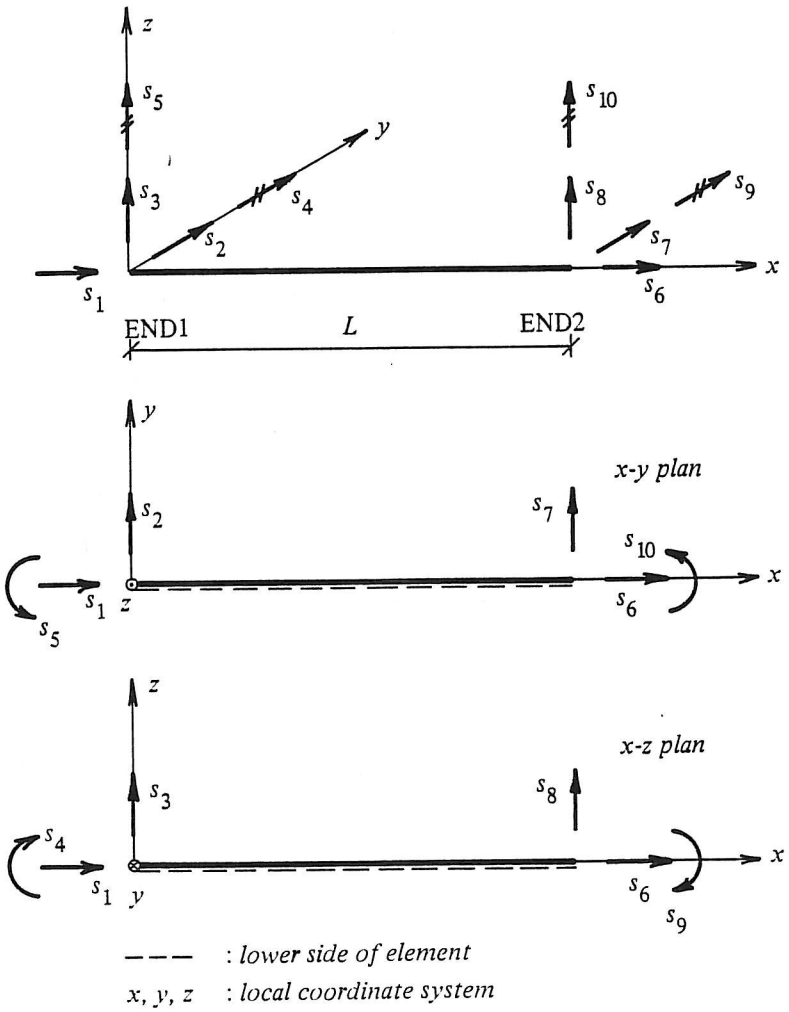

Figure 3.4.1. Definition of generalised coordinates $\overline{s}$ for a space beam element.

Unless a yield hinge is formed within a member, the member must move as a rigid body within the mechanism. Therefore it is necessary to formulate equations that can enforce this requirement. For this purpose a coordinate transformation is introduced into the member-generalised coordinates separating the rigid body motion from the member deformation. For this purpose it is useful to introduce two sets of generalised coordinates, i.e. a set $\overline{s}$ which describes the motion of the member ends and a set $\overline{s}'$ which describes the motion of the members (the member deformation and the rigid body motion of the members). Further, the transformation between $\overline{s}'$ and $\overline{s}$ will be described by a transformation matrix $\overline{\overline{T}}$ i.e.

$$\overline{s}' = \overline{\overline{T}}\,\overline{s} \tag{3.4.2}$$

Consider a space beam element. Definition of the set $\overline{s}$ for the element is shown in figure 3.4.1.

The set $\overline{s}'$ can be defined, in terms of the set $\overline{s}$ in the following way (note that member rotations about ends which give tension in the lower side of the beam are defined as positive)

$s'_1 = s_6 - s_1$	member elongation (displacement of end 2 in relation to end 1)
$s'_2 = s_5 + \frac{1}{L}(s_7 - s_2)$	positive member end rotation of end 1 about the z-axis
$s'_3 = -s_{10} + \frac{1}{L}(s_2 - s_7)$	positive member end rotation of end 2 about the z-axis
$s'_4 = -s_4 + \frac{1}{L}(s_8 - s_3)$	positive member end rotation of end 1 about the y-axis
$s'_5 = s_9 + \frac{1}{L}(s_3 - s_8)$	positive member end rotation of end 2 about the y-axis
$s'_6 = s_1$	rigid member translation in the x-direction
$s'_7 = s_2$	rigid member translation in the y-direction
$s'_8 = s_3$	rigid member translation in the z-direction
$s'_9 = \frac{1}{L}(s_8 - s_3)$	rigid member rotation about the y-axis from end 1 to end 2
$s'_{10} = \frac{1}{L}(s_2 - s_7)$	rigid member rotation about the z-axis from end 1 to end 2

where the two last-mentioned rotations are defined positive when the rotation is counterclockwise. These definitions are illustrated in figure 3.4.2. Note that any member deformation (except axial rotation, which is not included here) can be expressed by some combinations of s'_i , $i = 1, \ldots, 5$, and any rigid member motion (except axial rotation) can be expressed by some combination of s'_i, $i = 6, \ldots, 10$.

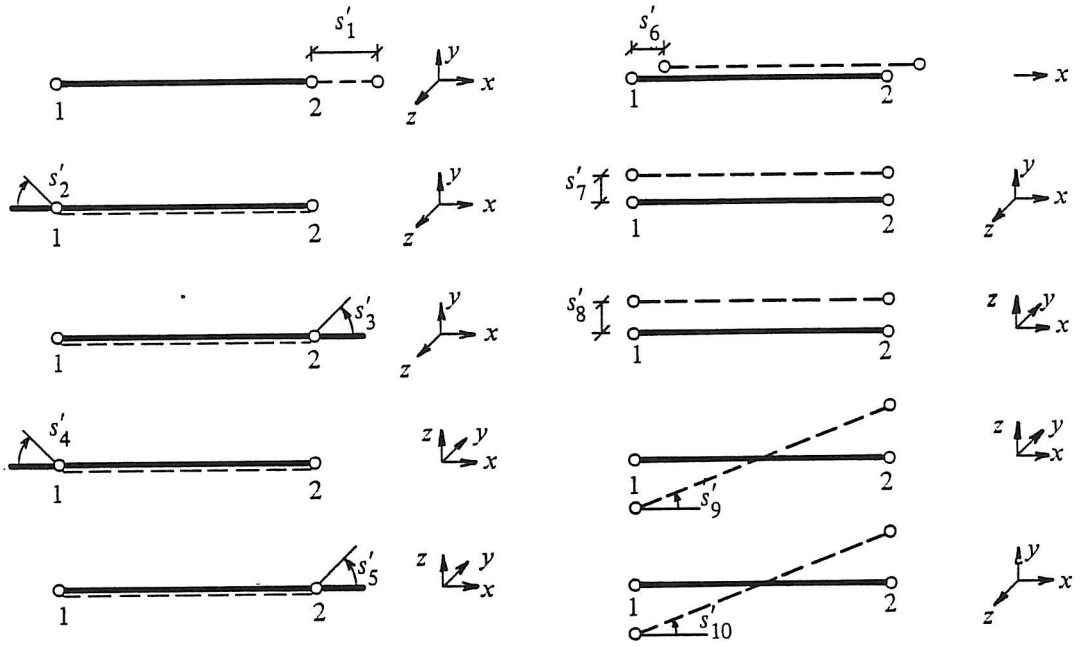

Figure 3.4.2. Definition of generalised coordinates $\bar{s}'$ for space beam element.

The transformation matrix $\bar{\bar{T}}$ can now be expressed as

$$\bar{\bar{T}} = \begin{bmatrix} -1 & 0 & 0 & 0 & 0 & 1 & 0 & 0 & 0 & 0 \\ 0 & -1/L & 0 & 0 & 1 & 0 & 1/L & 0 & 0 & 0 \\ 0 & 1/L & 0 & 0 & 0 & 0 & -1/L & 0 & 0 & -1 \\ 0 & 0 & -1/L & -1 & 0 & 0 & 0 & 1/L & 0 & 0 \\ 0 & 0 & 1/L & 0 & 0 & 0 & 0 & -1/L & 1 & 0 \\ 1 & 0 & 0 & 0 & 0 & 0 & 0 & 0 & 0 & 0 \\ 0 & 1 & 0 & 0 & 0 & 0 & 0 & 0 & 0 & 0 \\ 0 & 0 & 1 & 0 & 0 & 0 & 0 & 0 & 0 & 0 \\ 0 & 0 & -1/L & 0 & 0 & 0 & 0 & 1/L & 0 & 0 \\ 0 & 1/L & 0 & 0 & 0 & 0 & -1/L & 0 & 0 & 0 \end{bmatrix} \tag{3.4.3}$$

When a mechanism is formed all members of the structure will behave as rigid bodies. Deformation of each member must be prevented by enforcing the deformation coordinates $s'_1, \ldots, s'_5$ for each member to remain zero during the mechanisms. To enforce these constraints formally, we first introduce a constraint matrix $\bar{\bar{C}}^j$ for the jth element which is made up of the first five rows of $\bar{\bar{T}}$, i.e.

$$\bar{\bar{C}}^j = \begin{bmatrix} -1 & 0 & 0 & 0 & 0 & 1 & 0 & 0 & 0 & 0 \\ 0 & -1/L & 0 & 0 & 1 & 0 & 1/L & 0 & 0 & 0 \\ 0 & 1/L & 0 & 0 & 0 & 0 & -1/L & 0 & 0 & -1 \\ 0 & 0 & -1/L & -1 & 0 & 0 & 0 & 1/L & 0 & 0 \\ 0 & 0 & 1/L & 0 & 0 & 0 & 0 & -1/L & 1 & 0 \end{bmatrix} \tag{3.4.4}$$

Let the structural system consist of m elements. The constraint matrix $\overline{\overline{C}}$ for the entire structure is constructed by assembling the $\overline{\overline{C}}^j$, $j = 1, \ldots, m$ for the members as follows

$$\overline{\overline{C}} = \begin{bmatrix} \overline{\overline{C}}^1 & \overline{\overline{0}} & . & . & . & \overline{\overline{0}} \\ \overline{\overline{0}} & \overline{\overline{C}}^2 & \overline{\overline{0}} & . & . & \overline{\overline{0}} \\ \overline{\overline{0}} & \overline{\overline{0}} & \overline{\overline{C}}^3 & \overline{\overline{0}} & . & \overline{\overline{0}} \\ . & . & . & . & & \\ . & . & . & & . & . \\ . & . & . & & . & . \\ \overline{\overline{0}} & \overline{\overline{0}} & \overline{\overline{0}} & . & . & \overline{\overline{C}}^m \end{bmatrix} \tag{3.4.5}$$

where $\overline{\overline{0}}$ is a 5×10 matrix with only zero components. The $\overline{\overline{C}}$ is a $5m \times 10m$ matrix. The set of deformation generalised coordinated $(s'_1, \ldots, s'_5)$ for each element in the structure is now assembled in a global vector $\overline{S}'$ defined by

$$\overline{S}' = (s'_{1_1}, \ldots, s'_{5_1}, s'_{1_2}, \ldots, s'_{5_2}, \ldots, s'_{1_m}, \ldots, s'_{5_m})^T \tag{3.4.6}$$

where s'_{i_j} denotes the deformation generalised coordinate i for the structural element j.

Likewise, the generalised coordinates $(s_1, \ldots, s_{10})$, for each element in the structure, are assembled in a global vector $\overline{S}$ defined by

$$\overline{S} = (s_{1_1}, \ldots, s_{10_1}, s_{1_2}, \ldots, s_{10_2}, \ldots, s_{1_m}, \ldots, s_{10_m})^T \tag{3.4.7}$$

where s_{i_j} denote the generalised coordinate i for the structural element j.

This provides the relation

$$\overline{S}' = \overline{\overline{C}}\,\overline{S} \tag{3.4.8}$$

Clearly the components of $\overline{S}$ are not independent, but restrained so that the structural elements move in such a way that the compatibility of the assembled structure are preserved. This can be enforced by introduction of the general compatibility condition

$$\overline{S}^* = \overline{\overline{A}}\,\overline{r} \tag{3.4.9}$$

where the components of $\overline{S}^*$ are the generalised coordinates of all elements expressed in the global coordinate system, $\overline{r}$ is the column matrix of the external degrees of freedom (in general three per joint in plane structures, and six per joint in spatial structures, unless constraints are imposed) expressed in the global coordinate system and finally, $\overline{\overline{A}}$ is the compatibility matrix.

It now remains to introduce the coordinate transformations to link the element coordinates expressed in the local system $\overline{S}$, to the element coordinates expressed in the global system $\overline{S}^*$. This can be expressed as

$$\overline{S} = \overline{\overline{Q}}\,\overline{S}^* \tag{3.4.10}$$

where $\overline{\overline{Q}}$ is the transformation matrix.

Combining eqs.(3.4.8),(3.4.9) and (3.4.10) leads to

$$\overline{\overline{C}}_1\,\overline{r} = \overline{S}' \tag{3.4.11}$$

where

$$\overline{\overline{C}}_1 = \overline{\overline{C}}\,\overline{\overline{Q}}\,\overline{\overline{A}} \tag{3.4.12}$$

To find a mechanism, one must find a solution to eq.(3.4.11) so that $\overline{S}'$ is zero

$$\overline{\overline{C}}_1\,\overline{r} = \overline{0} \tag{3.4.13}$$

However, unless the structure is already a mechanism no such solution exists. In fact, $\overline{\overline{C}}_1$ generally has the dimension $3m \times r$ for plane frames, and for spatial frames, $5m \times r$ (unless constrains are imposed), where m is the number of structural elements and r is the number of external degrees of freedom.

At this point releases are introduced which will provide the possibility of mechanism formation. To keep the methods as general as possible five releases per element will be inserted. The five releases inserted are two rotational possibilities at each end of each element (about the two local axis) plus detaching (axial only) at end one from its joint. This is shown for a simple space frame in figure 3.4.3. Insertion of a release is equivalent to adding an external degree of freedom. By combining eq.(3.4.9) and eq.(3.4.10) leads to

$$\overline{S} = \overline{\overline{Q}}\,\overline{\overline{A}}\,\overline{r} \tag{3.4.14}$$

The releases must be made with respect to the local coordinates $\overline{s}$. In accordance with the definition of the coordinates shown in figure 3.4.3, the rows of the matrix $\overline{\overline{Q}}\,\overline{\overline{A}}$ are replaced by zeros where they correspond to $s_1, s_4, s_5, s_9, s_{10}, s_{11}, s_{14}, s_{15}, s_{19}$ and s_{20}. This is equivalent to releasing the corresponding degree of freedom. Also, a column is added to $\overline{\overline{Q}}\,\overline{\overline{A}}$ in which the number one is placed in the row that was zeroed out earlier. Of course, $\overline{r}$ must be expanded by one component for each column added to $\overline{\overline{Q}}\,\overline{\overline{A}}$. This modified form of eq.(3.4.14) is then inserted into eq.(3.4.8) resulting in

$$\overline{\overline{C}}_2\,\overline{r}_M = \overline{S}' \tag{3.4.15}$$

where $\overline{\overline{C}}_2$ is $\overline{\overline{C}}$ multiplied by the modified form of $\overline{\overline{Q}}\,\overline{\overline{A}}$, and $\overline{r}_M$ is the matrix of external degrees of freedom, $\overline{r}$, augmented by the member releases.

Putting $\overline{S}' = \overline{0}$ (as before) the following is obtained

$$\overline{\overline{C}}_2\,\overline{r}_M = \overline{0} \tag{3.4.16}$$

The solution of eq.(3.4.16) defines the fundamental solutions. Note that for plane structures $\overline{\overline{C}}_2$ is a $3m \times r_M$ matrix, where m is the number of elements, and where r_M is equal to the number of external degrees of freedom plus the number of internal degrees of freedom. For space structures $\overline{\overline{C}}_2$ is a $5m \times r_M$ matrix. The difference $r_M - \gamma m$ (where γ is equal to 3 or 5) is the number of independent solutions of eq.(3.4.16) and therefore also the number of fundamental mechanisms.

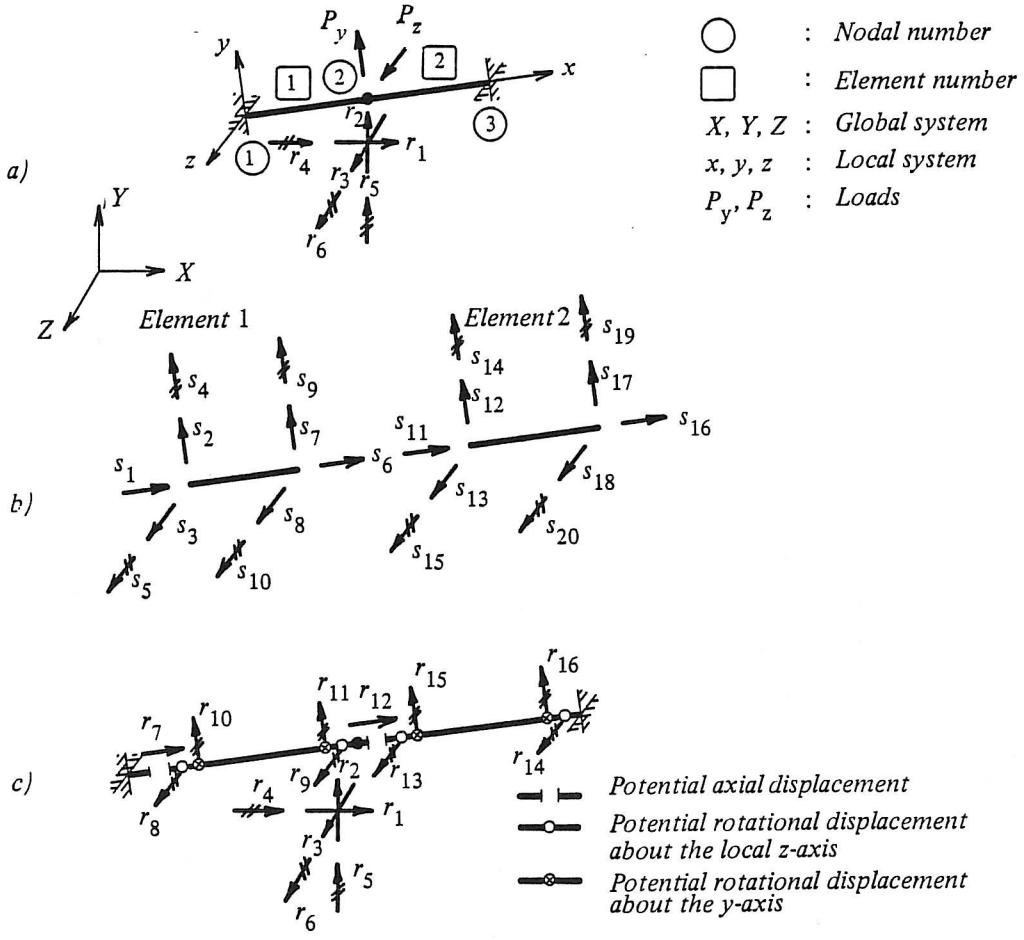

Figure 3.4.3. Simple space frame example.

When estimating the reliability of the complete structure it is important to be able to identify the most significant mechanisms, i.e mechanisms that contribute significantly to the probability of failure of the structure. When each yield hinge in the structure has only one possible strain rate the MDOF mechanisms will not become significant

for estimation of the reliability. For this kind of structure a heuristic method used to identify the most significant mechanisms can be formulated similarly to the β-unzipping method described in Thoft-Christensen & Murotsu[b] 1986.

First, the fundamental mechanisms are divided into two groups namely real mechanisms (mechanisms with non-zero external work) and fictitious mechanisms (mechanisms with zero external work). The real mechanisms with safety index β indices in the interval $[\beta^f_{min}, \beta^f_{min} + \Delta_1]$, where β^f_{min} is the smallest safety index of all fundamental mechanisms and where $\Delta_1 \geq 0$ is a given constant, are used to define the starting points for a failure tree. Each of these selected starting mechanisms is in turn combined with the remaining fundamental mechanisms in such a way that the new mechanisms fulfil the following condition

- they are real mechanisms with positive external work
- only fundamental mechanisms with at least one common failure element are combined with the selected mechanisms

The lowest β index among the combined mechanisms is called β_{min}. The combined mechanisms with β indices in the interval $[\beta_{min}, \beta_{min} + \Delta_2]$, where $\Delta_2 \geq 0$ is a given constant then define the branches in the failure tree originating from the fundamental mechanisms. These combined mechanisms now form the basis of new branches. Each branch symbolises that the mechanism belonging to the node at the end of the branch is obtained by combination of a combined mechanism and a fundamental mechanism using the same conditions as mentioned above.

This procedure is terminated when at least one of the following criteria is fulfilled

- the number of combined fundamental mechanism which form a combined mechanisms exceeds a critical number N_{max}
- the lowest β index calculated in a ramification is greater than ξ multiplied by the β index for the mechanism which forms the basis, where ξ is some given real number, e.g. $\xi = 2$
- all new combinations of combined mechanisms and fundamental mechanisms have been identified before

During the formation of a failure tree some of the identified mechanisms are insignificant (mechanisms with high β indices and mechanisms which are fully correlated with a mechanism with a lower β index). Evaluation of the reliability of the structure is made by modelling the significant mechanisms as elements in a series system, and by including only not fully correlated mechanisms with β indices in the interval $[\beta^s_{min}, \beta^s_{min} + \Delta_3]$, where β^s_{min} is the lowest β index for any mechanism in the failure tree and $\Delta_3 \geq 0$ is a given constant.

It is seen from this brief description of the above method, that the procedure can be performed in the following three steps

1. Generation of a set of fundamental mechanisms.
2. Identification of significant mechanisms.

3. Estimate of the reliability of the structure on the basis of the significant mechanisms.

In example 3.4.1, it is illustrated how the method works for a plane 2- storey frame structure, when each yield hinge in the structure is assumed to have only one possible strain rate, namely rotational.

It is important to note that this procedure leads to identification of ODOF mechanisms. However, when each yield hinge in the structure has more than one possible strain rate, the MDOF mechanisms can become significant, see example 3.3.1 in section 3.3. In section 3.3 it is discussed how the most significant mechanisms for MDOF mechanisms can be estimated using optimisation. The results of the optimisation problem will often depend strongly on which optimisation algorithm is chosen and on the starting point in the optimisation problem. An obvious choice of starting points is the most significant ODOF mechanisms obtained by the above method.

Example 3.4.1

The 2-storey frame structure in figure 3.4.4 is considered in this example. The loading and locations of potential yield hinges are also shown in figure 3.4.4. This example have been analysed before by Bjerager[4] 1984, but by another method. The structure is 6 times statically indeterminate, i.e. $r = 6$. The number of internal degrees of freedom of the structure is equal to possible locations of potential yield hinges so that each yield hinge is assumed only to have one possible strain rate, namely rotational (ODOF yield hinge), i.e. $n = 12$. The number of fundamental mechanisms then is

$$m = n - r = 6$$

The yield moment capacity $M_{F_i}, i = 1, \ldots, 12$ and the external loading $P_i, i = 1, \ldots, 4$ are assumed to be Gaussian random variables. The expected values and the coefficient of variation for the stochastic variables are shown in table 3.4.1.

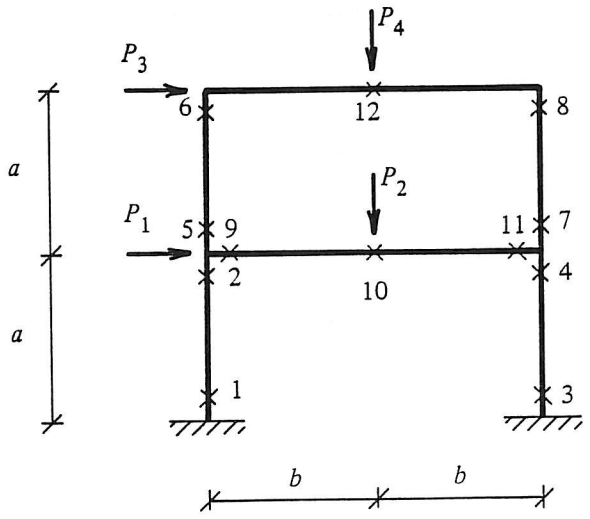

Figure 3.4.4. Geometry, loading and possible location of potential yield hinges (×).

Variable	Expected value	Coefficient of variation
P_1	$2.0\mu_P$	0.30
P_2	$2.5\mu_P$	0.15
P_3	$1.0\mu_P$	0.30
P_4	$1.5\mu_P$	0.20
$M_{F_i}, i = 1, \ldots, 12$	$a\mu_P$	0.10

Table 3.4.1. Expected values and coefficient of variation for the stochastic variables (μ_P is an arbitrary constant and a is defined in figure 3.4.4)

Further, the yield moment capacities are equicorrelated with correlation coefficient 0.5, but are uncorrelated with the loads, and the loads are mutually uncorrelated except for $\rho_{P_1 P_3} = 1$. Finally it is assumed that $a = b$ in figure 3.4.4.

In figure 3.4.5 a set of fundamental mechanisms with the respective safety indices β is shown. On the basis of $\Delta_1 = 10$ the fundamental mechanisms 1,2,3 and 4 (see figure 3.4.5) are selected as starting points in the failure tree. In the case of $N_{max} = 6$ and $\Delta_2 = 1$ the failure tree becomes as shown in figure 3.4.6. With $\Delta_3 = 1$, 6 not fully correlated ODOF significant mechanisms are identified. The significant mechanisms with the respective β-indices are shown in figure 3.4.7.

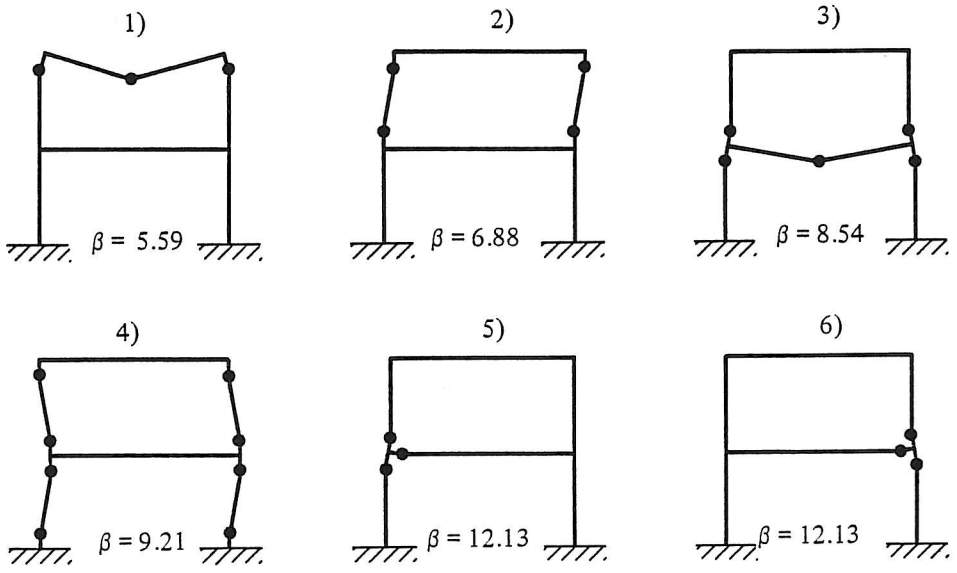

Figure 3.4.5. A set of fundamental mechanisms of the frame in figure 3.4.4.

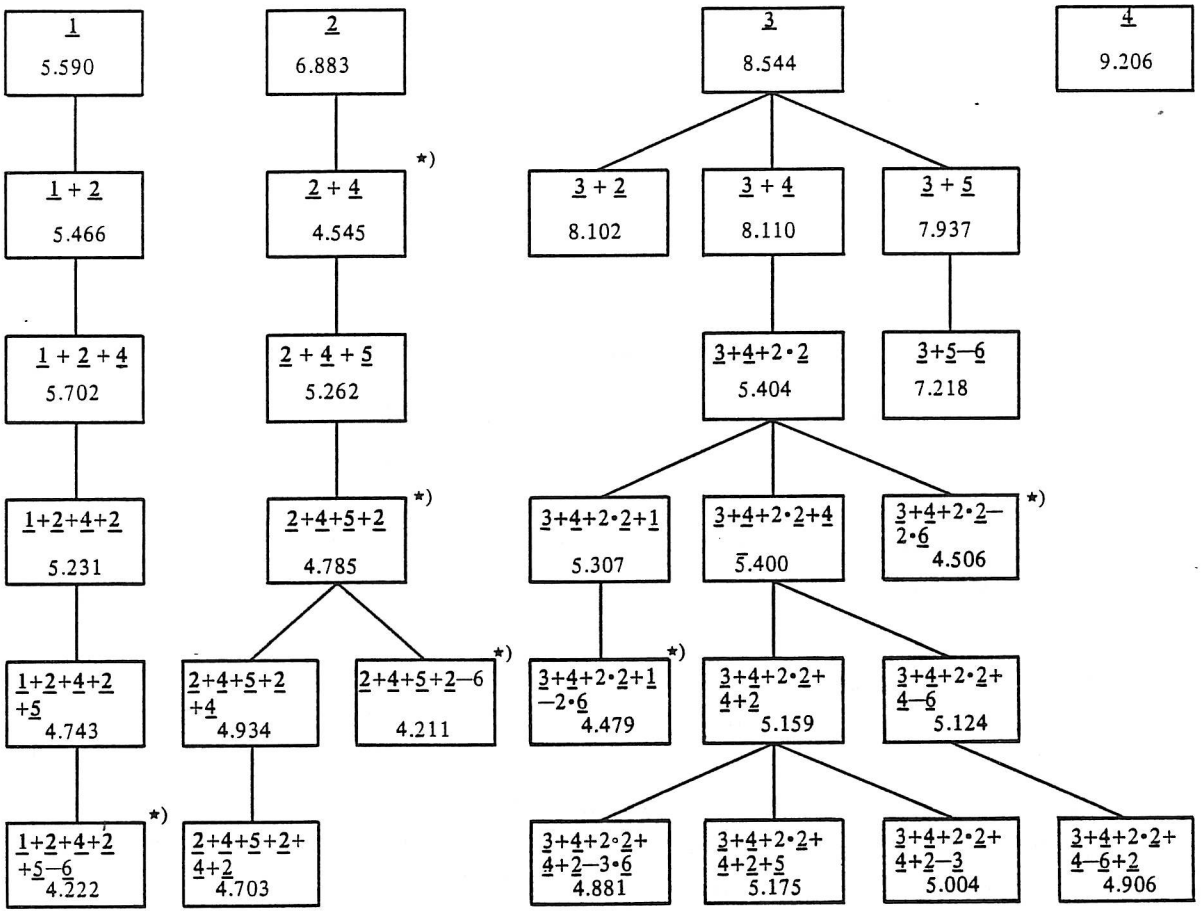

Figure 3.4.6. Failure tree for the frame in figure 3.4.4, in case of $\Delta_1 = 10$ and $\Delta_2 = 1$. 3+4+2•2 5.404 denotes a new mechanism obtained by combining one time fundamental mechanisms no.3 and no. 4 and two times fundamental mechanism no. 2 and the safety index β for the new mechanism becomes equal to 5.404. $*)$ denotes significant mechanism.

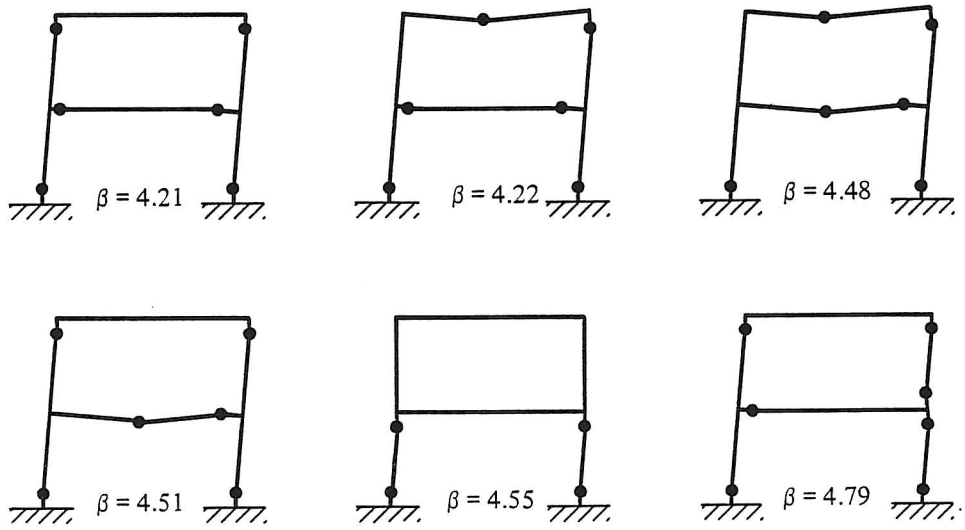

Figure 3.4.7. Significant mechanisms for the frame in figure 3.4.4, in case of $\Delta_3 = 3$.

The correlation coefficient matrix of the safety margin of the significant failure modes

(mechanisms) is

$$\bar{\bar{\rho}} = \begin{bmatrix} 1.00 & 0.97 & 0.92 & 0.94 & 0.97 & 0.99 \\ & 1.00 & 0.95 & 0.93 & 0.95 & 0.96 \\ & & 1.00 & 0.98 & 0.90 & 0.91 \\ & & & 1.00 & 0.92 & 0.93 \\ & & & & 1.00 & 0.98 \\ \text{sym.} & & & & & 1.00 \end{bmatrix}$$

Estimates of the upper bounds of the system reliability index β_s are (Ditlevsen bounds, Ditlevsen[p] 1979)

$$4.11 \leq \beta_s \leq 4.14$$

In Bjerager[t] 1984 the exact value of the reliability index is found to be between 4.06 and 4.14.

3.5. Application

In the sections above a method for estimating the probability of failure with respect to plastic collapse of truss and frame structures of ideal rigid plastic materials is briefly described. To make this method applicable a new program package "COLLAPSE" has been made. The program package which contains approx. 3200 source lines written in FORTRAN77, consists of four calculation blocks, namely

1) AUTOMEK
   This program reads the structural data and generates a set of fundamental mechanisms by creating and solving eq.(3.4.16)

2) SIGNMEK
   This program uses the method described in section 3.4 to identify the most significant mechanisms. The parameters N_{max}, Δ_1, Δ_2, Δ_3 and ξ are defined by the user.

3) OPTMEK
   This program is only used for MDOF yield hinges. Identification of a new significant mechanisms is formulated as an optimisation problem as shown in eq.(3.3.10), with the most significant mechanisms obtained in program SIGNMEK as a starting points in the optimisation problem. In example 3.3.1 some results from OPTMEK are illustrated. The user can choose between two different optimisation algorithms namely the NLPQL-algorithm, Schittkowski[p] 1986, and the Nelder&Mead-algorithm, Kuester & Mize[b] 1973.

4) SERIESYS
   This program estimate the system reliability index β_s on the basis of the significant mechanisms obtained in the programs SIGNMEK and OPTMEK.
   The following methods are available in the program
   - Ditlevsen bounds, Ditlevsen[p] 1979
   - Hohenbichler approximation, Hohenbichler[p] 1983
   - PNET approximation, Sørensen[t] 1984
   - approximation based on the average correlation coefficient, Sørensen[t] 1984
   - approximation based on the equivalent correlation coefficient, Sørensen[t] 1984
   - bound based on min. and max. correlation coefficient, Sørensen[t] 1984

Example 3.5.1

Consider the plane frame shown in figure 3.5.1. It is part of an offshore platform. It has 15 structural elements which are all tubular beam elements made of steel. Each yield hinge is assumed to have two types of deformation, namely axial elongation

and rotation. The loading and yield stresses in potential yield hinges in a structural element are assumed to be fully correlated, and the coefficient of correlation between yield stresses in failure elements with the same cross-section is chosen to be 0.7. Otherwise the yield stresses are uncorrelated. The concentrated loads P_1 and P_2 are uncorrelated. The expected values and the coefficient of variation for the loads $P_i, i = 1,2$ and the yield stresses $Y_i, i = 1,\ldots,30$ are shown in table 3.5.1. The geometrical cross-sectional data for the failure elements are shown in table 3.5.2.

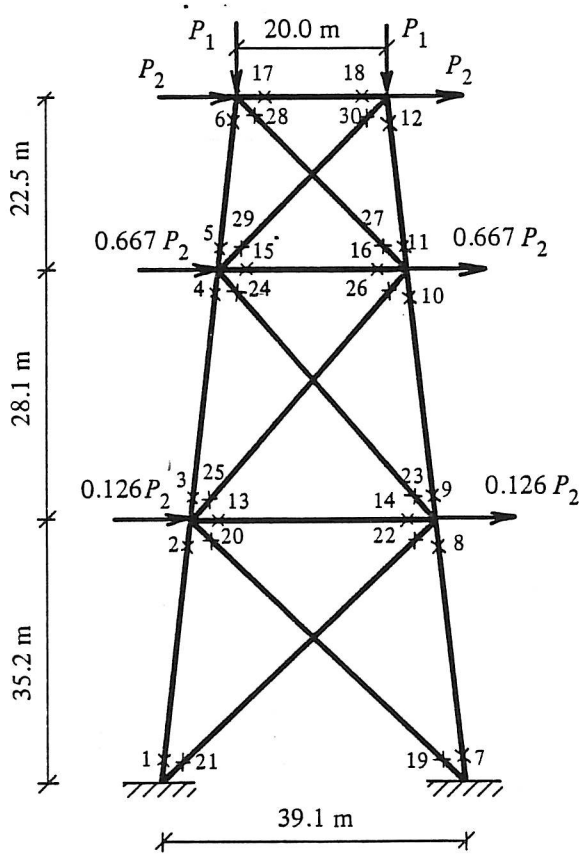

Figure 3.5.1. Geometry, loading and possible location of potential yield hinges (×).

Variables	Expected value	Coefficient of variation
$Y_i, i = 1,\ldots,30$	3.2 10^5 kN/m^2	0.15
P_1	4.5 10^4 kN	0.05
P_2	1.0 10^3 kN	0.30

Table 3.5.1. Expected values and coefficients of variation for the stochastic variables.

With $N_{max} = 7$, $\Delta_1 = 10, \Delta_2 = 0.3$ and $\Delta_3 = 1$, three not fully correlated significant mechanisms are identified. The significant mechanisms and respective reliability indices are shown in figure 3.5.2. The system reliability index, estimated by Ditlevsen

bounds, are

$$3.75 \leq \beta^s \leq 3.75$$

Failure element i	D (m)	t (m)	A (m^2)	W_p (m^3)
$i = 1, \ldots, 12$	2.5	0.042	0.3243	0.2538
$i = 13, 14$	2.0	0.034	0.2100	0.1314
$i = 15, 16, 19, \ldots, 22$	1.5	0.025	0.1158	0.0544
$i = 17, 18$	1.0	0.017	0.0525	0.0164
$i = 23, \ldots, 26$	1.2	0.020	0.0741	0.0279
$i = 27, \ldots, 30$	0.9	0.015	0.0417	0.0133

cross-section: 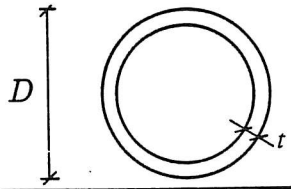

A : cross-sectional area
$A \approx \pi t(D-t)$
W_p : plastic modulus
$W_p \approx t(D-t)^2$

Table 3.5.2. Cross-sectional data.

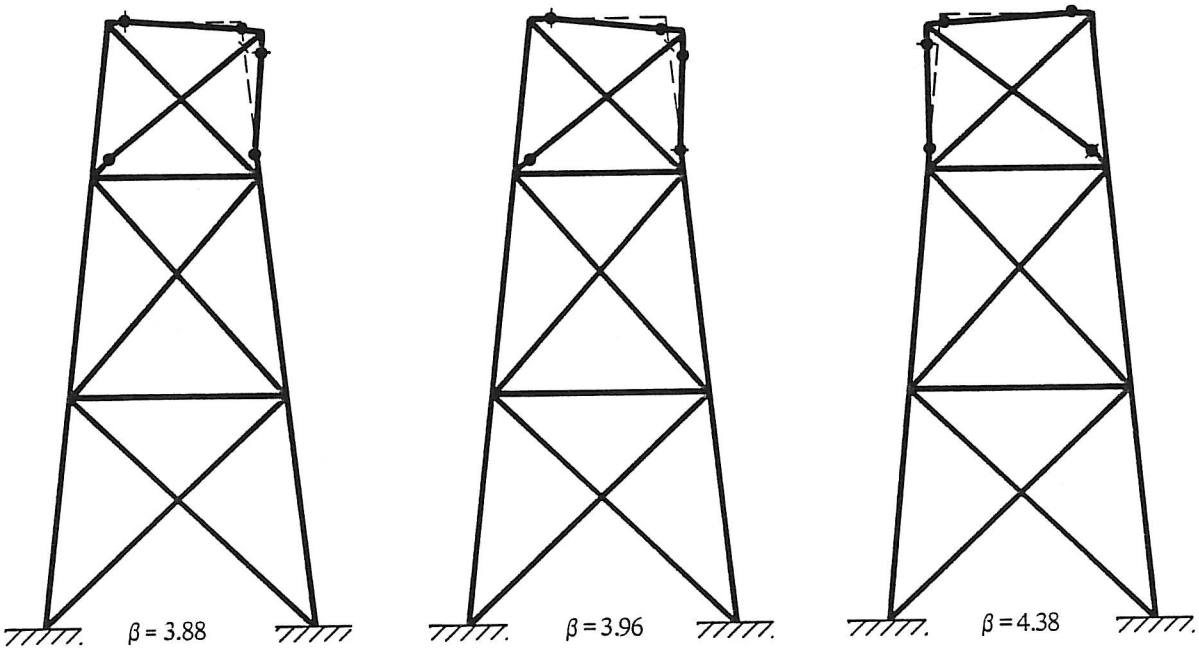

Figure 3.5.2. Significant mechanisms.

Example 3.5.2

Consider the model of a steel jacket offshore platform in figure 3.5.3. The structure is

a 12 times statically indeterminate spatial truss tower, having 48 structural elements. Each structural element is supposed to have one failure element with one possible strain rate, namely axial elongation. Therefore, the number of fundamental mechanisms is $m = 48 - 12 = 36$. The expected values of the axial strength capacities in tension $E[N_{F_i}^+]$ for the failure elements are shown in figure 3.5.3.

This example has been analysed before by Sigurdsson, Sørensen & Thoft-Christensen[p] 1985 and by Bjerager[t] 1984, but by different methods.

The expected values of yield capacities in compression, $E[N_{F_i}^-]$, are

$$E[N_{F_i}^-] = 0.5\, E[N_{F_i}^+] \qquad i = 1, 2, \ldots, 48$$

All yield capacities N_{F_i} are assumed to be equicorrelated with correlation coefficient 0.5, and coefficients of variation equal to 0.15.

The structure is subjected to 4 vertical dead loads each of the magnitude P_1, see figure 3.5.4, and 12 horizontal wave loads all of the magnitude proportional to the quantity P_2 and all having the same direction given by the angle θ, see figure 3.5.4.

Further, it is assumed that there is no correlation between resistance and load variables, and that the constants in the wave load model are

$$(\theta, \gamma_1, \gamma_2, \gamma_3) = (30°, 1.000, 0.667, 0.126)$$

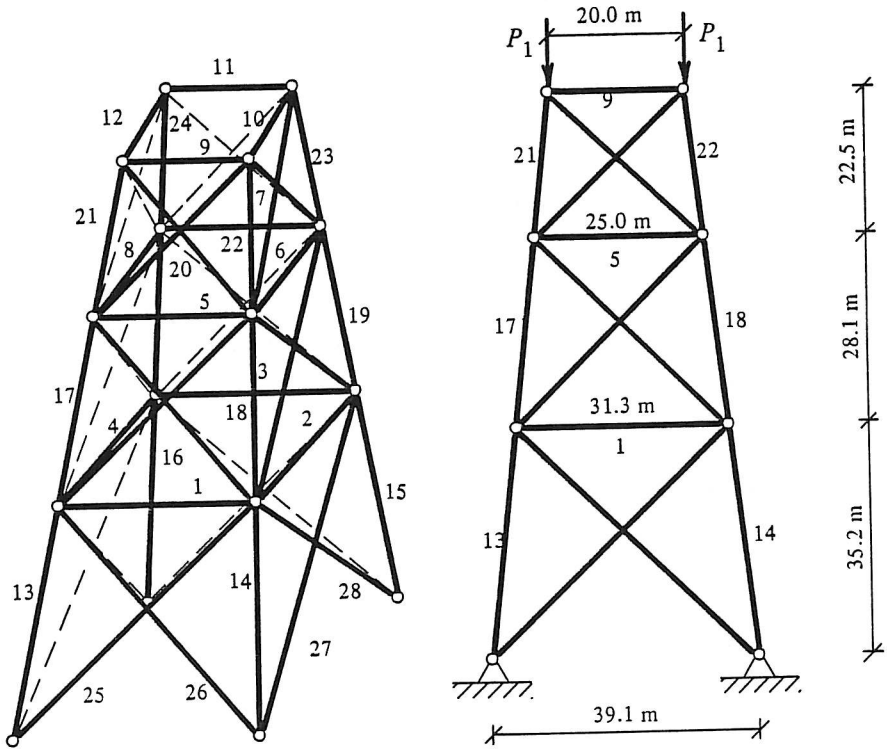

$E[N_{F_i}^+]$ (kN)

67200	$i = 1, \ldots, 4$
37070	$i = 5, \ldots, 8$
16800	$i = 9, \ldots, 12$
103780	$i = 13, \ldots, 24$
370370	$i = 25, \ldots, 32$
23070	$i = 33, \ldots, 40$
13350	$i = 41, \ldots, 48$

Figure 3.5.3. Spatial truss tower.

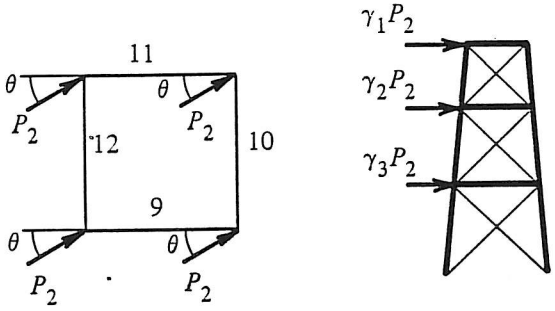

$E[P_1] = 40000$ kN $V[P_1] = 0.05$
$E[P_2] = 278$ kN $V[P_2] = 0.30$
$\rho_{P_1P_2} = 0$

Figure 3.5.4. Illustration of the wave loading ($V[\cdot]$ denotes coefficient of variation).

With $N_{max} = 6$, $\Delta_1 = 1.0$, $\Delta_2 = 1.0$ and $\Delta_3 = 2.0$, 12 not fully correlated significant mechanisms are identified. The mutual axial and rotational deformation rates for the failure elements, $\dot{u}_i$, the displacement rates for the external loads, v_i, and the reliability indices, β_i for the significant mechanisms are shown in table 3.5.3.

Mech. no.	1	2	3	4	5	6	7	8	9	10	11	12
$\dot{u}_9$						-1.42						
$\dot{u}_{11}$					-1.42							
$\dot{u}_{12}$							-1.42					
$\dot{u}_{21}$				1.4		1.73	1.73		-0.16	0.17	0.17	
$\dot{u}_{22}$		0.17									-0.02	-0.17
$\dot{u}_{23}$	1.56				1.73			1.56				1.57
$\dot{u}_{24}$			1.56					-0.16	1.56	-0.02		
$\dot{u}_{41}$							1.23				0.11	-0.12
$\dot{u}_{42}$		0.12		1		0.12			-0.11	0.12		
$\dot{u}_{43}$	1.11							1.11				-0.11
$\dot{u}_{44}$		0.12			1.23						-0.01	1.11
$\dot{u}_{45}$	1.11		1.11					1	1.11	-0.01		
$\dot{u}_{46}$					0.12							1.12
$\dot{u}_{47}$			1.11	1			0.12		1		0.12	
$\dot{u}_{48}$						1.23		-0.11		0.11		
disp. rate:												
v_1	1.58	0.18	1.58	1.42	1.59	1.59	1.59	1.42	1.42	0.16	0.16	1.42
v_2	2.46	0.27	1.42		2.80	-2.80	-3.44	2.46	1.42	-0.16	-0.27	1.58
β_i	2.33	2.33	2.35	2.38	3.49	3.59	3.60	3.65	3.67	3.72	3.74	3.87

Table 3.5.3. The 12 most significant mechanisms.

The system reliability index, estimated by Ditlevsen bounds are

$$1.85 \leq \beta_s \leq 1.92$$

The results obtained in this example are very well in accordance with results from Sigurdsson, Sørensen & Thoft-Christensen[p] 1985 and from Bjerager[t] 1984, where β_s was estimated to 1.86 and 1.90, respectively.

3.6. Conclusions

In this chapter a reliability analysis of truss and frame structures of ideal rigid plastic materials is discussed. Failure modes corresponding to plastic collapse are used. The reliability analysis is carried out using the upper-bound theorem of plasticity (kinematic theorem of mechanisms).

A technique for identifying the most significant failure modes is presented. It is shown that the most significant failure modes depend significantly on the cross-section.

A new program package "COLLAPSE" is presented. The program is illustrated by two examples, i.e. two different models of steel jacket offshore platforms. The second example, example 3.5.2, has been analysed before by Sigurdsson, Sørensen & Thoft-Christensen[p] 1985 and Bjerager[t] 1984, but by different methods. The results obtained here are very well in according to their results.

4. PROBABILISTIC FATIGUE ANALYSIS OF OFFSHORE STRUCTURES

4.1. Introduction

Offshore structures of all types are generally subjected to cyclic loading from wind, current, earthquakes and waves acting simultaneously, which cause time-varying stress effects in the structure. The environmental quantities are of a random nature and are more or less correlated to each other through the generating and driving mechanism. Waves and earthquakes are generally considered to be the most important sources of the structural excitations. However, earthquake loads are only taken into account in the analysis of offshore structures close to or in tectonic offshore fields. For fixed offshore structures in deep water environments wind loads represent a contribution of about 5 % to the environmental loading, Watt[p] 1978. Current loads are usually considered to be unimportant in the dynamic analysis of offshore structures, because their frequencies are not sufficient to excite the structures. A reliability calculation of offshore structures due to a fatigue failure is a difficult task due to the random nature of the loading, and also due to insufficient information of structural failure under these conditions. A stochastic assessment of the reliability analysis of structures is therefore inevitable. Dynamic loads, such as wave loads, produce stress fluctuations in the structural members and joints and are the primary cause of fatigue damages. A fatigue analysis of offshore structures can be described in general terms as a calculation procedure, starting from the waves and perhaps ending with fatigue damage occurring in the material. The links between the waves and the damage are formed by mathematical models for the wave forces, the structural behaviour and the material behaviour. In view of the stochastic and dynamic character of the waves it is an obvious choice to apply spectral fatigue analysis methods to the fatigue problem, when the structural system and loading are modelled linear. In this chapter, a stochastic reliability assessment for jacket type offshore structures subjected to wave loads in deep water environments is outlined. To estimate statistical measures of structural stress variations the modal spectral analysis method is applied.

The probabilistic fatigue analysis is divided into four steps:

I Probabilistic modelling of the sea states
   a) short-term modelling of the sea states
   b) long-term modelling of the sea states

II Probabilistic modelling of the wave loading

III Structural response analysis (global and local)

IV Stochastic modelling of fatigue failure

Step I is considered in section 4.2, where the sea surface, for a short-term period, is assumed to be a realisation of a zero-mean ergodic Gaussian process, and it is shown how the long-term probability distribution of the sea states can be modelled. The short-term modelling of the sea state is mainly based on Sigbjørnsson[p] 1979, Sigbjørnsson & Smith[p] 1980, Sarpkaya & Isaacson[b] 1981, Haver[p] 1985[1], Sigbjørnsson, Bell & Holand[p] 1978, Olufsen, Farnes & Fergestad[p] 1986 and Haver & Moan[p] 1983. The long-term modelling of the sea states is mainly based on Haver[p] 1985[2], Haver & Nyhus[p] 1986 and Haver[p] 1985[3]. In section 4.3 it is shown how the wave loading on structural members can be modelled by using Morison's equation, and how the cross-spectral densities of the load process can be obtained. This section is mainly based on Sarpkaya & Isaacson[b] 1981, Sigbjørnsson[p] 1979, Atalik & Utku[p] 1976 and Langen & Sigbjørnsson[b] 1979. In section 4.4 it is shown how the cross-spectral densities of the stresses in the structure can be obtained. And in section 4.5 it is shown how the probability of fatigue failure can be estimated by three different damage accumulations models, namely by Miner's rule combined with the so-called S-N approach, by using crack growth model (fracture mechanics) and by using a model introduced by Bogdanoff et al.[p] 1978[1,2,3], 1980.
In section 4.6 a new computer package "SAOFF" is presented. The program, which is based on the methods and assumptions described in sections 4.2-4.5, is illustrated by a single example.

4.2. Probabilistic Model of the Sea States

Short-Term Sea Model

The observed sea elevation, $\eta(\overline{r},t)$, at the fixed location $\overline{r}$ at a time t, can be considered as a realisation of a non-stationary stochastic process, whose characteristic parameters vary slowly with time. Further, it is assumed that for short-term periods (a few hours) the sea surface $\eta(\overline{r},t)$ can be considered as a realisation of a stationary stochastic process. This process is assumed to be a zero-mean ergodic Gaussian process. A consequence of these simplifying assumptions is that within the short-term time scale the sea surface elevation is completely defined by the cross correlation function $R_{\eta_n\eta_m}(\Delta\overline{r},\tau)$.

$$R_{\eta_n\eta_m}(\Delta\overline{r},\tau) = E[\eta(\overline{r},t)\ \eta(\overline{r}+\Delta\overline{r},t+\tau)] \tag{4.2.1}$$

$$= \int_{-\infty}^{+\infty}\int_{\overline{k}} exp(\epsilon(\omega\tau - \overline{k}^T\Delta\overline{r}))\ S^{(3)}_{\eta\eta}(\overline{k},\omega)d\overline{\kappa}d\omega \tag{4.2.2}$$

where $\epsilon=\sqrt{-1}$, $\Delta\overline{r}=(x_n-x_m,y_n-y_m)$, $\tau=t_n-t_m$, and n and m refer to points with spatial coordinates (x_n,y_n) and (x_m,y_m), respectively in the time space, $\overline{k}$ is the two-dimensional wave number vector and ω is the frequency. $S^{(3)}_{\eta_n\eta_m}(\overline{k},\omega)$ is the three-dimensional wave spectral density.

The wave number vector $\overline{k}$ can be expressed by polar coordinates

$$\overline{k} = \kappa cos(\theta)\ \overline{i} + \kappa sin(\theta)\ \overline{j} \tag{4.2.3}$$

where $\overline{i}$ and $\overline{j}$ represent the base vectors and κ is the wave number.

The correlation function can now be expressed by polar coordinates

$$R_{\eta_n\eta_m}(\Delta\overline{r},\tau) = \int_{-\infty}^{+\infty}\int_{\overline{\theta}-\pi/2}^{\overline{\theta}+\pi/2}\int_{\kappa} S^{(3)}_{\eta\eta}(\kappa,\theta,\omega)\ exp(\epsilon\omega\tau)\ exp(-\epsilon\kappa (\Delta x cos\theta + \Delta y sin\theta))d\kappa d\theta d\omega \tag{4.2.4}$$

where $\Delta x = x_n - x_m$, $\Delta y = y_n - y_m$ and $\overline{\theta}$ is the average direction of wave propagation.

In structural analysis it is more convenient to use spectral densities than correlation functions. The corresponding spectral density is defined by the Wiener-Khinchine relation as

$$S_{\eta_n\eta_m}(\omega) = \frac{1}{2\pi}\int_{-\infty}^{+\infty} R_{\eta_n\eta_m}(\Delta\overline{r},\tau)\ exp(-\epsilon\omega\tau)d\tau \tag{4.2.5}$$

Substitution of eq.(4.2.4) into eq.(4.2.5) yields

$$S_{\eta_n\eta_m}(\omega) = \int_{\bar{\theta}-\pi/2}^{\bar{\theta}+\pi/2} \int_{\kappa} S^{(3)}_{\eta\eta}(\kappa,\theta,\omega)\ exp(-\epsilon\kappa(\Delta x cos\theta + \Delta y sin\theta))d\kappa d\theta \quad (4.2.6)$$

The existence of one-to-one mapping of the modulus of the wave number κ into the frequency ω is assumed. An expression suitable for this purpose is the dispersion relation known from the Airy wave theory

$$\omega^2 = \kappa\ g\ tanh(\kappa d) \qquad \omega \geq 0 \quad ,\kappa \geq 0 \quad (4.2.7)$$

where g is the acceleration of gravity and d is the water depth. Equation (4.2.7) is based on the small-amplitude wave theory. However, experience indicates that it may be used with confidence in engineering for waves with moderate amplitudes, Sigbjørnsson & Smith[p] 1980. The spectral density can now be expressed in terms of the directional frequency spectral density

$$S_{\eta_n\eta_m}(\omega) = \int_{\bar{\theta}-\pi/2}^{\bar{\theta}+\pi/2} S^{(2)}_{\eta\eta}(\theta,\omega)\ exp(-\epsilon\kappa(\omega)(\Delta x cos\theta + \Delta y sin\theta))d\theta \quad (4.2.8)$$

In practical application it is commonly assumed that the two-dimensional wave spectral density $S^{(2)}_{\eta\eta}(\theta,\omega)$ can be written, see Sigbjørnsson[p] 1979

$$S^{(2)}_{\eta\eta}(\theta,\omega) = S_{\eta\eta}(\omega)\ \psi(\theta) \quad (4.2.9)$$

where $S_{\eta\eta}(\omega)$ is the one-dimensional wave spectral density and $\psi(\theta)$ is the so-called spreading function, which is assumed frequency independent. By using equations (4.2.8) and (4.2.9) the following expression for the cross-spectral density of the sea surface is obtained

$$S_{\eta_n\eta_m}(\omega) = S_{\eta\eta}(\omega) \int_{\bar{\theta}-\pi/2}^{\bar{\theta}+\pi/2} \psi(\theta)\ exp(-\epsilon\kappa(\omega)(\Delta x cos\theta + \Delta y sin\theta))d\theta \quad (4.2.10)$$

It is seen that the spectral density, eq.(4.2.10), is reduced to the one-dimensional spectral density of wave elevation when the points n and m coincide. When the one-dimensional spectral density and the spreading function are known the short-term properties of the wave field are completely specified in terms of eq.(4.2.10). In most practical applications a standard formula involving a few sea state characteristics is usually used for $S_{\eta\eta}(\omega)$. Over the last 30 years many spectral expressions have been suggested, Sarpkaya & Isaacson[b] 1981. A common feature of most spectral models is that they are of a unimodal form and mainly meant to characterise a pure wind driven sea, but real seas are very often of a combined nature, e.g. comprising wind sea and swell components. These two parts will normally correspond

to different directions of propagation, making the concept of a mean direction of a questionable value. An accurate description of a general sea state in terms of characteristic parameters will require a large number of parameters. However, for these purposes a sea state with a given average direction of propagation $\overline{\theta}$ can reasonably well be described by two parameters, namely by the significant wave height H_s, and the spectral peak period T_p. In other words, it is assumed that the variability in the spectral parameter set does not affect the predicted response significantly. The spectral variability over the $H_s - T_p$ space is indicated qualitatively in figure 4.2.1, Haver^p 1985[1]. Within area 2 the sea states can on average be reasonably well modelled by single peaked model spectra. Beyond this area sea states will typically be of a combined nature. It is expected that the bulk of extreme sea states is located within area 2, but for lower and moderate sea states which are of importance in the present fatigue studies, the percentage of sea states beyond area 2 is increasing. However, the sea states are assumed to be more or less pure wind sea.

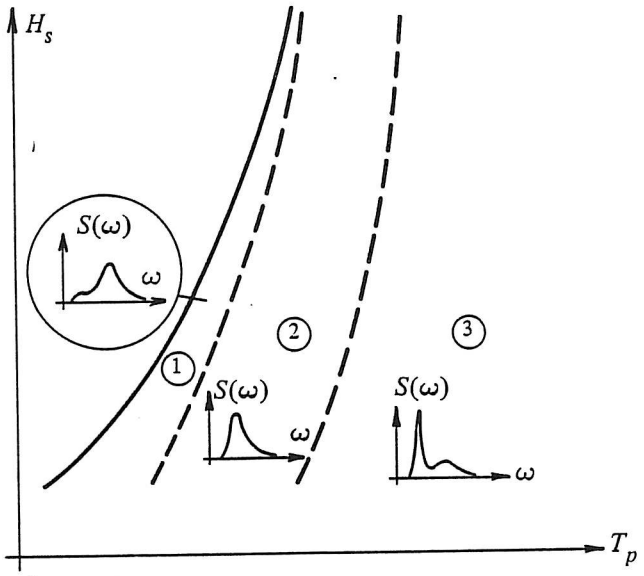

1) Sea states combined by wind sea but significantly influenced by some swell components.

2) More or less pure wind seas (or, possibly some swell components located well inside the wind sea frequency band).

3) Sea states more or less dominated by swell but significantly influenced by wind sea.

Figure 4.2.1 Qualitative indication of spectral variability, Haver^p 1985[1].

Here, the JONSWAP spectrum is adopted as a model for wind sea. This spectrum

can be written, Sigbjørnsson, Bell & Holand[p] 1978

$$S_{\eta\eta}(\omega) = \alpha g^2 \omega^{-5} exp\left(-\frac{5}{4}\left(\frac{\omega}{\omega_p}\right)^{-4}\right)\gamma^{exp\left(-\frac{1}{2}\left(\left(\frac{\omega}{\omega_p}-1\right)/\sigma\right)^2\right)} \tag{4.2.11}$$

where

ω is the frequency (rad/sec)

α is the equilibrium range parameter

g is the acceleration of gravity

ω_p is the spectral peak frequency ($= 2\pi/T_p$)

γ is the spectral peak parameter

σ is the spectral peak width parameter

Regarding σ the mean values from the JONSWAP experiment are usually adopted, i.e. $\sigma = 0.07$ for $\omega \leq \omega_p$ and $\sigma = 0.09$ for $\omega > \omega_p$, Haver[p] 1985[1]. Here σ is chosen to be 0.08 for all frequencies and all sea states. For a sea state with a given value of the significant wave height H_s the remaining parameters (α, γ and ω_p) are related to each other through the following equation, Haver[p] 1985[1]

$$\gamma = exp\left(3.484\left(1 - 0.1975\,\alpha\, T_p^4/H_s^2\right)\right) \tag{4.2.12}$$

It should be noted that eq.(4.2.12) can be used as "physically correct" only within the so-called JONSWAP range, i.e. the subspace of area 2 in figure 4.2.1, where a JONSWAP formula is expected to be a reasonable spectral model. In Haver[p] 1985[1] the JONSWAP range is given by

$$3.6\sqrt{H_s} \leq T_p \leq 5\sqrt{H_s} \tag{4.2.13}$$

The lower bound corresponds to $\alpha = 0.016$ and $\gamma = 5.0$, and the upper bound (corresponding to fully developed sea) to $\alpha = 0.0081$ and $\gamma = 1.0$, where the JONSWAP wave spectrum equals the Pierson-Moskowitz wave spectrum (PM-spectrum). Within the JONSWAP range α is assumed to vary linearly with T_p at a fixed H_s, i.e.

$$\alpha = 0.036 - 0.0056\, T_p/\sqrt{H_s} \tag{4.2.14}$$

Experience seems to indicate that the suggested lower bound for the JONSWAP range, eq.(4.2.13), is located on the edge of area 1 in figure 4.2.1. A fairly good fit is obtained with a single peaked spectrum up to $T_p/\sqrt{H_s} \approx 6.0 - 6.5$. For sea states located above the JONSWAP range it is assumed that the JONSWAP spectrum with $\gamma = 1$ can be used, and for a sea state located below the JONSWAP range it is assumed that the JONSWAP spectrum with $\gamma = 5$ can be used.

In some case it is more convenient to use the expected zero-upcrossing wave period T_z instead of T_p.

$$T_z = 2\pi\sqrt{m_0/m_2} \tag{4.2.15}$$

where

$$m_i = \int_0^\infty \omega^i S_{\eta\eta}(\omega) d\omega$$

and the relation between T_p and T_z can be estimated by, Olufsen, Farnes & Fergestad[p] 1986

$$T_p = \frac{T_z}{0.43365 + 0.27594\ \gamma^{0.1842}} \tag{4.2.16}$$

The accuracy in eq.(4.2.16) is rather good. If T_p is in the range of 1-20 sec. and if γ is between 1-8 the error will be less than 1 % .

Several analytical expressions have been suggested for the spreading function $\psi(\theta)$. Normally, a cosine function is used

$$\psi(\theta) = \begin{cases} K\ cos^{2n}(\theta - \overline{\theta}) & -\frac{\pi}{2} \leq (\theta - \overline{\theta}) \leq \frac{\pi}{2} \\ 0 & \text{elsewhere} \end{cases} \tag{4.2.17}$$

where K is a normalisation factor defined so that the integral of the spreading function between $-\frac{\pi}{2}$ and $\frac{\pi}{2}$ is equal to one

$$K = \frac{1}{\sqrt{\pi}} \frac{\Gamma(n+1)}{\Gamma(n+\frac{1}{2})} \tag{4.2.18}$$

where Γ is the Gamma function and n is a parameter describing the width of the distribution. For the limiting case $n \to \infty$ eq.(4.2.17) approaches the Dirac delta function corresponding to long crested waves.

Long-Term Sea Model

As mentioned earlier it is assumed that the sea surface elevation at a fixed location for short-term periods can be accurately modelled by a zero-mean ergodic Gaussian process. This process is completely characterised by the frequency spectrum $S_{\eta\eta}(\omega)$ which, for a given average direction of wave propagation $\overline{\theta}$, can be described by two parameters, namely by the significant wave height H_s and the spectral peak periods T_p. The long-term probability distribution of the sea state , $p_{H_s T_p \overline{\theta}}(h_s, t_p, \theta)$, is then given as a joint distribution of $\overline{\theta}, H_s$ and T_p. It is not possible to derive this distribution theoretically. The distribution has to be estimated from wave observations in the ocean area concerned or derived applying hidcasting models, i.e. the chosen analytical model has to fit in the best possible way to the data.

In most wave observations no information of the mean direction of propagation $\overline{\theta}$ has been included. If it is assumed that the joint distribution of H_s and T_p is independent of $\overline{\theta}$, the joint distribution $p_{H_sT_p\overline{\theta}}(h_s, t_p, \theta)$ can be written as

$$p_{H_sT_p\overline{\theta}}(h_s, t_p, \theta) = p_{H_sT_p}(h_s, t_p)\, p_{\overline{\theta}}(\theta) \tag{4.2.19}$$

For the present purpose the probability density function $p_{H_sT_p}(h_s, t_p)$ is conveniently written as

$$p_{H_sT_p}(h_s, t_p) = p_{T_p|H_s}(t_p|h_s)\, p_{H_s}(h_s) \tag{4.2.20}$$

where $p_{H_s}(h_s)$ is the marginal probability density function for H_s and $p_{T_p|H_s}(t_p|h_s)$ is the conditional probability density function for T_p given H_s. $p_{T_p|H_s}(t_p|h_s)$ and $p_{H_s}(h_s)$ are fitted to the observations separately. The numerical values for $p_{H_sT_p}(h_s, t_p)$ are obtained by means of eq.(4.2.20). In this thesis $p_{H_s}(h_s)$ is modelled by a log-normal distribution for $h_s \leq v$ and by a Weibull distribution for $h_s > v$, i.e.

$$p_{H_s}(h_s) = \begin{cases} \frac{1}{\sqrt{2\pi}\sigma_{H_s} h_s}\, exp\left(\frac{-(ln\, h_s - \mu_{H_s})^2}{2\sigma^2_{H_s}}\right) & h_s \leq v \\ \frac{\xi}{\rho}\left(\frac{h_s}{\rho}\right)^{\xi-1} exp\left(-\frac{h_s}{\rho}\right)^{\xi} & \rho > 0\,, \xi > 0\,, h_s > v \end{cases} \tag{4.2.21}$$

where μ_{H_s} and $\sigma^2_{H_s}$ are the mean and variance of the variable $ln\,(H_s)$, respectively, and where continuity is required for $p_{H_s}(h_s)$ and $P_{H_s}(h_s)$ at $h_s = v$. The conditional distribution of T_p given H_s is modelled by the log-normal distribution, i.e.

$$p_{T_p|H_s}(t_p|h_s) = \frac{1}{\sqrt{2\pi}\sigma_{T_p} t_p}\, exp\left(\frac{-(ln\, t_p - \mu_{T_p})^2}{2\sigma^2_{T_p}}\right) \tag{4.2.22}$$

where μ_{T_p} and $\sigma^2_{T_p}$ are the mean and variance of the variable $ln\,(T_p)$, respectively.
The long-term probability distribution of the sea state can also be given by some other characteristic periods than T_p together with H_s, i.e by using the expected zero-upcrossing wave periods T_z instead of T_p (see eq.(4.2.16)). The reason for choosing T_p is that these periods are less correlated to the significant wave height H_s than the other periods, Haver[p] 1985[2]. Together with H_s it will therefore include some additional information about a general sea state.
The marginal probability density function $p_{\overline{\theta}}(\theta)$ can be estimated by dividing the circle into a certain number of sectors and associating each sector with a point probability $p_{\overline{\theta}}(\theta_k), k = 1, ..., n$ where θ_k is the midpoint of sector no. k, and n is the number of sectors.

4.3. Probabilistic Modelling of the Wave Loading

In chapter 4.2 the statistical nature of the waves themselves was dealt with. Now consider the consequential loading on a structural element. It is well known that the force on a vertically placed circular cylinder subjected to wave action consists of a drag as well as an inertia component, Sarpkaya & Isaacson[b] 1981. It is generally assumed that the total wave force per unit length of a fixed vertical cylinder of the diameter D at position $\overline{r}_0 = (x_0, y_0, z_0)$ at the time t is

$$\overline{f}(\overline{r}_0, t) = \begin{bmatrix} f_x(\overline{r}_0, t) \\ f_y(\overline{r}_0, t) \\ f_z(\overline{r}_0, t) \end{bmatrix} = \overline{f}_D(\overline{r}_0, t) + \overline{f}_I(\overline{r}_0, t) \tag{4.3.1}$$

where

$\overline{f}_D(\overline{r}_0, t) = K_D \, |\overline{\dot{u}}(\overline{r}_0, t)| \, \overline{\dot{u}}(\overline{r}_0, t)$

$\overline{f}_I(\overline{r}_0, t) = K_I \, \overline{\ddot{u}}(\overline{r}_0, t)$

$K_D = 1/2 \, C_D \, \rho D$

$K_I = 1/4 \, C_M \, \pi \, \rho \, D^2$

$\overline{\dot{u}}(\overline{r}_0, t)$ is the horizontal water particle velocity vector at position $\overline{r}_0$ at the time t.

$\overline{\ddot{u}}(\overline{r}_0, t)$ is the horizontal water particle acceleration vector at position $\overline{r}_0$ at the time t.

x, y, z is the global coordinate system.

C_D is the drag coefficient.

C_M is the inertia coefficient.

ρ is the density of water.

Eq.(4.3.1), usually denoted as Morison's equation, assumes that the cylinder is vertical and fixed and that the velocity $\overline{\dot{u}}$ and the acceleration $\overline{\ddot{u}}$ of the water particles are horizontal and exactly normal to the vertical cylinder. In real offshore structures the structural elements are in general not vertical and under dynamic loading they are not fixed. However, it is assumed in this thesis that the load on the structure can be calculated without taking into account that the structure is moving, which means that the response velocity and the acceleration of the structure are assumed to be much less than the water particle velocity and the acceleration respectively. Further, it is assumed that Morison's equation can be applied to a cylindrical member orientated in a random manner as

$$\overline{f}_n(\overline{r}_0, t) = \begin{bmatrix} f_{nx}(\overline{r}_0, t) \\ f_{ny}(\overline{r}_0, t) \\ f_{nz}(\overline{r}_0, t) \end{bmatrix} = \overline{f}_{nD}(\overline{r}_0, t) + \overline{f}_{nI}(\overline{r}_0, t) \tag{4.3.2}$$

where

$$\overline{f}_{nD}(\overline{r}_0,t) = K_D\,|\dot{\overline{u}}_n(\overline{r}_0,t)|\,\dot{\overline{u}}_n(\overline{r}_0,t)$$
$$\overline{f}_{nI}(\overline{r}_0,t) = K_I\,\ddot{\overline{u}}_n(\overline{r}_0,t)$$

where the subscript n refers to a direction perpendicular to the cylinder.
The non-linear drag term $\overline{f}_{nD}$ in eq.(4.3.2) makes the computations for correlations and spectral densities extremely difficult and intractable. Therefore, a recourse to linearization of the drag term in eq.(4.3.2) is made. The "minimum square error linearization method" ,Atalik & Utku[p.] 1976, is used for this purpose. The linearized version of the drag term $\overline{f}_{nD}$ becomes

$$\overline{f}_{DL}(\overline{r}_0,t) = K_D\,\overline{\overline{L}}\,\dot{\overline{u}}_n(\overline{r}_0,t) = K_D \begin{bmatrix} l_{11} & l_{12} & l_{13} \\ l_{21} & l_{22} & l_{23} \\ l_{31} & l_{32} & l_{33} \end{bmatrix} \begin{bmatrix} \dot{u}_{nx} \\ \dot{u}_{ny} \\ \dot{u}_{nz} \end{bmatrix} \tag{4.3.3}$$

where the linearization coefficient matrix $\overline{\overline{L}}$ is given in appendix B.
Eq.(4.3.3) can now be written as

$$\overline{f}_n(\overline{r}_0,t) = \begin{bmatrix} f_{nx}(\overline{r}_0,t) \\ f_{ny}(\overline{r}_0,t) \\ f_{nz}(\overline{r}_0,t) \end{bmatrix} = K_D\,\overline{\overline{L}}\,\dot{\overline{u}}_n(\overline{r}_0,t) + K_I\ddot{\overline{u}}_n(\overline{r}_0,t) \tag{4.3.4}$$

The normal vectors $\dot{\overline{u}}_n$ and $\ddot{\overline{u}}_n$ in eq.(4.3.4) can be expressed in terms of a unit vector $\overline{c} = (c_x, c_y, c_z)$ along the cylinder axis as follows (see appendix B)

$$\dot{\overline{u}}_n = (\overline{c} \times (\dot{\overline{u}}^T \times \overline{c}))^T = \overline{\overline{C}}\,\dot{\overline{u}}$$

$$\ddot{\overline{u}}_n = (\overline{c} \times (\ddot{\overline{u}}^T \times \overline{c}))^T = \overline{\overline{C}}\,\ddot{\overline{u}} \tag{4.3.5}$$

where

$$\overline{\overline{C}} = \begin{bmatrix} (1-c_x^2) & -c_xc_y & -c_xc_z \\ & (1-c_y^2) & -c_yc_z \\ \text{sym.} & & (1-c_z^2) \end{bmatrix} = \left[\{\overline{C}\}_x\ \{\overline{C}\}_y\ \{\overline{C}\}_z\right]$$

$$\dot{\overline{u}} = \begin{bmatrix} \dot{u}_x \\ \dot{u}_y \\ \dot{u}_z \end{bmatrix}$$

$$\ddot{\overline{u}} = \begin{bmatrix} \ddot{u}_x \\ \ddot{u}_y \\ \ddot{u}_z \end{bmatrix}$$

Now eq.(4.3.4) can be rewritten as

$$\overline{f}_n(\overline{r}_0,t) = \begin{bmatrix} f_{nx}(\overline{r}_0,t) \\ f_{ny}(\overline{r}_0,t) \\ f_{nz}(\overline{r}_0,t) \end{bmatrix} = K_D \, \overline{\overline{L}} \, \overline{\overline{C}} \, \dot{\overline{u}}(\overline{r}_0,t) + K_I \, \overline{\overline{C}} \, \ddot{\overline{u}}(\overline{r}_0,t) \tag{4.3.6}$$

Two points in the wave field are considered, i.e. point l with the coordinates $\overline{r}_l = (x_l, y_l, z_l)$ and point m with the coordinates $\overline{r}_m = (x_m, y_m, z_m)$. The point l belongs to a circular cylindrical element L with the diameter D_L and the unit vector $\overline{c}_L = (c_{x_L}, c_{y_L}, c_{z_L})$ along the cylinder axis and the point m belongs to a circular cylindrical element M with the diameter D_M and the unit vector $\overline{c}_M = (c_{x_M}, c_{y_M}, c_{z_M})$ along the cylinder axis. The cross-covariance function for the various combinations of wave force components at l and m can now be expressed as a function of the covariance functions of $\dot{\overline{u}}$ and $\ddot{\overline{u}}$. The cross-spectral densities between various components can be found by deriving the Fourier transforms of the corresponding cross-covariance functions. The cross-spectral density between the forces f_{nil} and f_{njm} becomes (subscripts nil and njm $(i,j = x,y,z)$ denotes the force perpendicular to the elements in the directions i and j in the points l and m)

$$\begin{aligned} S_{f_{nil}f_{njm}}(\omega) &= K_{D_L} \, K_{D_M} [\{\overline{B}_l\}_i \, \{\overline{B}_m\}_j] \, [S_{\dot{u}_l \dot{u}_m}] \\ &+ K_{D_L} \, K_{I_M} [\{\overline{B}_l\}_i \, \{\overline{C}_M\}_j] \, [S_{\dot{u}_l \ddot{u}_m}] \\ &+ K_{I_L} \, K_{D_M} [\{\overline{C}_L\}_i \, \{\overline{B}_m\}_j] \, [S_{\ddot{u}_l \dot{u}_m}] \\ &+ K_{I_L} \, K_{I_M} [\{\overline{C}_L\}_i \, \{\overline{C}_M\}_j] \, [S_{\ddot{u}_l \ddot{u}_m}] \end{aligned} \tag{4.3.7}$$

where

$$[\{\overline{B}_l\}_x \, \{\overline{B}_l\}_y \, \{\overline{B}_l\}_z] = \overline{\overline{L}}_l \, \overline{\overline{C}}_L$$

$$[\{\overline{B}_m\}_x \, \{\overline{B}_m\}_y \, \{\overline{B}_m\}_z] = \overline{\overline{L}}_m \, \overline{\overline{C}}_M$$

$$\overline{\overline{C}}_L = [\{\overline{C}_L\}_x \, \{\overline{C}_L\}_y \, \{\overline{C}_L\}_z] = \begin{bmatrix} (1-c_{x_L}^2) & -c_{x_L}c_{y_L} & -c_{x_L}c_{z_L} \\ & (1-c_{y_L}^2) & -c_{y_L}c_{z_L} \\ \text{sym.} & & (1-c_{z_L}^2) \end{bmatrix}$$

$$\overline{\overline{C}}_M = [\{\overline{C}_M\}_x \, \{\overline{C}_M\}_y \, \{\overline{C}_M\}_z] = \begin{bmatrix} (1-c_{x_M}^2) & -c_{x_M}c_{y_M} & -c_{x_M}c_{z_M} \\ & (1-c_{y_M}^2) & -c_{y_M}c_{z_M} \\ \text{sym.} & & (1-c_{z_M}^2) \end{bmatrix}$$

$\overline{\overline{L}}_l$ and $\overline{\overline{L}}_m$ are the linearization coefficient matrices for point l and point m, respec-

tively (see appendix B).

$$[S_{\dot{u}_l \dot{u}_m}] = \begin{bmatrix} S_{\dot{u}_{x_l}\dot{u}_{x_m}}(\omega) & S_{\dot{u}_{x_l}\dot{u}_{y_m}}(\omega) & S_{\dot{u}_{x_l}\dot{u}_{z_m}}(\omega) \\ S_{\dot{u}_{y_l}\dot{u}_{x_m}}(\omega) & S_{\dot{u}_{y_l}\dot{u}_{y_m}}(\omega) & S_{\dot{u}_{y_l}\dot{u}_{z_m}}(\omega) \\ S_{\dot{u}_{z_l}\dot{u}_{x_m}}(\omega) & S_{\dot{u}_{z_l}\dot{u}_{y_m}}(\omega) & S_{\dot{u}_{z_l}\dot{u}_{z_m}}(\omega) \end{bmatrix}$$

$$[S_{\dot{u}_l \ddot{u}_m}] = \begin{bmatrix} S_{\dot{u}_{x_l}\ddot{u}_{x_m}}(\omega) & S_{\dot{u}_{x_l}\ddot{u}_{y_m}}(\omega) & S_{\dot{u}_{x_l}\ddot{u}_{z_m}}(\omega) \\ S_{\dot{u}_{y_l}\ddot{u}_{x_m}}(\omega) & S_{\dot{u}_{y_l}\ddot{u}_{y_m}}(\omega) & S_{\dot{u}_{y_l}\ddot{u}_{z_m}}(\omega) \\ S_{\dot{u}_{z_l}\ddot{u}_{x_m}}(\omega) & S_{\dot{u}_{z_l}\ddot{u}_{y_m}}(\omega) & S_{\dot{u}_{z_l}\ddot{u}_{z_m}}(\omega) \end{bmatrix}$$

$$[S_{\ddot{u}_l \dot{u}_m}] = \begin{bmatrix} S_{\ddot{u}_{x_l}\dot{u}_{x_m}}(\omega) & S_{\ddot{u}_{x_l}\dot{u}_{y_m}}(\omega) & S_{\ddot{u}_{x_l}\dot{u}_{z_m}}(\omega) \\ S_{\ddot{u}_{y_l}\dot{u}_{x_m}}(\omega) & S_{\ddot{u}_{y_l}\dot{u}_{y_m}}(\omega) & S_{\ddot{u}_{y_l}\dot{u}_{z_m}}(\omega) \\ S_{\ddot{u}_{z_l}\dot{u}_{x_m}}(\omega) & S_{\ddot{u}_{z_l}\dot{u}_{y_m}}(\omega) & S_{\ddot{u}_{z_l}\dot{u}_{z_m}}(\omega) \end{bmatrix}$$

$$[S_{\dot{u}_l \dot{u}_m}] = \begin{bmatrix} S_{\ddot{u}_{x_l}\ddot{u}_{x_m}}(\omega) & S_{\ddot{u}_{x_l}\ddot{u}_{y_m}}(\omega) & S_{\ddot{u}_{x_l}\ddot{u}_{z_m}}(\omega) \\ S_{\ddot{u}_{y_l}\ddot{u}_{x_m}}(\omega) & S_{\ddot{u}_{y_l}\ddot{u}_{y_m}}(\omega) & S_{\ddot{u}_{y_l}\ddot{u}_{z_m}}(\omega) \\ S_{\ddot{u}_{z_l}\ddot{u}_{x_m}}(\omega) & S_{\ddot{u}_{z_l}\ddot{u}_{y_m}}(\omega) & S_{\ddot{u}_{z_l}\ddot{u}_{z_m}}(\omega) \end{bmatrix}$$

The notation [...][...] in eq.(4.3.7), and later in eq.(4.3.10), does not denote matrix multiplications in the conventional sense. They are used here only to denote a row-to-column multiplication. After one row-to-column multiplication a sum is made and added to the sum of the second row-to- column multiplication and so on, so that the final result is only a single term. The cross-spectral densities of the water particle velocity $[S_{\dot{u}_l \dot{u}_m}]$ may be expressed in terms of the one- dimensional wave spectral density $S_{\eta\eta}(\omega)$ by using eq.(4.2.10) as, Sigbjørnsson[p] 1979

$$[S_{\dot{u}_l \dot{u}_m}] = S_{\eta\eta}(\omega) \int_{\overline{\theta}-\pi/2}^{\overline{\theta}+\pi/2} \omega^2 \overline{\overline{\Lambda}}(\omega, z_l, z_m) \psi(\theta) exp(-\epsilon\kappa(\omega)(\Delta x \, cos\theta + \Delta y \, sin\theta)) d\theta \tag{4.3.8}$$

where

$$\overline{\overline{\Lambda}}(\omega, z_l, z_m) = \overline{A}(\overline{k}(\omega), z_l) \overline{A}^{*T}(\overline{k}(\omega), z_m)$$

$$\overline{A}(\overline{k}(\omega), z) = \frac{1}{sinh(\kappa(\omega)d)} \begin{bmatrix} cos\theta \; cosh(\kappa(\omega)z) \\ sin\theta \; cosh(\kappa(\omega)z) \\ \epsilon \; sinh(\kappa(\omega)z) \end{bmatrix}$$

$*$ denotes complex conjugated

ϵ $= \sqrt{-1}$

d is the water depth

Δx $= x_l - x_m$

$\Delta y \quad = y_l - y_m$

$\kappa(\omega)$ is the wave number, defined in eq.(4.2.7)

$\psi(\theta)$ is the spreading function, defined in eq.(4.2.17)

The z-coordinates are measured from bottom positive upwards.

The cross-spectral densities of water particle accelerations $[S_{\ddot{u}_l \ddot{u}_m}]$, acceleration and velocity $[S_{\ddot{u}_l \dot{u}_m}]$ and velocity and acceleration $[S_{\dot{u}_l u_m}]$ can be obtained using the properties of the derived processes. This gives

$$[S_{\ddot{u}_l \ddot{u}_m}] = \omega^2 [S_{\dot{u}_l \dot{u}_m}]$$

$$[S_{\dot{u}_l \ddot{u}_m}] = -[S_{\ddot{u}_l \dot{u}_m}] = \epsilon\omega \, [S_{\dot{u}_l \dot{u}_m}] \tag{4.3.9}$$

Applying eq.(4.3.9), eq.(4.3.7) can be rewritten as

$$S_{f_{nil} f_{njm}}(\omega) = [K_{D_L} \, K_{D_M}(\{\overline{B}_l\}_i \{\overline{B}_m\}_j) + \omega^2 K_{I_L} \, K_{I_M}(\{\overline{C}_L\}_i \{\overline{C}_M\}_j)$$

$$+ \epsilon\omega (K_{D_L} K_{I_M}(\{\overline{B}_l\}_i \, \{\overline{C}_M\}_j) - K_{I_L} K_{D_M}(\{\overline{C}_L\}_i \, \{\overline{B}_m\}_j))] \, [S_{\dot{u}_l \dot{u}_m}] \tag{4.3.10}$$

4.4. Structural Response Analysis

It is assumed that the structure can be modelled as a space frame of three-dimensional beam elements connected by nodal points, where each structural member in the structure has one or more beam elements. If the structural system is modelled by a linear system and by a finite number of degrees of freedom then the dynamic equations may written as

$$\overline{\overline{M}}\,\ddot{\overline{x}} + \overline{\overline{C}}\,\dot{\overline{x}} + \overline{\overline{K}}\,\overline{x} = \overline{F} \tag{4.4.1}$$

where

$\overline{x}$ is the displacement vector

$\overline{\overline{M}}$ is the mass matrix

$\overline{\overline{C}}$ is the damping matrix

$\overline{\overline{K}}$ is the stiffness matrix

$\overline{F}$ is the load vector which varies with time

The matrix equation (4.4.1) represents a finite number of coupled differential equations. A "modal analysis" is chosen for transforming the coupled system into an uncoupled system (i.e. it is assumed that the system is slightly damped). The linear transformation is written as

$$\overline{x} = \overline{\overline{\Phi}}\,\overline{q} \tag{4.4.2}$$

where the transformation matrix $\overline{\overline{\Phi}}$ is the mode shape matrix, i.e. $\overline{\overline{\Phi}} = [\{\overline{\phi}_1\}, \{\overline{\phi}_2\}, \ldots, \{\overline{\phi}_n\}]$, where $\{\overline{\phi}_i\}$ denotes the mode shape vector corresponding to the ith natural frequency. Substituting eq.(4.4.2) into eq.(4.4.1) and pre-multiplying by $\overline{\overline{\Phi}}^T$ gives

$$\overline{\overline{\Phi}}^T\,\overline{\overline{M}}\,\overline{\overline{\Phi}}\,\ddot{\overline{q}} + \overline{\overline{\Phi}}^T\,\overline{\overline{C}}\,\overline{\overline{\Phi}}\,\dot{\overline{q}} + \overline{\overline{\Phi}}^T\,\overline{\overline{K}}\,\overline{\overline{\Phi}}\,\overline{q} = \overline{\overline{\Phi}}^T\,\overline{F} \tag{4.4.3}$$

Taking account of the orthogonality of the modes, the mass and stiffness matrices diagonalise.
$\overline{\overline{\Phi}}$ is normalised as

$$\overline{\overline{\Phi}}^T\,\overline{\overline{M}}\,\overline{\overline{\Phi}} = \overline{\overline{I}} \tag{4.4.4}$$

where $\overline{\overline{I}}$ is the unit matrix. Assuming proportional damping, the damping matrix $\overline{\overline{C}}$ will also be diagonalised. The matrix eq.(4.4.3) represents a finite number of uncoupled differential equations given as

$$\ddot{q}_i + 2\zeta_i\omega_i\dot{q}_i + \omega_i^2 q_i = f_i \quad ; \quad i = 1, \ldots, m \tag{4.4.5}$$

where m is the number of degrees of freedom, q_i is the modal coordinates defined in eq.(4.4.2), ω_i is the ith natural frequency and ζ_i is the damping ratio which is normally prescribed in practical applications, Penzien & Tseng[p] 1978. The modal loading f_i is obtained from

$$\overline{f} = \overline{\overline{\Phi}}^T \overline{F} \tag{4.4.6}$$

Finally, the stresses $\overline{s}$ at internal points in the structure may be found as

$$\overline{s} = \overline{\overline{T}}\,\overline{q} \tag{4.4.7}$$

where the components T_{ij} in the matrix $\overline{\overline{T}}$ indicate the stress at point i due to displacement in mode j, and $\overline{q}$ is the solution of eq.(4.4.5). From the theory of vibration, Cronin, Godfrey, Hook & Watt[p] 1978, it follows that the cross-spectral density of the stresses at points k and l may be written as (see eq.(4.4.7))

$$S_{s_k s_l}(\omega) = \sum_{i=1}^{n}\sum_{j=1}^{n} T_{ki}T_{lj}S_{q_i q_j}(\omega) \tag{4.4.8}$$

where n is the number of mode shapes.

The cross-spectral density of the modal displacements q_i and q_j, $S_{q_i q_j}(\omega)$ in eq.(4.4.8) may be found as

$$S_{q_i q_j}(\omega) = H^*_{q_i f_i}(\omega)H_{q_j f_j}(\omega)S_{f_i f_j}(\omega) \tag{4.4.9}$$

where $*$ denotes the complex conjugate and where $H_{q_i f_i}$ is the frequency response function of the system (in eq.(4.4.5)) defined as

$$H_{q_i f_i}(\omega) = \frac{1}{\omega_i^2 - \omega^2 + 2\epsilon\zeta_i\omega\omega_i} \tag{4.4.10}$$

The cross-spectral density of the modal loading f_i and f_j, $S_{f_i f_j}(\omega)$ in eq.(4.4.9) can be found as (see eq.(4.4.6))

$$S_{f_i f_j}(\omega) = \sum_{r=1}^{m}\sum_{s=1}^{m} \phi_{ir}\phi_{js}S_{F_r F_s}(\omega) \tag{4.4.11}$$

where ϕ_{ir} is the (i,r) element in the mode shape matrix $\overline{\overline{\Phi}}$.

The cross-spectral density of the load at the nodal points r and s, $S_{F_r F_s}$, may be found by double integration of eq.(4.3.10) over half the lengths of all elements corresponding to nodal points r and s.

Equations (4.4.8) to (4.4.11) yield the cross-spectral density for the stresses in the structure, which may be summarised as

$$S_{s_k s_l}(\omega) = \sum_{i=1}^{n}\sum_{j=1}^{n} T_{ki}T_{lj}S_{q_i q_j}(\omega) \tag{4.4.12a}$$

where

$$S_{q_i q_j}(\omega) = H^*_{q_i f_i}(\omega)H_{q_j f_j}(\omega)S_{f_i f_j}(\omega) \tag{4.4.12b}$$

and where

$$S_{f_i f_j}(\omega) = \sum_{r=1}^{m}\sum_{s=1}^{m} \phi_{ir}\phi_{js}S_{F_r F_s}(\omega) \tag{4.4.12c}$$

For an exact solution of eq.(4.4.12a) the number of mode shapes is equal to the number of degrees of freedom, i.e. $n = m$. In general it is sufficient to take just a few mode shapes into account (i.e. the mode shapes with the lowest natural frequencies), namely $n \ll m$.

For the fatigue analysis in section 4.5 the cross-spectral density for the stresses as a whole is not interesting. However, three characteristics, namely the area m_0, the second moment m_2 and the fourth moment m_4 of the auto-spectral density (i.e. $k = l$ in eq.(4.4.12)) are of interest. the area of the auto-spectral density can be derived as

$$m_0(s_k) = \sigma^2(s_k) = \int_0^\infty S_{s_k s_k}(\omega)d\omega \tag{4.4.13}$$

and the second and the fourth moment of the auto-spectral density as

$$m_2(s_k) = \int_0^\infty \omega^2 S_{s_k s_k}(\omega)d\omega \tag{4.4.14}$$

$$m_4(s_k) = \int_0^\infty \omega^4 S_{s_k s_k}(\omega)d\omega \tag{4.4.15}$$

Applying equations (4.4.12a),(4.4.13),(4.4.14) and (4.4.15) the expressions

$$\begin{aligned} m_0(s_k) = \sigma^2(s_k) &= \sum_{i=1}^{n}\sum_{j=1}^{n} T_{ki}T_{kj}\int_0^\infty S_{q_i q_j}(\omega)d\omega \\ &= \sum_{i=1}^{n}\sum_{j=1}^{n} T_{ki}T_{kj}Cov(q_i, q_j) \end{aligned} \tag{4.4.16}$$

and

$$m_2(s_k) = \sum_{i=1}^{n}\sum_{j=1}^{n} T_{ki}T_{kj}\int_0^\infty \omega^2 S_{q_i q_j}(\omega)d\omega \tag{4.4.17}$$

and

$$m_4(s_k) = \sum_{i=1}^{n}\sum_{j=1}^{n} T_{ki}T_{kj}\int_0^\infty \omega^4 S_{q_i q_j}(\omega)d\omega \tag{4.4.18}$$

can be derived. They introduce a time saving modification of the computational procedure.

4.5. Stochastic Modelling of Fatigue Failure

Fatigue is one of the most common form of failure for structure which are subjected to time-varying loads of significant like offshore structure. It is also a failure mode which there is very large uncertainty in the number of load-cycle which will actually cause failure, and therefore a natural candidate for the using of probabilistic methods.

In section 4.4 it was shown how the spectral densities for the stresses in a given hot spot in the structure can be estimated. In this thesis fatigue damage is defined as a result of cumulative damage because of stress fluctuations (the stress ranges). In section 4.5.1 it is shown how the distribution of the stress amplitudes for a given stress spectral density, can be estimated by using the rain-flow-counting method (RFC-method) and the range-counting method (RC-method). In section 4.5.2 it is be shown how the probability of fatigue failure can be estimated by three different damage accumulation models, namely by using Miner's rule combined with the so-called S-N approach, by using a crack growth model (fracture mechanics) and by using a model introduced by Bogdanoff et al.[p] 1978[1,2,3], 1980.

4.5.1. Distribution of Stress Amplitudes

For a short-term period the sea state is assumed to be a zero-mean ergodic Gaussian process, see section 4.2. By using the linearized version of the Morison equation (see section 4.3), and by modelling the structural system linearly (see section 4.4) the stress response S becomes a zero-mean ergodic Gaussian process too. In this section it is shown how the distribution function of stress amplitudes in a stationary Gaussian random process with a given spectral density can be estimated.
A number of cycles counting algorithms have been proposed. Two of the counting methods, namely the range count method (RC-method) and the rainflow count method (RFC-method) are generally recognised as the method which produces the best results, and will be included here. Both methods give the same result for an ideal narrow-banded stress history, but for wide-banded stress history the result can be very different.

We consider a stationary Gaussian stochastic process $X(t)$ with mean μ_X, which is taken for simplicity as zero in the following description, and spectral density $S_X(\omega)$. The process is completely determined by the mean value μ_X and the covariance function $C_X(\tau)$

$$E[X(t)] = \mu_X = 0 \tag{4.5.1}$$

$$C_X(\tau) = Cov[X(t), X(t+\tau)]$$

$$= \int_0^\infty S_X(\omega)\, cos(\omega\tau) d\omega \tag{4.5.2}$$

The spectral moments m_j are defined as

$$m_j = \int_0^\infty \omega^j S_X(\omega) d\omega \qquad j = 0, 1, 2, \ldots \tag{4.5.3}$$

The mean period of upcrossing of the mean level μ_X=0 is, Lin^b 1967

$$T_z = 2\,\pi \sqrt{\frac{m_0}{m_2}} \tag{4.5.4}$$

and the mean period of the peaks (local maxima) is, Lin^b 1967

$$T_{mp} = 2\,\pi \sqrt{\frac{m_2}{m_4}} \tag{4.5.5}$$

The iregularity factor α is defined as the ratio of the mean period of peaks and the mean period of upcrossing of the mean level, i.e $\frac{1}{\alpha}$ is the mean number of peaks between the upcrossing and following down-crossing of the mean level.

$$\alpha = \frac{T_{mp}}{T_z} = \frac{m_2}{\sqrt{m_0 m_4}} \quad ; \quad 0 < \alpha \leq 1 \tag{4.5.6}$$

If $\alpha \approx 1$ the process is called narrow banded and if $\alpha \ll 1$ the process is called wide-banded. It can be shown, Lin[b] 1967, that the peaks u_i (local maxima) of stationary Gaussian processes are distributed according to the Rice distribution, Madsen, Krenk & Lind[b] 1986, with following distribution function

$$f_U(u) = \sqrt{1-\alpha^2}\,\phi\left(\frac{u}{\sqrt{1-\alpha^2}\sqrt{m_0}}\right) + \frac{\alpha\, u}{\sqrt{m_0}}\, e^{\frac{-u^2}{2m_0}}\,\Phi\left(\frac{\alpha\, u}{\sqrt{1-\alpha^2}\sqrt{m_0}}\right) \tag{4.5.7}$$

where the functions $\phi(\cdot)$ and $\Phi(\cdot)$ are the standard Gaussian density and distribution functions respectively.
For $\alpha = 0$ U_i becomes Gaussian distributed and for $\alpha = 1$ U_i becomes Rayleigh distributed.
Our purpose is to approximate the density distribution function, $f_H(h)$, for the stress amplitudes (cycles) H. It will dependent on definition of the amplitudes.

Rain-Flow Counting Method

The rain-flow method can be used to count cycles from a realisation of the random process $X(t)$. A realisation of $X(t)$ is converted to a point process of peaks and troughs as shown in figure 4.5.1. The peaks are identified by the even numbers and the troughs by the odd numbers. The time series is plotted so that the time axis is downward vertical, and the lines connecting the peaks and troughs are imagined to be a series of pagoda roofs. The following rules are imposed on rain dripping on these roofs, so that cycles and half cycles are defined, Wirsching & Shehata[p] 1977

1) A rain-flow is started at each peak and trough.
2) When a rain-flow part started at a trough comes to a tip of the roof, the flow stops if the opposite trough is more negative than that at the start of the path under consideration (e.g. in figure 4.5.1, path[1-8], path[9-10], etc.). For a path started at a peak, it is stopped by a peak which is more positive than that at the start of the rain path under consideration (e.g. in figure 4.5.1, path[2-3], path[4-5] and path[6-7]).
3) If the rain flowing down a roof intercepts a flow from the previous path, the present path is stopped, (e.g. in figure 4.5.1, path[3-3a], path[5-5a], etc.)
4) A new path is not started until the path under consideration is stopped.

Half-cycles of trough-originated range magnitudes h_i are projected distances on the X axis (e.g. in figure 4.5.1, [1-8],[3-3a],[5-5a] etc.). If the realisation of $X(t)$ is sufficiently long, any trough-originated half-cycle will be followed by another peak-originated half-cycle of the same range.

Because of the complexity of the rain-flow algorithm, it would be extraordinary difficult to derive $f_H(h)$ from a given spectral density $S_X(\omega)$. However, $f_H(h)$ can be estimated by simulating $X(t)$ e.g. by using the Monte-Carlo method, and counting the amplitudes (cycles) by using the above rules.

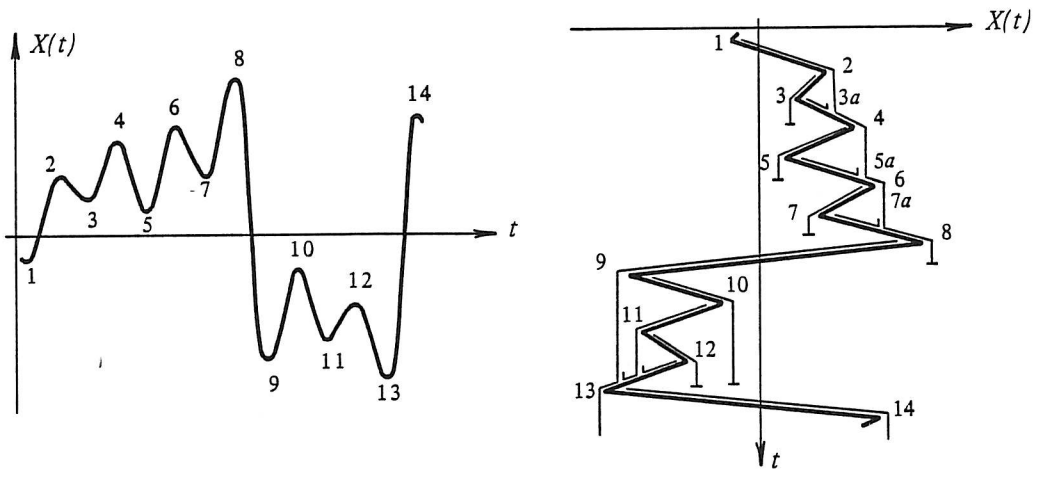

Figure 4.5.1. Illustration of the rain-flow cycle counting applied to sample of $X(t)$, Wirsching & Shehata[p] 1977.

Range Counting Method

In the range counting method a half-cycle is defined as the difference between two successive local extremes (local maxima (peak) and the following local minima (trough)). The distribution function for the amplitude, $f_H(h)$ can be estimated by simulating realisation of $X(t)$ and counting the number of half-cycles. Analytical estimation of the range distribution through the range counting method can be obtained relatively easily. Figure 4.5.2 illustrates the definition of range h_j and the half wave length τ_j.

The wave length τ_j and the amplitude h_j depend strongly upon the peak heights u_j. The joint distribution function of amplitudes H and half wave length τ is defined by, Madsen, Krenk & Lind[b] 1986

$$f_{UHT}(u,h,\tau) =$$

$$\frac{\int_0^\infty \left(\int_{-\infty}^0 -\ddot{x}_1 \ddot{x}_2 \, f_{X_1 X_2 \dot{X}_1 \dot{X}_2 \ddot{X}_1 \ddot{X}_2}(u, u-h, 0, 0, \ddot{x}_1, \ddot{x}_2) d\ddot{x}_1 \right) d\ddot{x}_2}{\int_0^\infty \left(\int_{-\infty}^0 -\ddot{x}_1 \ddot{x}_2 f_{\dot{X}_1 \dot{X}_2 \ddot{X}_1 \ddot{X}_2}(0,0,\ddot{x}_1,\ddot{x}_2) d\ddot{x}_1 \right) d\ddot{x}_2} \qquad (4.5.8)$$

where $f_{X_1X_2\dot{X}_1\dot{X}_2\ddot{X}_1\ddot{X}_2}$ is the joint density function of $X_1, X_2, \dot{X}_1, \dot{X}_2, \ddot{X}_1$ and $\ddot{X}_2$, where $X_1 = X(t)$ and $X_2 = X(t+\tau)$.

In order to estimate the density function of the range between two successive extremes h, it is also necessary to estimate the density function of half the wave length τ, $f_T(\tau)$.

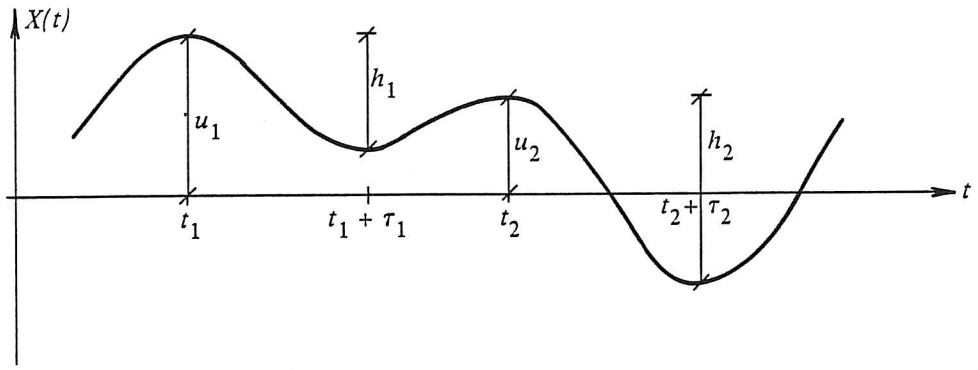

Figure 4.5.2. Definition of range h_j and half wave length τ_j in the RC-method.

This is a first passage problem which cannot generally be solved analytically. A simple estimate of $f_T(\tau)$ can be obtained by using the upper bound, Sørensen & Brincker[p] 1989

$$f_T(\tau) = \int_0^\infty \left(\int_{-\infty}^0 -\ddot{x}_1\ddot{x}_2 \; f_{\dot{X}_1\dot{X}_2\dot{X}_1\dot{X}_2}(0,0,\ddot{x}_1,\ddot{x}_2) d\ddot{x}_1 \right) d\ddot{x}_2 \; ; \; 0 \leq \tau \leq T_1 \quad (4.5.9)$$

where T_1 is determined from the normalisation condition

$$\int_0^{T_1} f_T(\tau) d\tau \; = \; 1 \quad (4.5.10)$$

When $\tau > T_1$, $f_T(\tau)$=0 is used. From eq.(4.5.8) and eq.(4.5.9) the density function of the amplitude h, $f_H(h)$, can be estimated by

$$f_H(h) \; = \; \int_0^{T_1} \left(\int_{-\infty}^\infty f_T(\tau) \; f_{UH|T}(u,h,|\tau) du \right) d\tau \quad (4.5.11)$$

In appendix C it is shown how eq.(4.5.11) can be calculated.

4.5.2. Damage Accumulation

It is often convenient to assume a fatigue failure to be a result of the accumulation of some measure of damage beyond a critical level. This damage measure may have direct physical meaning e.g. the length of a fatigue crack, maximum deformation, etc. or it may represent an indicator variable (typically unity at fatigue) whose growth is unobservable. In any of these cases, it is necessary to formulate empirical "laws" that govern the damage accumulation process under deterministic loading. A probabilistic structure in a cumulative damage model can be introduced by starting with a deterministic model for damage accumulation and then modelling the model parameters as a random variables or random processes. Alternatively, the evolutionary probabilistic structure can be assumed from the start. In the first approach, the accumulated damage is described as a function of the time, whereas in the second approach, the probabilistic distribution of the accumulated damage is described as a function of time. In section 4.5.2.1 the first approach is exemplified in connection with Miner's rule and the so-called S-N approach. In section 4.5.2.2 the same approach is exemplified for crack growth. In section 4.5.2.3 the second approach is elaborated with a model introduced by Bogdanoff et al.[p] 1978[1,2,3], 1980.

In fatigue analysis of jackets, the analysis will primarily focus on the welded joint between the members. When considering a fatigue failure in tubular joints the geometry of the nodal point becomes very important, since stress concentrations will occur due to the non-uniform stiffness of the chord wall and the brace. The locations, or points at which the highest stress occurs, are called hot spots. In welded joints two different hot spots for each brace in the joint are defined, one at the weld toe on the brace side, the other on the chord side, i.e. for plan K-joints there are four hot spots. The stress concentration factor (SCF) is defined as the ratio of the hot spot stress σ_{max} to the nominal stress σ_N in the brace, i.e.

$$SCF = \frac{\sigma_{max}}{\sigma_N} \tag{4.5.12}$$

The SCFs for a given joint geometry and loads can be estimated either by full-scale tests of by a FEM-analysis. Here the SCFs are estimated by using some empirical formulas suggested by Kuang, Almar-Næs (ed.)[b] 1985, which are based on thin shell FEM-analysis of different joint-geometries and loads. Two modes of fatigue failure, called failure elements, are defined to occur for each brace in a tubular joint; cracking at the hot spot toe of the weld jointing the brace to the chord (brace fatigue) and cracking at the hot spot in the wall of the chord itself (punching shear fatigue). The locations in the chord/brace intersection, where the hot spot stresses occur, depend on the external loads. In Almar-Næs (ed.)[b] 1985 checking of the 8 points along the brace/chord intersection is recommended to locate the hot spots, see figure 4.5.3

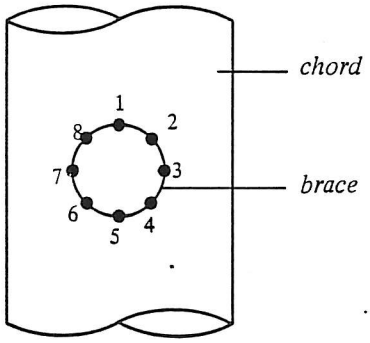

Figure 4.5.3. Points in the brace/chord intersection where the stress concentrations are checked.

4.5.2.1. Miner's Rule and S-N Approach

The relationship between the stress fluctuations and the damage can be found by using Miner's rule, which states in essence that every stress cycle i results in a degree of damage D_i equal to

$$D_i = \frac{1}{N_i} \tag{4.5.13}$$

where N_i is the number of cycles to failure, if the same stress cycle is repeated over and over again. The most commonly used model to determine N_i is the so-called $S-N$ approach

$$N_i = \left(\frac{2\hat{S}_i}{K}\right)^{-m} \tag{4.5.14}$$

where $\hat{S}_i$ is the stress amplitude and K and m are assumed for normal design purposes to be constants which can be determined by constant-amplitude tests. The relationship between $\hat{S}_i$ and N_i for a homogeneous regime has a very definite random character even under the most controlled and uniform test conditions. It is therefore meaningless to speak of a deterministic relationship between $\hat{S}_i$ and N_i. To allow for the randomness in the relationship, m and K are modelled as random variables. The value of K can depend on the mean stress in the stress cycles. The effect can be accounted i.e. by using the Goodman criterion, Madsen, Krenk & Lind[b] 1986

$$K = K_0\left(1-\frac{S_{a_i}}{S_u}\right)^m \tag{4.5.15}$$

where K_0 is the value of K from tests with zero-mean stress cycles, S_{a_i} is the mean stress in the stress cycle i and S_u is the ultimate tensile strength. However, in this thesis this dependence is assumed to have no effect on the fatigue life. To allow for the uncertainty in the estimation of the stress amplitude a new random variable B is introduced. Eq.(4.5.14) then becomes

$$N_i = \left(\frac{2\hat{S}_i B}{K}\right)^{-m} \tag{4.5.16}$$

Eq.(4.5.13) can now be rewritten as

$$D_i = \left(\frac{2\hat{S}_i B}{K}\right)^{m} \tag{4.5.17}$$

Under constant amplitude loading failure occurs by definition when the total degree

of damage $D_{tot} = \sum_{i=1}^{N} D_i$ attains the value D_{fail} equal to 1. However, with variable-amplitude random loading the influences due to the loading history may cause failure at the value D_{fail} different from 1. To take into account the uncertainty of the failure definition, D_{fail} will be modelled as a random variable.

Consider a zero-mean ergodic Gaussian stress process $S_{ss}(\omega)$, acting in a given period T. The expected fatigue damage per stress cycle i, given m, K and B, $E[D_i \mid m, K, B]$ can be determined as

$$E[D_i \mid m, K, B] = \int_0^\infty D_i(\hat{s})\, p_{\hat{S}}(\hat{s})\, d\hat{s} \tag{4.5.18}$$

where $p_{\hat{S}}(\hat{s})$ is the distribution function of the stress amplitudes. The expected total damage in the period T given m and B, $E[D_{tot} \mid m, K, B]$ is obtained by multiplying the expected damage per cycle by the number of cycles

$$E[D_{tot} \mid m, K, B] = \frac{T}{T_{mp}} E[D_i \mid m, K, B] \tag{4.5.19}$$

where T_{mp} is mean period of a stress cycle in the period T.

For a narrow-banded stress process ($\alpha \rightarrow 1$), $p_{\hat{S}}(\hat{s})$ becomes Rayleigh distributed and $E[D_i \mid m, K, B]$ can be written as

$$E[D_i \mid m, K, B] = \int_0^\infty B^m \left(\frac{2\hat{s}}{K}\right)^m \frac{\hat{s}}{\sigma_S^2}\, exp\left(-\frac{\hat{s}^2}{2\sigma_S^2}\right) d\hat{s} \tag{4.5.20}$$

$$= B^m \frac{\sigma_S^m}{K^m} \left(2\sqrt{2}\right)^m \Gamma(1 + \frac{m}{2}) \tag{4.5.21}$$

where $\Gamma(\cdots)$ is the gamma function, $\sigma_S = \sqrt{m_o}$ and where T_{mp} can be estimated as the expected zero-upcrossing period T_z

$$T_{mp} \approx T_z = 2\,\pi \sqrt{\frac{m_0}{m_2}} \tag{4.5.22}$$

m_0 and m_2 are the area and the second moment of the auto-spectral density of the stress process $S_{ss}(\omega)$, see eq.(4.4.12), eq.(4.4.13) and eq.(4.4.14).

For the case in which the stress process is wide-banded, it is much more difficult to calculate the expected total damage, because the true distribution of wide-banded stress cycles $p_{\hat{S}}(\hat{s})$ is unknown. The primary reason for this lack of knowledge is that the true distribution of wide-banded stress cycles depends on the definition of the stress cycle. The most common methods for estimating $p_{\hat{S}}(s)$ and T_{mp} are the

RFC-method and RC-method, see section 4.5.1. The expected total damage can be obtained using eq.(4.5.19) and eq.(4.5.20).

Another approach to predict the total damage of the wide-banded problems is to calculate the equivalent narrow-banded damage, which is the damage calculated from eq.(4.5.19) and eq.(4.5.20) without taking into account to either the correct number of stress cycles, $\frac{T}{T_{mp}}$, or their true distribution $p_{\hat{S}}(\hat{s})$, i.e. eq.(4.5.22) is used to estimate T_{mp}, and the Rayleigh distribution is used instead of the true distribution of the stress cycles.
The correct expected number of stress cycles in a wide-banded process, $\frac{T}{T_{mp}}$, is greater than in a narrow-banded process, $\frac{T}{T_z}$, with the same spectral moments. This tends to make the wide-banded damage larger than the equivalent narrow-banded damage. However, the estimation of the true distribution of stress cycles $f_{\hat{S}}(\hat{s})$ is strongly dependent on the shape of the stress spectrum and the definition of the stress cycles. It does therefore not apply generally that the wide-banded fatigue damage is less than the narrow-banded damage.

Wirsching & Light[p] 1980 present a simulation study of estimation of the expected total damage given m and K, $E[D_{tot} \mid m, K]$ (B was not introduced in their model). They performed simulations of random processes with various bandwidth parameter $\epsilon = \sqrt{1-\alpha^2}$, where α is defined in eq.(4.5.6), and with four different spectral density models shown in figure 4.5.4, and for five different values of m.

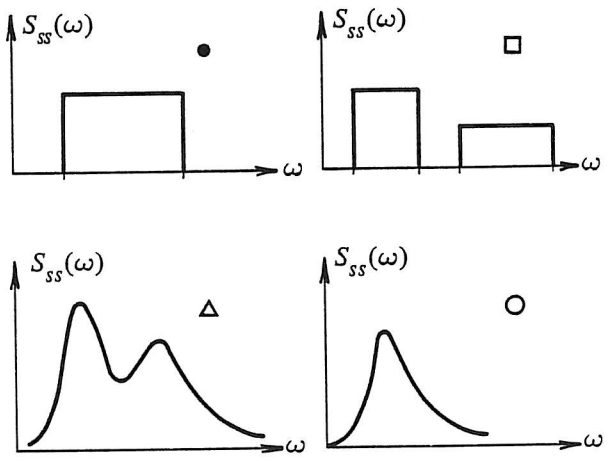

Figure 4.5.4. Spectral density models (symbols are used to define spectra in figure 4.5.5) Wirsching & Light[p] 1980.

For each simulation they calculated $E[D_{tot} \mid m, K]$ by the equivalent narrow-banded method and by using the RFC-method to estimate $p_{\hat{S}}(\hat{s})$ and T_{mp}. The ratio of the expected wide-banded damage $E[D_{wb}]$ and the expected equivalent narrow-banded damage $E[D_{nb}]$, called the "rainflow damage factor", λ_{RFC}, was calculated for each simulation as

$$\lambda_{RFC} = \frac{E[D_{wb}]}{E[D_{nb}]} \tag{4.5.23}$$

The results from the simulation study are shown in figure 4.5.5.
To obtain an estimate of λ_{RFC} as a function of ϵ and m, $\hat{\lambda}_{RFC}(\epsilon, m)$, characterising the relationship, a least square analysis was used. Wirsching and Light determined the equation

$$\hat{\lambda}_{RFC} = a(m) + (1 - a(m))(1 - \epsilon)^{b(m)} \tag{4.5.24}$$

where

$$a(m) = 0.926 - 0.033m$$

$$b(m) = 1.587m - 2.323$$

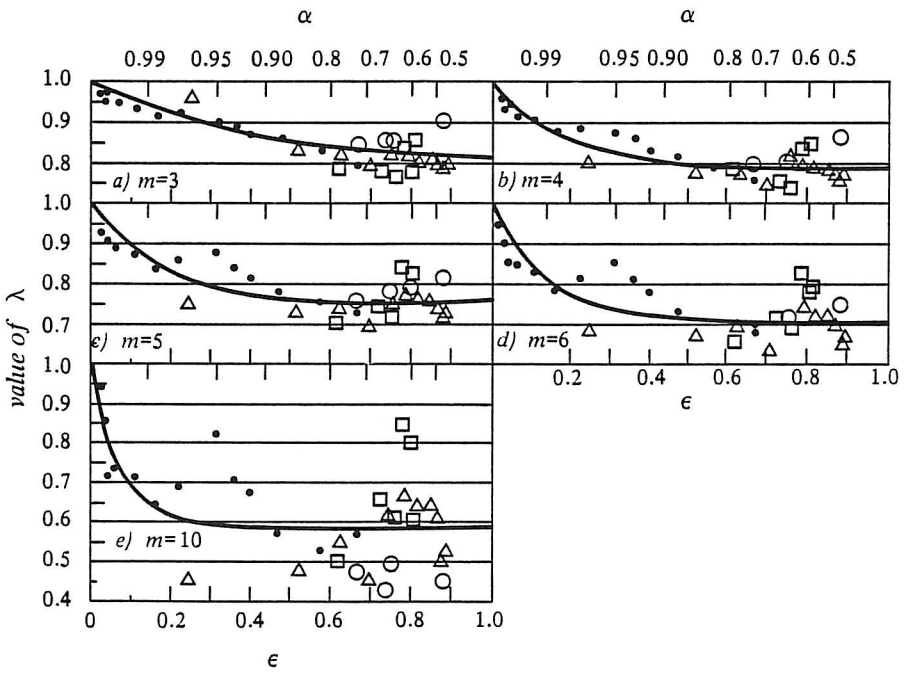

Figure 4.5.5. Estimates of λ_{RFC} versus ϵ (a) m=3; (b) m=4; (c) m=5; (d) m=6; (e) m=10 (symbols defined in figure 4.5.4, Wirsching & Light[p] 1980.

Knowing ϵ the expected wide-banded damage for a given m can now be estimated by using eq.(4.5.21) and eq.(4.5.24) as

$$E\left[D_{wb} \mid m, K, B\right] = \hat{\lambda}_{RFC}(\epsilon, m)\, E\left[D_{nb} \mid m, K, B\right]$$

$$= \hat{\lambda}_{RFC}(\epsilon, m)\, B^m \frac{\sigma_S^m}{K^m} \left(2\sqrt{2}\right)^m \Gamma(1 + \frac{m}{2}) \tag{4.5.25}$$

Lutes et al.[p] 1984 suggested that the λ_{RFC} might be a function of an adjustable band-width factor β_b, defined as

$$\beta_b = \sqrt{\frac{m_b}{m_o\, m_{2b}}} \tag{4.5.26}$$

where m_i is the ith moment of the stress spectrum.
Their study found that for given m, b can be optimised to produce a linear relationship between λ_{RFC} and β_b, which fits the data better than eq.(4.5.24). However the optimum value of b for different values of m is completely unpredictable and therefore useless for design.
Ortiz[t] 1985 showed that the distribution of peaks of a stationary Gaussian process has, approximately, a Rayleigh distribution with the parameter θ_s, given by

$$\theta_s = 2\, \sigma_S\, \alpha \tag{4.5.27}$$

Using eq.(4.5.27) the expected total fatigue damage given m (B is not included) becomes

$$E\left[D_{tot} \mid m, K\right] = \frac{T}{T_{mp}} \frac{\left(2\sqrt{2}\sigma_S\, \alpha\right)^m}{K^m} \Gamma(1 + \frac{m}{2}) \tag{4.5.28}$$

and the corresponding damage factor is

$$\lambda_{\theta_s} = \frac{T_{mp}}{T_z}\, \alpha^m \tag{4.5.29}$$

Realising that $T_{mp}/T_z = \frac{1}{\alpha}$, eq.(4.5.29) becomes

$$\lambda_{\theta_s} = \alpha^{m-1} \tag{4.5.30}$$

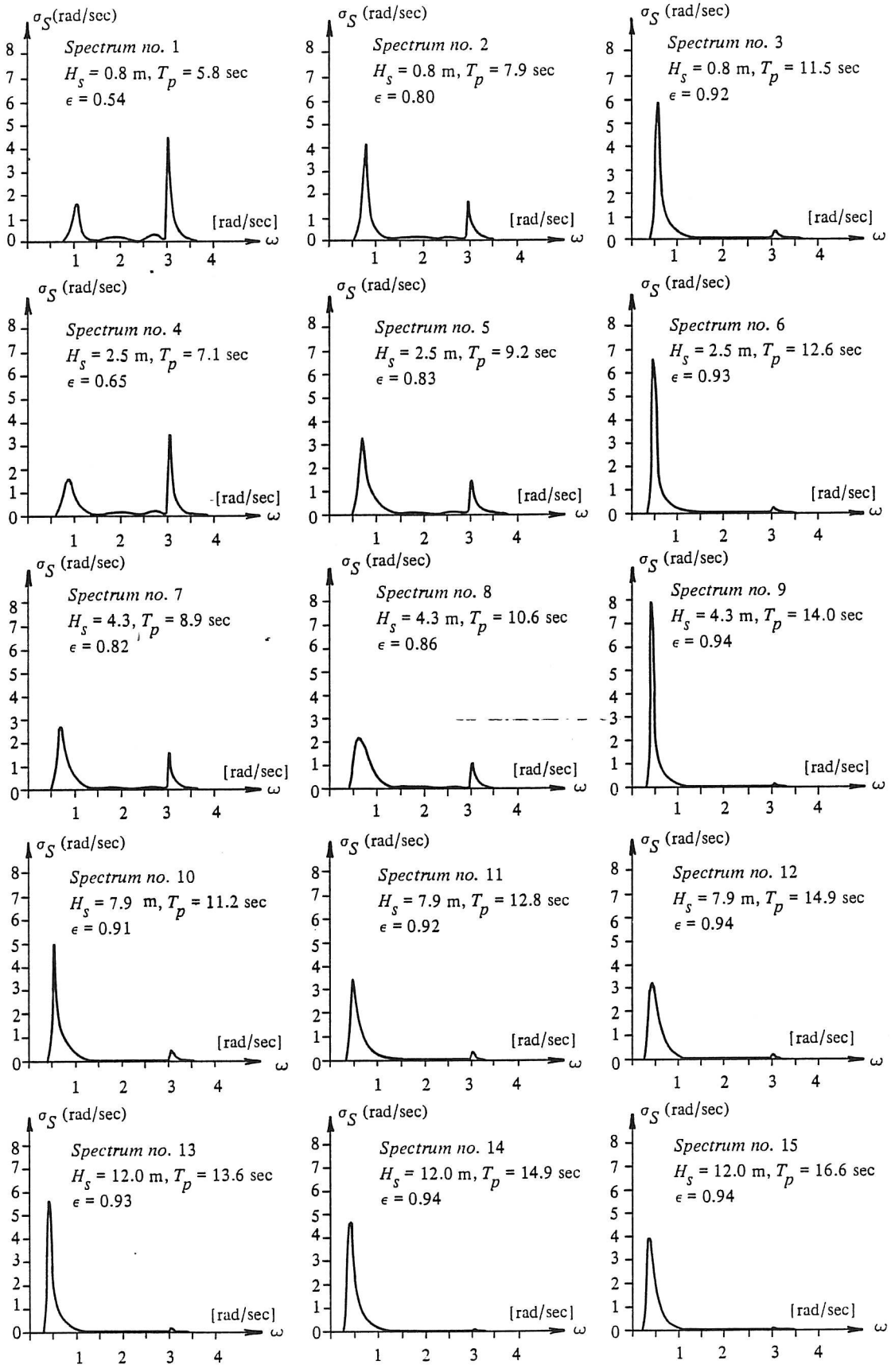

Figure 4.5.6. Normalised stress spectra for a hot spot.

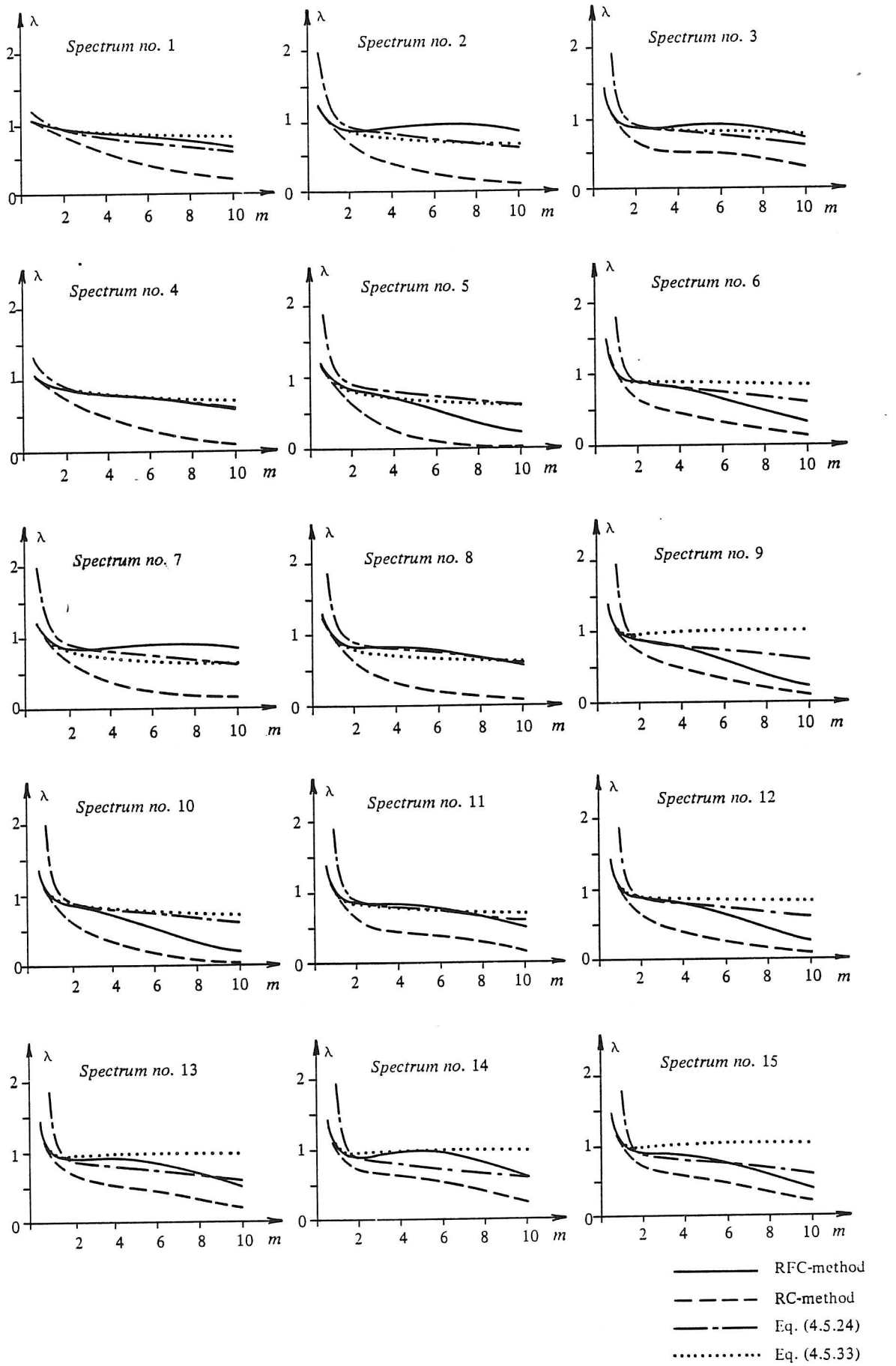

Figure 4.5.7. Wide-banded damage factor λ as a function of m for the spectra shown in figure 4.5.6.

Ortiz & Chen[p] 1987 compared eq.(4.5.30) with the simulation results and found that the use of λ_{θ_s} gives much too unconservative results. Therefore they suggested a new parameter θ_k instead of θ_s, given by

$$\theta_k = 2\ \sigma_S\ \beta_k \tag{4.5.31}$$

where β_k is an adjustable band-width measure defined by

$$\beta_k = \sqrt{\frac{m_2\ m_k}{m_o\ m_{k+2}}} \tag{4.5.32}$$

Analogues to eq.(4.5.29) the corresponding damage factor becomes

$$\lambda_{\theta_k} = \frac{\beta_k^m}{\alpha} \tag{4.5.33}$$

To estimate k as a function of m they re-analysed the simulation results of Wirsching & Light[p] 1980, and Lutes et al.[p] 1984. For a given value of m, the value of k was determined by minimising the sum of the squared errors. The result was

$$log(k)\ =\ log(2.0) - 0.89\ log(m) \tag{4.5.34}$$

However, due to the small sample size of their simulation study, they recommended the following convenient and conservative simplification

$$k\ =\ \frac{2}{m} \tag{4.5.35}$$

The expected wide-banded damage for given m can now be estimated as

$$E\left[D_{wb} \mid m, K\right] = \lambda_{\theta_k}(\epsilon, m)\ E\left[D_{nb} \mid m, K\right] \tag{4.5.36}$$

Several other empirical and semi-theoretical predictions of $E\left[D_{wb} \mid m, K\right]$ exist see e.g. Kam & Dover[p] 1987.

The above results are based on the assumption that the true distribution of stress cycles are estimated using the RFC-method.

To evaluate eq.(4.5.24) and eq.(4.5.33) simulation studies similar to those above have been used. However,the auto-spectral densities of a hot spot of a jacket type offshore structure are now estimated using eq.(4.4.12). The simulation is carried out for 15 different sea states. In figure 4.5.6 a normalised stress spectrum for the hot spot is shown (normalised as $m_o = 1.0$). The expected damage for each sea state is estimated

using eq.(4.5.25), eq.(4.5.36) and eq.(4.5.19) where $p_{\hat{S}}(\hat{s})$ is estimated by simulation and T_{mp} is obtained by eq.(4.5.5), where two methods for counting the stress cycles are used, namely the RFC-method and RC-method. In figure 4.5.8, an estimation of $p_{\hat{S}}(\hat{s})$ using the RFC-method, the RC-method and the narrow-banded approach (Rayleigh distribution) for spectrum no. 8, see figure 4.4.6, is shown The calculation was carried out for 20 different values of m, namely m=0.5, 1.0, 1.5, ... , 10.0. The results are shown in figure 4.5.7.

It can be seen from figure 4.5.7, that there is a significant difference between damage estimated from the RFC-method and from the RC-method. This indicates that the damage accumulation model must be calibrated, depending on the definition of the stress cycle.

The results shown in figure 4.5.7 lead to the following comments

- for $m > 2$ the rainflow damage factor $\lambda_{RFC} \leq 1$, (the simulation results), which indicates that the expected wide-banded damage $E[D_{wb}]$ is greater than the expected equivalent narrow-banded damage $E[D_{nb}]$.
- the use of eq.(4.5.35) instead of eq.(4.5.34) to estimate k in eq.(4.5.32) leads to a conservative estimate of the damage factor λ_{RFC} (not shown in figure 4.5.7).
- eq.(4.5.24) and eq.(4.5.33), where k is obtained from eq.(4.5.34), gives acceptable results for $2 \leq m \leq 4$.
- for $m > 4$, eq.(4.5.24) and eq.(4.5.33) generally give conservative estimates of λ_{RFC}, in some cases much too conservative.

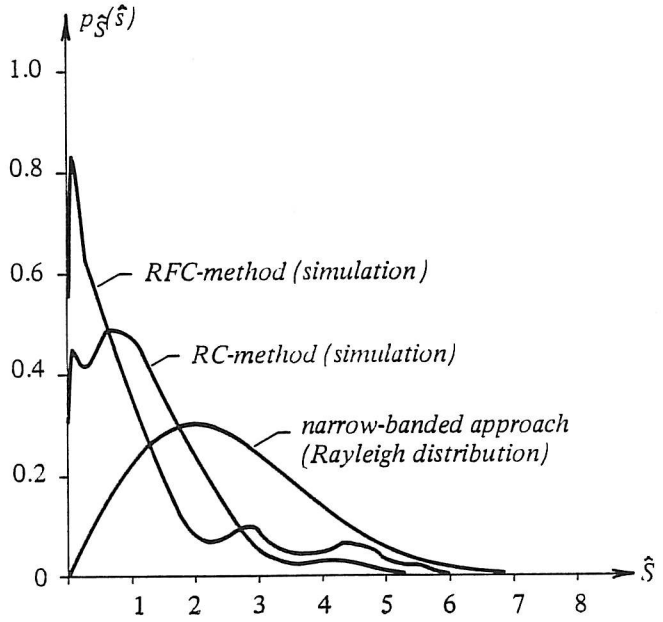

Figure 4.5.8. Estimation of the distribution density function of stress cycles using the RFC-method, the RC-method and the narrow-banded approach (the Rayleigh distribution).

Until now only the expected total damage of one sea state has been considered. The expected total damage at the failure element in a real offshore jacket structure, $E[D_{tot}]$ is obtained by summing up the expected damage $E[D_i]$ per stress cycle over the service life of the structure, taking account of the long-term distribution of the sea states (see eq.(4.2.21) and eq.(4.2.22) in section 4.2)

$$E[D_{tot}] = \int_0^{2\pi}\int_0^{\infty}\int_0^{\infty} \frac{T_L}{T_{mp}(t_p,h_s,\theta)}\, E\left[D_i(t_p,h_s,\theta)\right]\; p_{T_p|H_s}(t_p|h_s)$$

$$p_{H_s}(h_s)\; p_{\bar{\theta}}(\theta)\; dt_p\, dh_s\, d\theta \tag{4.5.37}$$

where $p_{H_s}(h_s)$ is the marginal probability density function for the significant wave height H_s, $p_{T_p|H_s}(t_p|h_s)$ is the conditional probability density function for the wave spectral peak periods T_p, given H_s, $p_{\bar{\theta}}(\theta)$ is the probability density function for the mean direction of the wave propagation, $\bar{\theta}$, T_L is the total service life and T_{mp} is mean period of a stress cycle within the sea state.
The fatigue failure mode for the failure element can be described by a safety margin M, defined as

$$M = D_{fail} - E[D_{tot}] \tag{4.5.38}$$

and the probability of fatigue failure of one failure element P_f is

$$P_f = P(M \leq 0) \tag{4.5.39}$$

For a narrow-banded stress process $p_{\hat{S}}(\hat{s})$ becomes Rayleigh distributed. And the total degree of damage $E[D_{tot}]$ can be written as

$$E[D_{tot}] = \int_0^{2\pi}\int_0^{\infty}\int_0^{\infty} \frac{T_L B^m}{T_{mp}(t_p,h_s,\theta)}\, \frac{\sigma_S^m(t_p,h_s,\theta)}{K^m}\, \left(2\sqrt{2}\right)^m \Gamma(1+\frac{m}{2})$$

$$p_{T_p|H_s}(t_p|h_s)\; p_{H_s}(h_s)\; p_{\bar{\theta}}(\theta)\; dt_p\, dh_s\, d\theta \tag{4.5.40}$$

where T_{mp} can be estimated as shown in eq.(4.5.22).
By using the rainflow damage factor λ_{RFC} the total damage can be estimated as

$$E[D_{tot}] = \int_0^{2\pi}\int_0^{\infty}\int_0^{\infty} \frac{T_L B^m}{T_{mp}(t_p,h_s,\theta)}\, \lambda_{RFC}(t_p,h_s,\theta)\, \frac{\sigma_S^m(t,h,\theta)}{K^m}\, \left(2\sqrt{2}\right)^m$$

$$\Gamma(1+\frac{m}{2})\; p_{T_p|H_s}(t_p|h_s)\; p_{H_s}(h_s)\; p_{\bar{\theta}}(\theta)\; dt_p\, dh_s\, d\theta \tag{4.5.41}$$

where for given θ, h_s and t_p the λ_{RFC} can be estimated from eq.(4.5.24).

4.5.2.2. Fracture Mechanics

Fracture mechanics seek to define the local condition of stress and strain around a crack, in terms of the global parameters of loads, geometry, etc., under which the crack will extend. Fracture mechanics can be subdivided into two general categories, namely linear-elastic and elastic-plastic. Various approaches have been employed in the analysis of fracture problems, leading to the introduction of various fracture mechanics parameters. The most popular among these parameters is the stress intensity factor K. In fact, a fundamental principle of linear-elastic fracture mechanics is that the stress field ahead of a sharp crack can be characterised in terms of this single parameter K.

The stress intensity factor K is computed by linear elastic fracture mechanics and is expressed as

$$K = YS\sqrt{\pi a} \tag{4.5.42}$$

where S is the stress applied, Y is a factor depending on geometry, including the crack geometry and size and a is the current crack or defect size.

It is commonly accepted that the stress intensity factor range, ΔK, can be used to describe fatigue crack growth under cyclic loading and the most frequently used law is the Paris law, Paris & Erdogan[p] 1963

$$\frac{da}{dN} = C(\Delta K)^m \tag{4.5.43}$$

where $\frac{da}{dN}$ is the rate of crack growth which is understood as the crack extension of a crack of a length a during one stress cycle, m and C are experimental constants depending on such factors as the mean stress, the test environment and the cycling frequency, etc., and $\Delta K = K_{max} - K_{min}$ is the range of the stress intensity factor defined in eq.(4.5.42)

$$\Delta K = Y\hat{S}\sqrt{\pi a} \tag{4.5.44}$$

where $\hat{S}$ is the range of the stress (stress cycle) applied.

If eq.(4.5.43) was correct then a plot of $log\left(\frac{da}{dN}\right)$ against $log(\Delta K)$ would show a straight line. However, a schematic plot of typical fatigue crack growth data shown in figure 4.5.9 shows that this is not true. Therefore, the fatigue process is divided into three regions:

Region I where the crack growth rate goes asymptotically towards zero as ΔK approaches a threshold value ΔK_{th}, which means that for stress intensity rates below ΔK_{th} there is no crack growth, i.e. there is a fatigue limit. Region II where $log\left(\frac{da}{dN}\right)/\ log(\Delta K)$ is constant and Region III where the crack growth rate is exhibiting a rapidly increasing growth rate towards infinity, i.e. ductile tearing and/or brittle fracture. The agreement between eq.(4.5.43) and the experiments is good

for Region II, typically 10^{-5} to 10^{-3} mm/cycle, Madsen, Krenk & Lind[b] 1986. For higher growth rates, Region III, eq.(4.5.43) underestimates the propagation rate, and for lower growth rates, Region I, eq.(4.5.43) overestimates the propagation rate.

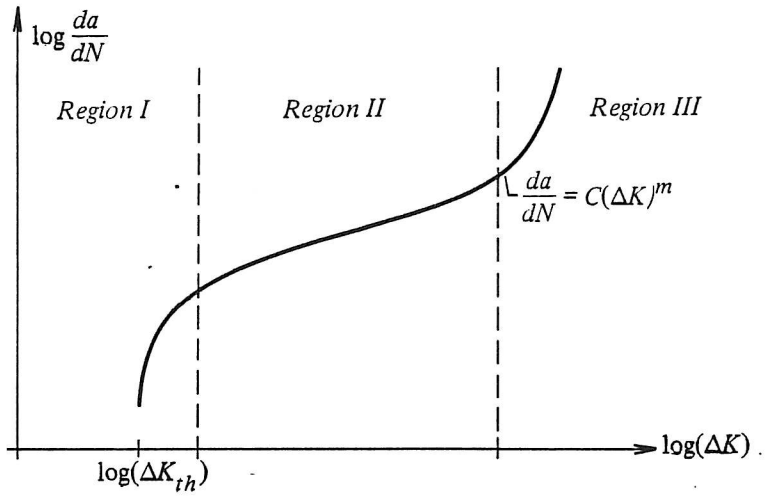

Figure 4.5.9. Schematic plot of typical fatigue crack growth data.

Crack growth in Region III is of minor importance for marine structures. The reason is that the cycle rate and the stress spectra are of such nature that the final fracture will be imminent, Almar-Næs(ed.)[b] 1985. A commonly used engineering approximation is using eq.(4.5.43) and the threshold is approximated by cutting-off. The cut-off model is conservative in the threshold region, and the deviation from a more accurate model is in many cases negligible in relation to the uncertainty associated with an assessment of the threshold. The threshold need to be considered for each case, taking into account residual stresses and mean stresses in particular.

Inserting eq.(4.5.44) into eq.(4.5.43) yields

$$\frac{da}{dN} = CY^m \hat{S}^m \left(\sqrt{\pi a}\right)^m \tag{4.5.45}$$

Assuming that C and m are independent of $\hat{S}$ and that ΔK_{th} is independent of a, the solution to eq.(4.5.45) is obtained by separating the variables and integrating

$$\int_{a_0}^{a_N} \frac{1}{CY^m \left(\sqrt{\pi a}\right)^m} \, da = \int_0^N \hat{S}^m \, dN \tag{4.5.46}$$

where a_0 is the initial crack lenght and a_N is the crack length after N stress cycles. Let Y, m, C and $\hat{S}$ be independent of a and N, and by integrating eq.(4.5.46), the crack lenght can after N cycles, a_N, be expressed as

$$a_N = \begin{cases} \left(a_0^{\left(1-\frac{m}{2}\right)} + CN\hat{S}^m \left(1-\frac{m}{2}\right) Y^m \pi^{\frac{m}{2}}\right)^{\left(\frac{1}{1-\frac{m}{2}}\right)} & m \neq 2, \Delta K \geq \Delta K_{th} \\ a_0 \, exp\left(CN\hat{S}^2 Y^2 \pi\right) & m = 2, \Delta K \geq \Delta K_{th} \\ 0 & \Delta K < \Delta K_{th} \end{cases} \tag{4.5.47}$$

The failure criterion can be written in terms of the crack length a_N as

$$a_c - a_N \leq 0 \tag{4.5.48}$$

where a_c is a critical crack length, e.g. corresponding to crack growth through the thickness of an element or to initiation of a unstable fracture.

One way of defining a damage indicator, D, in terms of the crack lenght is

$$D = \frac{a_N}{a_c} \tag{4.5.49}$$

and the failure criterion can be written as

$$1 - D \leq 0 \tag{4.5.50}$$

Using this definition it follows from eq.(4.5.47) that the damage increases with the number of stress cycles from 0 to 1.

However, laboratory experiments with the fatigue of samples clearly indicate that Y varies considerably with the crack shape and the crack lenght and must be expressed as $Y(a)$, m is not constant and in most situations the real structural elements, e.g. joints in jacket structure, are subjected to a number of widely differing stress ranges, and the initial crack lenght a_0 can vary significantly, with the result that eq.(4.5.45) cannot be obtained in a closed form.

Assuming that a_0, C, m, N and $Y(a)$ are known and by ignoring possible effect of the order of succession of the stress cycles, which include that ΔK_{th} is assumed to be equal to zero, a_N can be obtained by numerical integration

$$\int_{a_0}^{a_N} \frac{1}{CY(a)^m \left(\sqrt{\pi a}\right)^m} \, da = \sum_{i=1}^{N} \hat{S}_i^m \tag{4.5.51}$$

For a reliability analysis, this last assumption can also be relaxed and each of these variables can be modelled by random variables.

For a given service life the crack lenght a_N in a real offshore structure can be determined taking into account the long-term distribution of the stress ranges by (see section 4.2)

$$\int_{a_0}^{a_N} \frac{1}{CY(a)^m \left(\sqrt{\pi a}\right)^m} \, da = \int_0^{2\pi} \int_0^{\infty} \int_0^{\infty} \frac{T_L}{T_{mp}(t_p, h_s, \theta)} \, p_{T_p|H_s}(t_p|h_s) \, p_{H_s}(h_s) \, p_{\bar{\theta}}(\theta)$$
$$\left(\int_0^{\infty} p_{\hat{S}|T_p,H_s,\bar{\theta}}(\hat{s}|t_p, h_s, \theta) \, \hat{s}^m \, d\hat{s} \right) dt_p \, dh_s \, d\theta \tag{4.5.52}$$

where $p_{H_s}(h_s)$ is the marginal probability density function for the significant wave height H_s, $p_{T_p|H_s}(t_p|h_s)$ is the conditional probability density function for the wave spectral peak periods T_p, given H_s, $p_{\overline{\theta}}(\theta)$ is the probability density function for the mean direction of the wave propagation, $\overline{\theta}$, $p_{\hat{S}|T_p,H_s,\overline{\theta}}(\hat{s}|t_p,h_s,\theta)$ is the conditional probability density function for the stress ranges given H_s, T_p and $\overline{\theta}$, T_L is the total service life and T_{mp} is the mean period of a stress cycle within the sea state.
The fatigue failure mode for the failure element is described by a safety margin M, defined as

$$M = 1 - D \tag{4.5.53}$$

and the probability of failure P_f is

$$P_f = P(M \leq 0) \tag{4.5.54}$$

It should be underlined that using eq.(4.5.52) to obtain a_N, the possible effect of the order of succession of the sea states and the possible effect of the order of succession of the stress ranges are ignored.
To evaluate the sequence effects of the stress ranges for a given sea state, a typical stress spectrum in a hot spot is considered. The spectrum no. 8 in figure 4.5.6 with $\sigma_S = 80$ N/mm^2 is chosen as stress spectrum. The density function of the stress cycles $p_{\hat{S}}(\hat{s})$ is estimated by simulating the stress process and using the RC-method to count the stress cycles (10^6 simulations with time step $\Delta t = 0.2$ sec). The density function $p_{\hat{S}}(\hat{s})$ and the corresponding distribution $P_{\hat{S}}(\hat{s})$ are shown in figure 4.5.10. The initial crack lenght a_0 is taken as 10 mm, m is taken as 3.0, C is taken as $1.21 \cdot 10^{-13}$ and the geometry function Y is modelled as

$$Y(a) = exp\left(\left(\frac{a}{50}\right)^2\right) \tag{4.5.55}$$

where the crack length, a, is measured in mm.
Now the sequence of the stress ranges is obtained by simulation, using $P_{\hat{S}}(\hat{s})$, and the crack propagation for stress range no. i, Δa_i, is obtained as

$$\Delta a_i = C Y(a_{i-1}) \hat{S}_i^m \left(\sqrt{\pi\, a_{i-1}}\right)^m \tag{4.5.56}$$

and the crack lenght after N stress cycles a_N is

$$a_N = a_0 + \sum_{i=1}^{N} \Delta a_i \tag{4.5.57}$$

The simulation is stopped when the crack lenght $a_N \geq a_c$, where a_c is a critical crack lenght. The stimulation is carried out 1000 times for five different values of a_c,

namely a_c=15, 20, 30, 40 and 50 mm.
Typical crack propagation for a_c=50 mm is shown in figure 4.5.11.

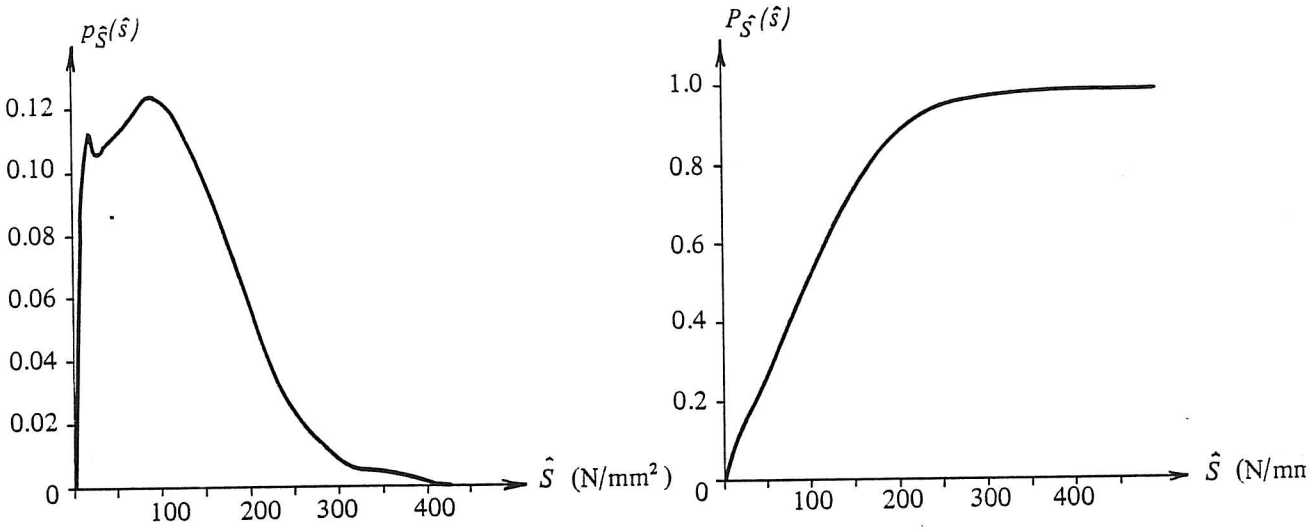

Figure 4.5.10. Density function $p_{\hat{S}}(\hat{s})$, and the corresponding distribution function $P_{\hat{S}}(\hat{s})$ of stress cycles.

The expected values $E[N]$, the standard deviation σ_N and the coefficient of variation $V[N]$ for N for the five different values of a_c are shown in table 4.5.1. A standardised density function of N, $p_N(n)$ (standardised as $E[N] = 0$ and $\sigma_N = 1$), for all five values of a_c became identical, and is shown in figure 4.5.12. As it follows from figure 4.5.12, $p_N(n)$ follows the Gaussian distribution very well, indicating that 1000 simulations are sufficient.

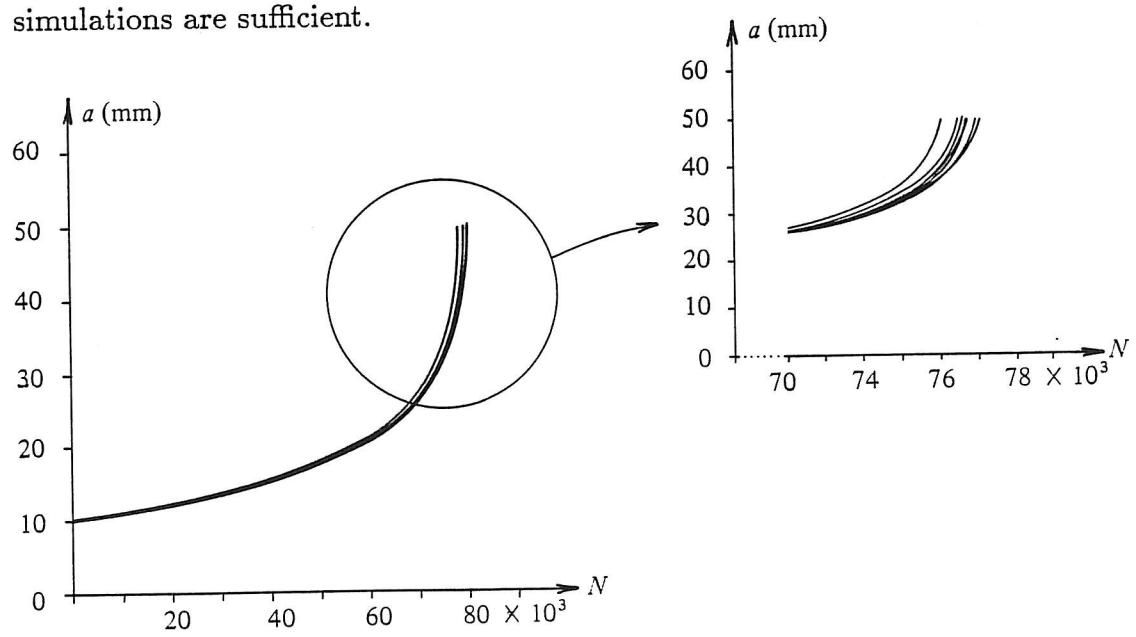

Figure 4.5.11. Typical crack propagation for a_c=50 mm.

As it follows from table 4.5.1, the coefficient of variation $V[N]$ is very small, indicating

that the effect of the order of succession of the stress cycles have minor influence on the crack propagation. It will therefore be concluded that eq.(4.5.52) can be used to estimate a_N, without gross error.

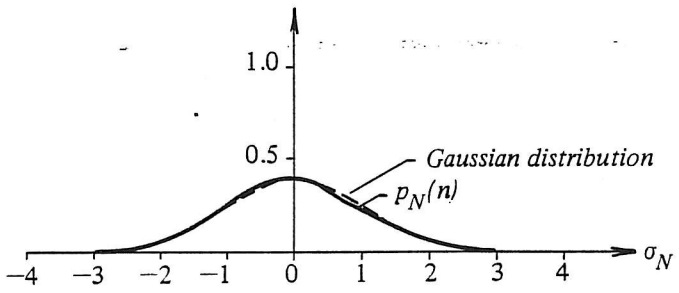

Figure 4.5.12. A standardised density function of N, $p_N(n)$.

a_c (mm)	$E[N]$	σ_N	$V[N]$
15	38412	289	0.0075
20	57634	433	0.0075
30	73564	529	0.0072
40	78282	550	0.0070
50	79554	557	0.0070

Table 4.5.1. The expected values $E[N]$, the standard deviation σ_N and the coefficient of variation $V[N]$, for the number of stress cycles N, for $a_N = a_c$, for five different values of a_c.

4.5.2.3. Bogdanoff Model

In sections 4.5.2.1 and 4.5.2.2 it was shown how a probabilistic structure in a cumulative damage model can be introduced using some deterministic models, and then introducing random variables instead of the model parameters. Another way is to assume an evolutionary probabilistic structure from the start. In this section the second approach is elaborated using the model of Bogdanoff et al.[p] 1978[1,2,3], 1980, called B-model, as starting point. The complete development of these models with examples and applications can be found in Bogdanoff & Kozin[b] 1985. The presentation here is mainly based on Bogdanoff & Kozin[b] 1985.

A basic element in the B-model is a duty cycle (DC) which is a repetitive period of operation in the life of a component during which damage may accumulate. The time x is measured in numbers of DCs and is discrete, i.e. $x = 0, 1, \ldots$. The damage is also assumed to be discrete with the states $d = 1, 2, \ldots, b$, where state b denotes a state of failure in some sense. It is assumed that the damage accumulation in a DC is non-negative and that the increment of damage at the end of a DC only depends, in a probabilistic manner, on the amount of damage present at the start of the DC and on DC itself, but it is independent of the accumulation of damage up to the start of the DC. These assumptions are the Markov assumptions and the damage process is viewed as a discrete-time, discrete-state Markov process and can be viewed as a Markov chain. The probability distribution of damage is completely determined by the transition matrix $\overline{\overline{P}} = [P_{ij}]$ for each DC and by the initial damage $\overline{p}_0$, at $x = 0$. The element P_{ij} in the transition matrix $\overline{\overline{P}}$ denotes the probability of being in state j after the DC, given that the damage is in state i at the beginning of the DC. As mentioned before, the damage accumulation in a DC is assumed to be non-negative, yielding that $P_{ij} = 0$ for $j < i$ and $\sum_{j=i}^{b} P_{ij} = 1$, $i = 1, 2, \ldots, b$. The transition matrix then has the form

$$\overline{\overline{P}} = \begin{bmatrix} P_{11} & P_{12} & \ldots & P_{1b-1} & P_{1b} \\ 0 & P_{22} & \ldots & P_{2b-1} & P_{2b} \\ \vdots & 0 & \ddots & \vdots & \vdots \\ \vdots & \vdots & \ddots & P_{b-1b-1} & P_{b-1b} \\ 0 & 0 & \ldots & 0 & 1 \end{bmatrix} \tag{4.5.58}$$

The corresponding Markov chain is shown in figure 4.5.13.

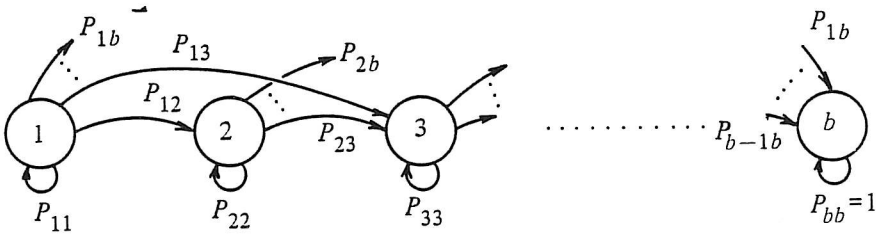

Figure 4.5.13. Markov chain with transition probabilities.

The presence of variability in the initial quality of components can be handled by

assigning a probability distribution to the initial state vector $\overline{p}_0$ as

$$\overline{p}_0 = (\pi_1, \pi_2, \ldots, \pi_b) \quad ; \quad \pi_i \geq 0, \quad \sum_{i=1}^{b} \pi_i = 1 \tag{4.5.59}$$

where π_i denotes the probability of being in state i at $x = 0$.
The state of damage at the time x is given by the vector $\overline{p}_x$ as

$$\overline{p}_x = (p_x(1), p_x(2), \ldots, p_x(b)) \quad ; \quad p_x(i) \geq 0, \quad \sum_{i=1}^{b} p_x(i) = 1 \tag{4.5.60}$$

where $p_x(i)$ is the probability that the damage is in state i at the time x.
Then, it follows from the Markov chain theory, Parzen[b] 1962, that

$$\overline{p}_x = \overline{p}_0 \prod_{i=1}^{x} \overline{\overline{P}}_i \tag{4.5.61}$$

where $\overline{\overline{P}}_i$ is the transition matrix for the ith duty cycle.
As follows from eq.(4.5.61) the probability distribution of damage is completely specified at any time and is calculated by simple matrix operations. Since matrix multiplication is generally not commutative, it follows from eq.(4.5.61) that the order of the DCs influences the damage accumulation. If all DCs have the same severity, eq.(4.5.61) reduces to

$$\overline{p}_x = \overline{p}_0 \, \overline{\overline{P}}^{x} \tag{4.5.62}$$

where $\overline{\overline{P}}$ is the common transition matrix.
In the above description the state b corresponded to failure. In many physical situations it is not possible to give such precise definition of the state that corresponds to failure. The state b at failure can be randomised, by assigning a probability at failure to a state as soon as that state is occupied, as

$$\overline{\rho} = (\rho_1, \rho_2, \ldots, \rho_b) \quad ; \quad \sum_{i=1}^{b} \rho_i = 1 \tag{4.5.63}$$

where ρ_i is the probability of being at failure in state i.
Eq.(4.5.62) is still valid when the transition matrix $\overline{\overline{P}}$ in eq.(4.5.58) is slightly modified, see Bogdanoff[p] 1978[3] for more details. Effects of inspection and replacement strategies can easily be incorporated into the B-model, see Bogdanoff[p] 1978[2] or Bogdanoff & Kozin[b] 1985. A formulation of the B-model consists in filling in the transition matrix. The number of parameters in the model is dependent on the number of state jumps from the transient state during a duty cycle. For an increasing number of

jumps during a duty cycle, the damage will increase, however, the statistical uncertainty resulting from parameter estimation based on a limited number of test results is consequently increased. Now a unit-jump version of the B-model is considered, e.g. damage can only increase in a DC from the state occupied at the start of the DC to the state one unit higher. The elements in the transition matrix $\overline{\overline{P}}$ becomes ; $P_{ii} = p_i$, $P_{ij} = q_i$ for $j = i+1$ and $P_{ij} = 0$ for $j < i$ and $j > i+1$, $i = 1, \ldots, b-1$ and $j = 1, \ldots, b-1$ i.e.

$$\overline{\overline{P}} = \begin{bmatrix} p_1 & q_1 & 0 & \ldots & 0 & 0 \\ 0 & p_2 & q_2 & \ddots & 0 & 0 \\ \vdots & \ddots & \ddots & \ddots & \vdots & \vdots \\ \vdots & \vdots & \ddots & \ddots & \vdots & \vdots \\ 0 & \ldots & \ldots & \ldots & p_{b-1} & q_{b-1} \\ 0 & \ldots & \ldots & \ldots & 0 & 1 \end{bmatrix} \tag{4.5.64}$$

The damage states are discrete and labelled $1, 2, \ldots, b$, where failure only occurs when the state b is reached, i.e. $\rho_b = 1$. The probability distribution of various random variables associated with the damage accumulation process can now be determined. Let the random variable W_b denote the time to failure at state b. Thus, the cumulative distribution function (CDF) of W_b is given by

$$F_{W_b}(x) = P(W_b \leq x) = p_x(b) \quad ; \qquad x = 0, 1, 2, \ldots \tag{4.5.65}$$

The mean value, $E[\cdot]$, and the variance, $Var[\cdot]$, of the lifetime W_b are

$$E[W_b] = \sum_{x=0}^{\infty} (1 - F_{W_b}(x)) \tag{4.5.66}$$

$$Var[W_b] = 2 \sum_{x=0}^{\infty} x\,(1 - F_{W_b}(x)) + E[W_b] - E[W_b]^2 \tag{4.5.67}$$

The CDF of the time W_i to reach state i, $F_{W_i}(x)$, can be found by eq.(4.5.65) where $p_x(b)$ is replaced with $\sum_{j=i}^{b} p_x(j)$, and the mean value and variance of W_i can be found similarly to eq.(4.5.66) and eq.(4.5.67), respectively.
The probability of damage D_x being in state j at the time x is determined by $p_x(j)$ as

$$p_x(j) = P(D_x = j) \quad ; \qquad j = 1, 2, \ldots, b \tag{4.5.68}$$

and the CDF of D_x is

$$F_{D_x}(j) = P(D_x \leq j) = \sum_{k=1}^{j} p_x(k) \qquad j = 1, 2, \ldots, b \tag{4.5.69}$$

The mean value and variance of D_x are given by

$$E[D_x] = \sum_{i=1}^{b} i\, p_x(i) \tag{4.5.70}$$

$$Var[D_x] = \sum_{i=1}^{b} (i^2 p_x(i)) - E[D_x]^2 \tag{4.5.71}$$

The time T_i spent in state i, where $i = 1, 2, \ldots, b-1$, has a geometric distribution

$$P(T_i = x) = q_i p_j^{x-1} \quad ; \quad x = 1, 2, \ldots \tag{4.5.72}$$

where q_i and p_i are the elements in the transition matrix defined in eq.(4.5.64).
The results above are all functions of the probability distribution to the initial state vector $\overline{p}_0$ and the elements in the transition matrix $\overline{\overline{P}}$. In some cases analytical results can be obtained in a closed form. This is illustrated in Bogdanoff & Kozin[b] 1985, where the analytical results are obtained by using geometrical transformations, i.e. for a stationary B-model with unit jumps the mean value and the 2nd, 3rd and the 4th central moments of W_b become

$$E[W_b] = \sum_{i=1}^{b-1}(1 + r_i) \equiv \mu_{W_b} \tag{4.5.73}$$

$$E[(W_b - E[W_b])^2] = Var[W_b] = \sum_{i=1}^{b-1} r_i(1 + r_i) \equiv \sigma^2_{W_b} \tag{4.5.74}$$

$$E[(W_b - E[W_b])^3] = \sum_{i=1}^{b-1} r_i(1 + r_i)(1 + 2r_i) \tag{4.5.75}$$

$$E[(W_b - E[W_b])^4] = 3\, Var[W_b]^2 + \sum_{i=1}^{b-1}(r_i(1 + r_i)(1 + 2r_i)(1 + 3r_i)) + \sum_{i=1}^{b-1} r_i^2(1 + r_i) \tag{4.5.76}$$

where $r_i = p_i/q_i$.

The central moments of W_i are found in a similar manner to eq.(4.5.73)-eq.(4.5.76)
Two crucial points for the applicability of the B-model are the possibilities of model

identification and parameter estimation. These points are not directly solvable since, from the outset of the model formulation, there is no immediate relation between damage and measurable physical quantities. The identification and parameter estimation, therefore, rely totally on test data.
Next it will be shown how the B-model can be formulated for fatigue crack data. Instead of using some given test data, the data are predicted by simulating the crack growth rate given by eq.(4.5.45) where C, Y and m are modelled as stochastic variables. The statistical characteristics for the stochastic variables are shown in table 4.5.2.

Variable	Distribution	Expected value	Coefficient of variation
C	LN	$1.21 \cdot 10^{-13}$	0.20
Y	LN	1.12	0.05
m	N	3.0	0.01

Table 4.5.2. Statistical characteristics for the stochastic variables.
(N: normal, LN: log-normal)

The simulation here is carried out 100 times for constant amplitude DCs, namely $\hat{S} = 50\text{N/mm}^2$. The initial crack size, a_0, is assumed to be constant, i.e. $a_0 = 10$ mm, and failure is defined in terms of the crack size $a = 50$ mm. The sample functions (SFs) of the fatigue crack growth for the 100 simulations are shown in figure 4.5.14.

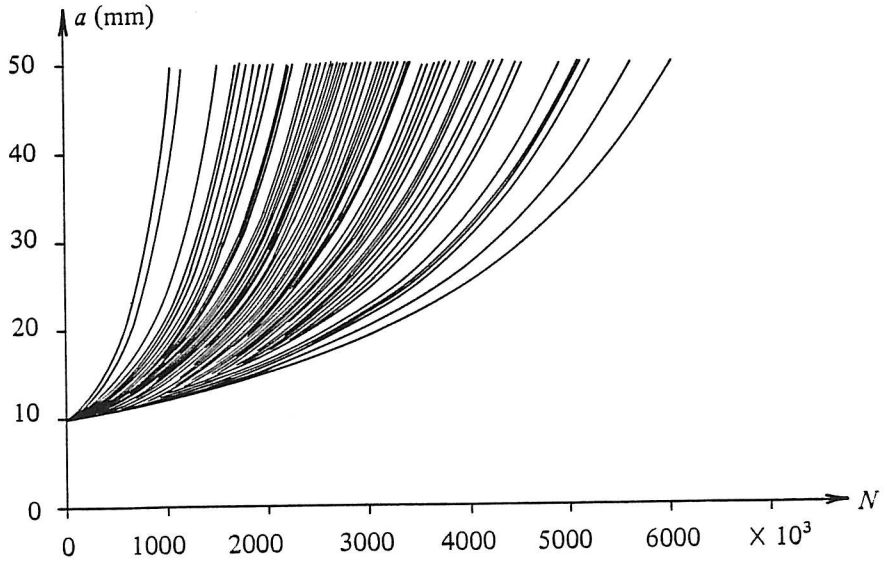

Figure 4.5.14. The sample functions of fatigue crack growth (simulation results).

The empirical distribution function (EDF) of the number of stress cycles N to reach 7 different crack lengths, $F(N|a)$, is shown in figure 4.5.15, and the estimated mean

value $\hat{\mu}_{N|a}$ and the standard deviation $\hat{\sigma}_{N|a}$ for the same crack lengths are shown in table 4.5.3.

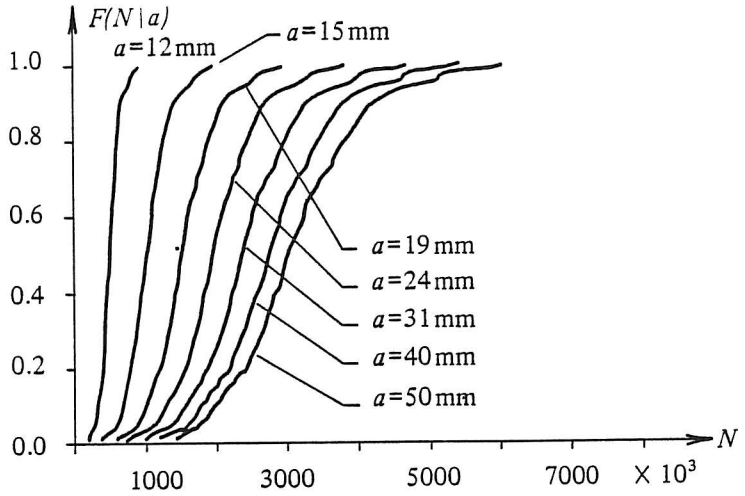

Figure 4.5.15. The EDFs of the number of stress cycles to reach 7 different crack lengths,
namely a=12, 15, 19, 24, 31, 40, 50 mm, (simulation results).

a (mm)	$\hat{\mu}_{N\|a}\ 10^{-3}$	$\hat{\sigma}_{N\|a}\ 10^{-3}$
12	491	141.3
15	1034	298.8
19	1548	449.0
24	1999	582.2
31	2437	712.6
40	2822	828.1
50	3121	918.7

Table 4.5.3. Estimate of the mean value and standard deviation of N for some given crack lengths (simulation results).

To formulate a B-model to describe the above data, it is necessary to know the estimates of the mean value and the variance of the number of cycles N to reach a crack length for at least one value of a. Clearly, $\pi_1 = 1$, since the initial crack size is assumed to be constant. Assume a stationary model with unit jumps and r_i constant in blocks.
First, assume that there are only data for N to reach a=50 mm, i.e. one block model, and take 1 DC as 10^3 stress cycles. From table 4.5.3 it follows that

$$\hat{\mu}_{N|a=50mm} = 3121 \cdot$$

$$\hat{\sigma}_{N|a=50mm} = 918.7$$

All simulations terminate at a=50 mm thus ρ_b=1. Using eq.(4.5.73) and eq.(4.5.74), remembering b must be an integer, it follows

$$b = 13$$

$$r_i = 259.1 \quad ; \quad i = 1, 2, \ldots, b-1$$

The mean sample function of state versus N is a straight line, which obviously cannot relate intermediate states to the crack length. However, the EDF of N to reach a=50 mm, obtained from the test data can be compared with the CDF generated by the B-model, see figure 4.5.16.

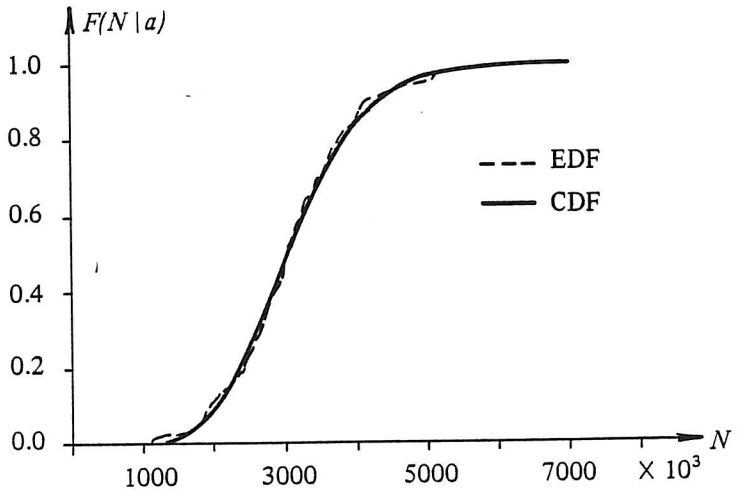

Figure 4.5.16. Comparison of the EDF of N to reach the crack length a=50 mm obtained from the predicted test data and CDF generated by the B-model.

It follows from figure 4.5.16 that the CDF generated from the B-model is very close the EDF obtained from the predicted test data.

Now assume that there exsist data for N to reach 7 different crack lengths, as shown in table 4.5.3, i.e. the 7 block model. Still assuming a stationary B-model with unit jumps, r_i constant in each block, ρ_b=1 and 1 DC is taken as 10^3 stress cycles. The model parameters b_i and r_i, for each block can now be obtained using eq.(4.5.73) and eq.(4.5.74), e.g.

for block 1, 10 mm $\leq$ a $\leq$ 12 mm

$$491 = (b_1 - 1)(1 + r_1)$$

$$141.3^2 = (b_1 - 1)r_1(1 + r_1)$$

and for block 2, 12 mm $\leq a \leq$ 15 mm

$$1034 = (b_1 - 1)(1 + r_1) + (b_2 - b_1)(1 + r_2)$$

$$298.8^2 = (b_1 - 1)r_1(1 + r_1) + (b_2 - b_1)r_2(1 + r_2)$$

The model states and r_i values for the 7 different blocks are shown in table 4.5.4.

states j	r_i
1,...,12	39.92
13,...,17	107.60
18,19,20	170.33
21,22	224.50
23	437.00
24	384.00
25	298.00

Table 4.5.4. The model states and r_i for the 7 different blocks

Each model state corresponds to a unique value of a. This relationship can be determined as follows: Each model state i has a mean number of cycles to reach the state i. The corresponding crack length a_i can be determined by requiring that the mean number of cycles to reach a_i much be the same as the number of cycles to reach state i. The relations thus obtained are shown in figure 4.5.17.

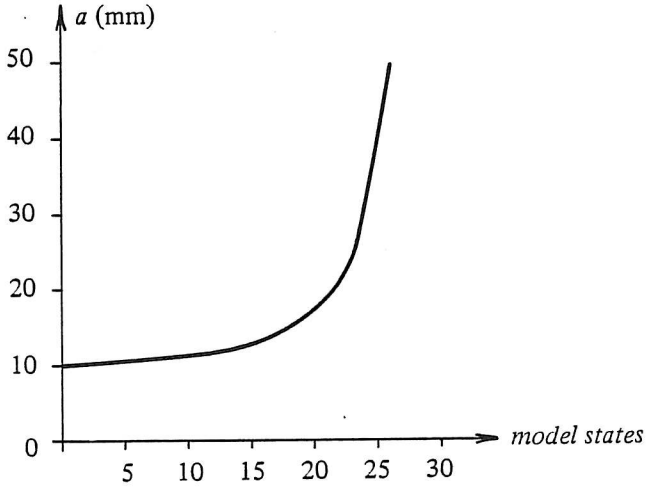

Figure 4.5.17. The relationship of the model states and the crack lengths.

Obviously, each a does not correspond to a model state since the model states are discrete. Now it is examined how well the model describes the data. Consider first the mean value and the standard deviation of N to reach a. It follows from figure 4.5.18 that the agreement is rather good. In the B-model the mean values are a little overestimated and the standard deviation is a little underestimated for $a \geq$40 mm.

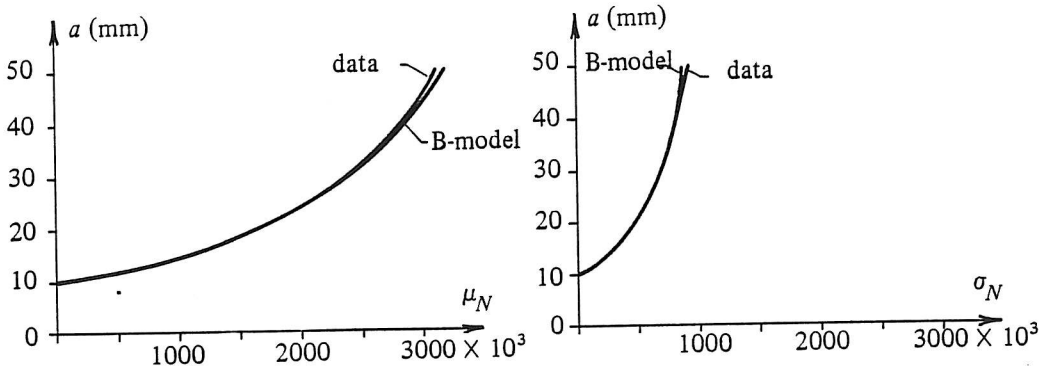

Figure 4.5.18. Comparison of the mean values and standard deviations of N to reach the crack length a

Now compare the EDFs of N to reach a obtained from the data and the corresponding CDFs obtained from the model. First the 7 values of a used to formulate the model are considered, see table 4.5.3. The results are shown in figure 4.5.19 a). Then consider a value of a which was not used to formulate the model, namely a=13 mm (which corresponds to state no. 15). The result is shown in figure 4.5.19 b). In all cases the agreement was good in the central and the upper region, but in the lower region, the CDFs rise too late (unconservative). These features of the CDFs is due the fact that the higher order central moment are not taken into account. The higher order moments cannot be taken into account in this model. However, they can be taken into account by changing from constant r_i in each block to variable r_i within blocks. The number of higher order moments is depending on the number of parameters used to describe r_i.
Comparing the results for a=50 mm in figure 4.5.16 and figure 4.5.19 a), it follows that the agreement is better in figure 4.5.16 where only the data on N to reach a=50 mm are used.

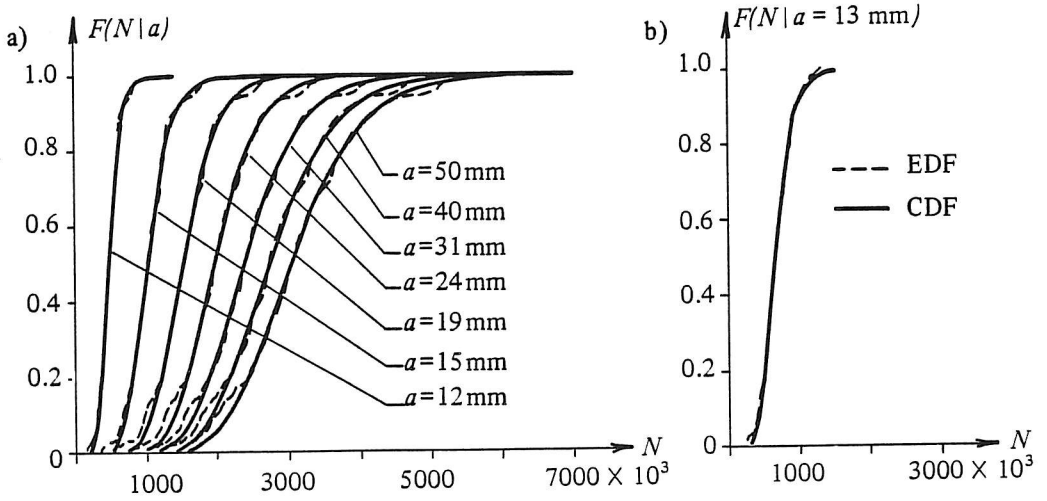

Figure 4.5.19. Comparison of EDFs and CDFs for 8 different crack lengths.

Above, it is shown how the stationary version of the B-model can be formulated from constant amplitude load data. However, in real structures, like offshore structures, the load (stress) amplitudes are not constant.
In section 4.4 it is shown how, for a given sea state, the stress spectrum in failure elements (hot spots) can be estimated, and in section 4.5.1 it is shown how the density function for the stress amplitudes can be estimated for a given stress spectrum. Using the B-model to predict life behaviour under a spectrum of loads, experimental testing under this type of loading is needed, because up to now there has been no satisfactory analytical method for combining the duty cycles of various severity to obtain reliable estimates of life behaviour, Bogdanoff & Kozin[b] 1985. The key problem in this kind of test is to infer life behaviour under a spectrum of loads, given the constant load cycles life behaviour for each of the components of the spectrum. The solution of this problem depends on those aspects of life behaviour concerned and on the generation of realisations for the test purposes. Next it is described how the spectrum and how the realisations of the stress cycles for testing might be generated for offshore structures. Taking into account the long-term distribution of the sea states (see section 4.2) the lifetime of the components (hot spots) can be divided into a finite number n of short-term periods with a constant length ΔT, denoted as sea state L_i with the probability p_{L_i}, $i = 1, \ldots, n$, where the stress process in the components can be characterised by a spectrum. For a given sea state L_i the density function for the stress amplitudes and the mean period of the peaks (local maxima) $T_{mp}(i)$ can be estimated e.g. by using the RC-method, see section 4.5.1. For each L_i the respective density function is discretized into a set l_{ij}, $j = 1, \ldots, m$, of single stress cycles, each having the probability $p_{l_{ij}}$. The experiens suggest that the sea states and the stress cycles in a given sea state do not come in strictly random order, i.e. the sea states of similar type are frequently grouping and the stress cycles of the same size come frequently grouping too. A number of methods exist for generating SFs having a specified long-term distribution of stress cycles, i.e $\{L_i,\ p_{L_i},\ l_{ij},\ p_{l_{ij}}\}$. In Bogdanoff & Kozin[b] 1985 three methods are measured and can be formulated as follows

1 Select successive L_is on a random basis using p_{L_i}. For each L_i the l_{ij}s are selected successively on a random basis by using $p_{l_{ij}}$ until the number of cycles is equal to $\Delta T / T_{mp}(i)$.

2 Form blocks, each having the same number of sea states L_i of just one type. For each block of L_i, form blocks, each having the same number of stress cycles l_{ij} of just one type. Select successive blocks of L_is on a random basis using p_{L_i}. For each block of L_i, the blocks of l_{ij}s are selected successively on random basis by using $p_{l_{ij}}$.

3 Form blocks of variable numbers of sea states L_i of just one type, where the numbers of L_i in each block is proportional to p_{L_i}. For each block of L_i, form blocks of variable number of stress cycles l_{ij}, where the number of l_{ij} in each block is proportional to $p_{l_{ij}}$. Select successive blocks of L_is randomly. For each block of L_i the blocks of l_{ij}s are selected successive randomly.

Each of the above methods represents the same long-term distribution of stress cycles, in the sense that, after suitably long time, all L_is will have occurred with relative frequencies close to or equal to p_{L_i} and the relative frequencies of l_{ij}s will be close to or equal to $p_{l_{ij}}$. In method 1, where the order of stress cycles is completely random, no characteristic stress cycles versus time patterns for the stress process are produced while methods 2 and 3 appear to be suitable for providing distinctive stress cycles versus time patterns, since the stress cycles are grouped, i.e. the blocks of L_i and l_{ij} have a suitable size relative to the lifetime and the total number of stress cycles in given sea state, respectively. The next point to consider is how the testing is to be carried out. All specimens can either be subjected to exactly the same realisation of stress cycles or each specimen can be subjected to randomly selected realisations of stress cycles. It is clear that the two methods of testing may give different results, which will be explained later.

Now method 2 for generating sample function of stress cycles using B-model will be considered.

For each block of L_i, the transition matrix $\overline{\overline{P}}_{ij}$ is formulated for each block of l_{ij}, i.e. if the number of sea states in each block is equal to N_1 and the number of stress cycles in each block in the sea state is equal to N_2 the $\overline{\overline{P}}_{ij}$ will be formulated based on a block size of $N_1 \times N_2$ stress cycles.

Let the $\{\overline{\overline{Q}}_k\}$ denote a sequence of the $\overline{\overline{P}}_{ij}$ generated by $\{L_i,\ p_{L_i},\ l_{ij},\ p_{l_{ij}}\}$. Thus each $\overline{\overline{Q}}_k$ is independently and randomly selected from $\overline{\overline{P}}_{ij}$, $i = 1, \ldots, n$, $j = 1, \ldots, m$, using the p_{L_i} and $p_{l_{ij}}$, and for each sample load sequence, the $\{\overline{\overline{Q}}_k\}$ represents a specific ordering of the $\overline{\overline{P}}_{ij}$. However, $\{\overline{\overline{Q}}_k\}$ may also be regarded as a sequence of independent random variables, since the each $\overline{\overline{Q}}_k$ is independently selected from the $\overline{\overline{P}}_{ij}$ with the probability $p_{L_i} \times p_{l_{ij}}$.

The state of damage at the time x is then given by (see eq.(4.5.61))

$$\overline{p}_x \;=\; \overline{p}_0 \prod_{k=1}^{x} \overline{\overline{Q}}_k \tag{4.5.77}$$

where x is the time in block units, where the block size is equal to $N_1 \times N_2$ stress cycles.

Following eq.(4.5.65) the CDF of the time to failure in state b, W_b, is given by

$$F_{W_b}(x) \;=\; p_x(b) \tag{4.5.78}$$

Since $\{\overline{\overline{Q}}_k\}$ is a sequence of random variables $\overline{p}_x$ and F_{W_b} become random functions of x. However, for a specific sample load sequence $\{\overline{\overline{Q}}_k\}$, $\overline{p}_x$ and F_{W_b} become deterministic functions.

Assuming that $\overline{p}_0$ is deterministic, and taking the expectation of eq.(4.5.77) at fixed but arbitrary x, it follows that

$$E[\overline{p}_x] \;=\; \overline{p}_0 \,(E[\overline{\overline{Q}}])^x \tag{4.5.79}$$

where

$$E[\overline{\overline{Q}}] = \sum_{i=1}^{n}\sum_{j=1}^{m} p_{L_i}\, p_{l_{ij}}\, \overline{\overline{P}}_{ij} \tag{4.5.80}$$

The expected value and the variance of the CDF of W_b can be expressed as

$$E[F_{W_b}(x)] = E[p_x(b)] \tag{4.5.81}$$

$$Var[F_{W_b}] = E[F^2_{W_b}(x)] - (E[F_{W_b}(x)])^2 \tag{4.5.82}$$

where the $Var[F_{W_b}]$ can be estimated by simulation.
The difference between the to different testing methods will then be evaluated. If all specimens are tested with exactly the same sequence of stress cycles $\{\overline{\overline{Q}}_k\}$, the EDF of W_b of the specimens will in this case approximate one sample CDF, but the location of this sample CDF, with respect to all sample CDFs, will in general be unknown. However, if the variance of $F_{W_b}(x)$ is small this uncertainty will not be important, while for a large variance the uncertainty can become significant.
If each specimen is tested under a randomly selected sequence of stress cycles $\{\overline{\overline{Q}}_k\}$, the EDF of W_b of the specimens in this case will approximate the $E[F_{W_b}]$.

4.6. Application

In the sections above a method for estimating the probability of fatigue failure is briefly described. To make this method applicable a new computer package "SAOFF" (Stochastic Analysis Of Fatigue Failure) has been made. The program package which contains approx. 7000 source lines written in FORTRAN77, consists of five calculation blocks, namely:

1) STIFFMAS
This program reads the structural data and creates the global stiffness and mass matrices for the structure.

2) EIGEN
This program evaluates the n smallest eigenfrequencies and corresponding eigenvectors (mode shapes), where n is defined by the user.

3) MODAL
This program is the most complex and time-consuming part of the whole program package. Here the 0-,2- and 4-moments of the cross-spectral density of the modal displacements are evaluated, namely (see chapters 3 and 4 for more details):
0-moment:

$$m_0 = \int_0^\infty S_{q_i q_j}(\omega) d\omega$$

2-moment:

$$m_2 = \int_0^\infty \omega^2 S_{q_i q_j}(\omega) d\omega$$

4-moment:

$$m_4 = \int_0^\infty \omega^4 S_{q_i q_j}(\omega) d\omega$$

4) SIGMA
In this program the auto-spectral densities and their moments for the hot spot stresses in joints defined by the user are evaluated. (Here the SCFs are taken into account in the calculation of T_{ki} and T_{kj}).

5) RELIA
In this program the probability of fatigue failure of failure elements in the joints (which was defined in SIGMA) is estimated. Here the user can choose between 3 different estimates of the distribution of the stress amplitudes $p_{\hat{S}}(\hat{s})$, namely:
1) Rayleigh distribution (narrow-banded approach)
2) Distribution defined by the RFC-method (simulation)
3) Distribution defined by the RC-method (analytical estimation or simulation).

The user can choose between two different damage accumulation models, namely the Miner rule described in section 4.5.2.1, where the rainflow damage factor λ_{RFC} defined in eq.(4.5.24) is included and the fracture mechanics models described in section 4.5.2.2. The Bogdanoff model described in section 4.5.2.3 has not yet been included in the program. The systems probability of fatigue failure is estimated by using Hohenbichler approximation, Hohenbichler[p] 1983.

Example 4.6.1

Consider the model of a steel jacket offshore platform shown in figure 4.6.1. All structural elements are tubular beam elements made of steel with modulus of elasticity $E = 0.205 \cdot 10^9$ kN/m^2 and density $\rho = 7800$kg/m^3.
The cross-sectional diameters and thicknesses are shown in table 4.6.1. The foundation is modelled as elastic springs with horizontal stiffness equal to $1.2 \cdot 10^5$kN/m, vertical stiffness equal to 10^6 kN/m and rotational stiffness equal to $1.2 \cdot 10^6$kNm/rad. The total mass of the deck is assumed to be $4.8 \cdot 10^6$kg. The service life of the structure is taken as 25 years.
The calculation is carried out by considering 3 directions of average wave propagation $\overline{\theta}$, namely $\overline{\theta}_1 = 0^o$ (x-direction), $\overline{\theta}_2 = 45^o$ and $\overline{\theta}_3 = 90^o$ (y-direction), where $\overline{\theta}$ is defined in figure 4.6.1. All three directions are assumed to have the same probability $p_{\overline{\theta}_i} = \frac{1}{3}$, $i = 1, 2, 3$. Long crested waves are assumed ($n = 0$ in eq.(4.2.17)).

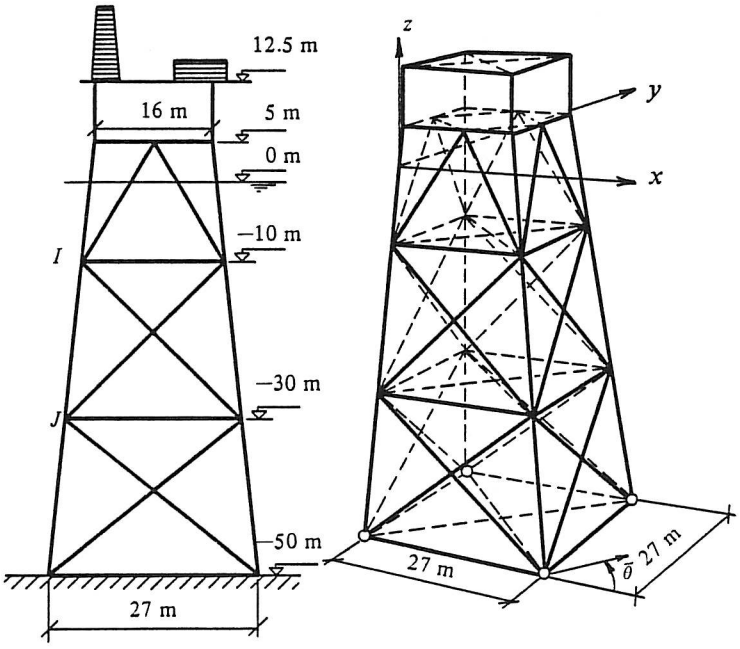

Figure 4.6.1 Steel jacket offshore platform.

The parameter in the long-term probability density function of the significant wave height H_s, $p_{H_s}(h)$, and conditional probability density function of the wave spectral peak periods T_p given H_s, $p_{T_p|H_s}(t|h)$ are estimated by fitting observations from the

northern part of the North Sea in the period 1980-1983 (8222 observations), see Haver & Nyhus[p] 1986 for more details. The parameters are (see eq.(4.2.21) and eq.(4.2.22)):

$\sigma^2_{H_s} = 0.376, \quad \mu_{H_s} = 0.836, \quad \upsilon = 3.27$ m, $\quad \rho = 2.822, \quad \xi = 1.547$

$\mu_{T_p} = 1.59 + 0.42\ ln(h_s + 2)$

$\sigma^2_{T_p} = 0.005 + 0.85\ exp\left(-0.13\ h_s^{1.35}\right)$

Members	Diameter (m)	Thickness (m)
deck legs	2.00	0.050
jacket legs	1.20	0.016
braces (vertical plane)	1.20	0.016
braces (horizontal plane):		
level +5	0.80	0.008
level -10	1.20	0.014
level -30	1.20	0.014
level -30 (diagonal)	1.20	0.016
level -50	1.20	0.014

Table 4.6.1 Cross-sectional data for structural elements.

The total damage calculation for each failure element is carried out by considering 45 sea states (15 sea states for each direction $\overline{\theta}$, see table 4.6.2).

H_s (m)	$P(H_s)$	T_p (sec)	$P(T_p\|H_s)$
0.8	0.30924	5.8	0.366318
		7.9	0.442132
		11.5	0.191550
2.5	0.42741	7.1	0.306097
		9.2	0.447116
		12.6	0.246787
4.3	0.22634	8.9	0.331933
		10.6	0.439235
		14.0	0.228832
7.9	0.03621	11.2	0.293697
		12.8	0.432785
		14.9	0.273518
12.0	0.00080	13.6	0.312393
		14.9	0.452909
		16.7	0.234698

Table 4.6.2. The sea states under consideration and their probabilities.

In figure 4.6.1 two joints in the structure are considered, namely joints I and J (two TK-joints with 12 failure elements). Detailed data and numbering of failure elements for the joints under consideration are shown in figure 4.6.2. The location of failure elements in the chord/brace intersection is determined by checking 8 points along the chord/brace intersection, see figure 4.5.3.
The Miner rule is used for damage accumulation (see section 4.5.2.1). The stochastic variables D_{fail} and B are assumed to be uncorrelated, but they are assumed to be fully correlated between failure elements and with the same statistical characteristics, respectively.. m and $log\ K$ are assumed to have correlation coefficient equal to -0.44 for each failure element, but uncorrelated between failure elements. The statistical characteristics for the stochastic variables are shown in table 4.6.3.

Basic variable	Variable	Distri-buted	Expected value	Standard deviation
X_1	D_{fail}	N	1.0	0.1
X_2	B	LN	1.0	0.2
$X_3, \ldots X_{14}$	$K_1, \ldots K_{12}$	LN	6400N/mm^2	1024N/mm^2
$X_{15}, \ldots X_{26}$	$m_1, \ldots m_{12}$	N	3.8	0.095

Table 4.6.3. Statistical characteristics for the stochastic variables (N: normal, LN: log-normal).

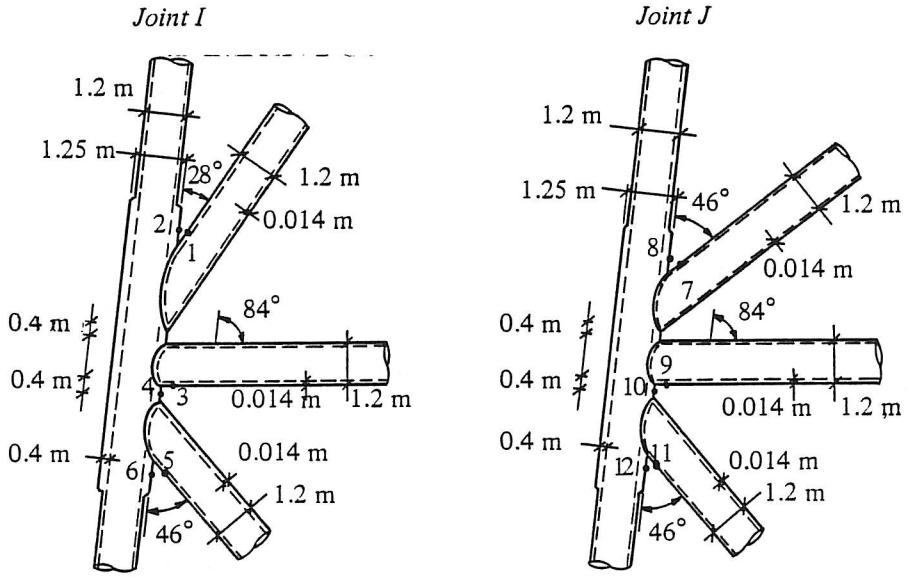

Figure 4.6.2. Detailed data and location of failure elements for joints under consideration (• means failure element).

The drag coefficient C_D in Morison's equation is taken as 1.3, but the coefficient of inertia C_M is assumed to vary as, Karadeniz[p] 1985 :

$$C_M = \begin{cases} 2 & \text{for } 0 \leq x \leq 0.6 \\ 2(1.65\ exp(-0.8974\ x)) & \text{for } 0.6 < x < 2.0 \\ 2(0.798/\sqrt{x^3}\ ) & \text{for } x \geq 2.0 \end{cases}$$

where $x = \frac{D}{2g}\,\omega^2$ in which D denotes a member diameter, g denotes the acceleration of gravity and ω is the frequency.

The number of eigenfrequencies (and mode shapes) in the modal analysis is taken as 3 and the damping ratio ζ is taken as 1 % for all mode shapes. The significant failure elements are defined as the failure elements which have safety indices less than $\beta_{min} + 1.5$, where β_{min} is the lowest safety index for the failure elements. The three lowest eigenfrequencies are obtained as:

$$\omega_1 = 3.01\ rad/sec$$
$$\omega_2 = 3.01\ rad/sec$$
$$\omega_3 = 6.48\ rad/sec$$

A run of the program SIGMA showed that the irregularity factor, α ($=\frac{m_2}{\sqrt{m_0\, m_4}}$, where m_i is the ith moment of the stress spectra), of the stress spectra in the failure elements is 0.37-0.6 for most of the sea states which means wide-banded stress spectra.
In figure 4.5.6 the normalised stress spectrum (normalised as $m_0 = 1.0$) for failure element no. 1, for the 15 different sea states, shown in table 4.6.2, for $\overline{\theta} = 0^o$, is shown.

The distribution of stress amplitudes is estimated by :

1 : Rayleigh distribution.

2 : Distribution defined by the RFC-method.

3 : Distribution defined by the RC-method.

Four not fully correlated significant failure elements are identified. They are given in table 4.6.4

Failure element i	1	7	12	11	System reliability index β^s
Rayleigh β_i	2.08	2.69	3.31	3.39	2.03
Rayleigh* β_i	2.32	2.83	3.54	3.63	2.27
RFC β_i	2.32	2.78	3.59	3.74	2.25
RC β_i	2.77	3.09	4.14	4.25	2.67

Table 4.6.4. Safety indices for the significant failure elements and Hohenbichler approximation of the system reliability index. (Rayleigh* β denote the reliability indices where the rainflow damage factor λ_{RFC} is used).

The correlation coefficient matrix of the linearized safety margins of the significant failure elements is:

$$\bar{\bar{\rho}} = \begin{bmatrix} 1.0 & 0.65 & 0.65 & 0.65 \\ & 1.0 & 0.65 & 0.65 \\ \text{sym.} & & 1.0 & 0.65 \\ & & & 1.0 \end{bmatrix}$$

As it can be seen from table 4.6.4, there are significant differences between the safety indices of a failure element dependent on the estimate of the distribution of the stress amplitudes. The safety indices obtained by using the Rayleigh distribution combined with the rain flow damage factor λ_{RFC} give a good estimation of the safety indices obtained by the RFC-method. The same results for the RC β_i were obtained by estimate the probability density functions of the stress cycles by simulation and by using the estimate given by eq.(4.5.11). In figure 4.6.3 a typical probability density function of the stress cycles, for a given sea state, in a failure element, estimated by the above methods is shown.

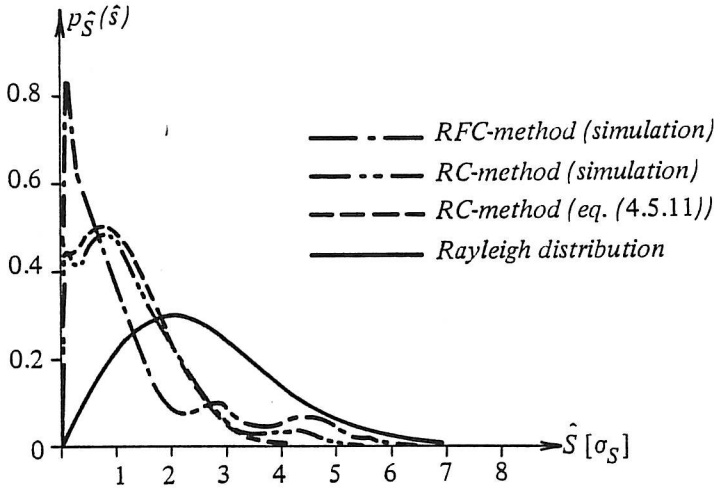

Figure 4.6.4 Estimation of the distribution density function of the stress amplitude, in a failure element, for a given sea state.

4.7. Conclusions

In this chapter a method to estimate the reliability of offshore structures subjected to wave loads in deep water environments is discussed. Failure modes corresponding to fatigue failure are considered. The reliability is estimated using a first-order reliability method and failure of the structure is defined as the event that one of the failure elements fails. To estimate statistical values of structural stress variations the modal spectral analysis method is applied.

Two methods to estimate the distribution of the stress cycles for a given stress spectral density are presented, namely the rain-flow-counting (RFC) method and the range-counting (RC) method. Three different models to estimate the damage in the failure elements are presented. Two deterministic models, where the uncertainties are taken into account by introducing random variables instead of the model parameters and one model where an evolutionary probabilistic structure is assumed from the start.

A new program package "SAOFF" (Stochastic Analysis Of Fatigue Failure) is presented. As an example a jacket structure is considered. The distribution function of the stress amplitudes, for a given sea state, is estimated by the Rayleigh distribution, a distribution obtained by the RFC method and a distribution obtained by the RC method. For most of the sea states under consideration the stress processes became broad-banded. Therefore, the results by using the Rayleigh distribution to estimate the distribution of the stress cycles cannot be expected to give satisfactory results. However, by taking into account the so-called rainflow damage factor, the results obtained using the Rayleigh distribution become very close to the results obtained using the RFC method. By comparing the results obtained using the RFC and the RC methods it is shown that the method used to define a stress cycle has significant influence on the results. This means that the definition of the stress cycles must be taken into account in the calibration of the model parameters and in the evaluation of the results. For this purpose more experimental and theoretical work are needed.

5. CONCLUSIONS

The development of some applicable methods for evaluating the reliability of offshore structure is studied.

Two different definitions of system failure modes of the structure are used, namely a failure mode due to formation of a mechanism (collapse), and failure mode due to a fatigue failure.

In chapter 2 a brief introduction of the reliability theory relevant in the thesis on structural reliability analysis is given.

In chapter 3 a system reliability analysis, with respect to plastic collapse, of truss and frame structures of ideal rigid-plastic materials, is discussed. Section 3.2 contains a general theory of plasticity for frame and truss structures. The reliability analysis is carried out using the upper-bound theorem of plasticity (kinematic theorem of mechanisms). A technique for identifying the most significant failure modes is presented. It is shown that the most significant failure modes depend significantly on the type of the cross-section. A new program package "COLLAPSE", which is based on the methods and assumptions described in sections 3.2 - 3.4, is presented. The program package is illustrated by two example, i.e. two different models of steel jacket offshore platforms. One of the examples has been analysed before in the literature, but a different method was used. The results obtained here are well in accordance with the results found in the literature.

Chapter 4 contains a reliability analysis of offshore structures, subjected to wave loads, with respect to fatigue failure. In section 4.2 a probabilistic modelling of the sea states is described, and both short-term and long-term modelling are considered. Section 4.3 contains a probabilistic modelling of the wave loading acting on the structural element, for a given sea state. In section 4.4 a structural response is considered. Section 4.5 contains stochastic modelling of fatigue failure. Two methods to estimate the distribution of the stress cycles for a given stress spectral density are described, namely the rain-flow-counting (RFC) method and the range-counting (RC) method. Three different models to estimate the damage in the failure elements are discussed. Two deterministic models, where the uncertainties are taken into account by introducing random variables instead of the model parameters, and one model where an evolutionary probability structure is assumed from the start. A new program package "SAOFF" (Stochastic Analysis Of Fatigue Failure), which is based on the methods and assumptions described in sections 4.2 - 4.5, is presented. As an example a jacket structure is considered. The distribution function of the stress amplitudes, for a given sea state, is estimated by the Rayleigh distribution, a distribution obtained by the RFC method and a distribution obtained by the RC method. For most of the sea states under consideration the stress processes became broad-banded. Therefore, the use of Rayleigh distribution to estimate the distribution of the stress cycles cannot be expected to give satisfactory results. However, by taking into account the so-called rainflow damage factor, the results obtained using the Rayleigh distribution become

very close to the results obtained using the RFC method. By comparing the results obtained using the RFC and the RC methods it is shown that the method used to define a stress cycle has significant influence on the results. This means that the definition of the stress cycles must be taken into account in the calibration of the model parameters and in the evaluation of the results. For this purpose more experimental and theoretical work are needed.

No examples have been found in the literature to compare the results obtained by "SAOFF".

6. BIBLIOGRAPHY

Books

Almar-Næs, A. (ed.) :
Fatigue Handbook. Tapir Publishers, Trondheim, 1985.

Augusti, G., A. Baratta & F. Casciati :
Probabilistic. Methods in Structural Engineering.
Chapman and Hall, London New York, 1984.

Bathe, K. -J. :
Finite Element Procedures in Engineering Analysis.
Prentice-Hall, Inc., Englewood Cliffs, New Jersey, 1982.

Bogdanoff, J. L. & F. Kozin :
Probabilistic Models of Cumulative Damage.
John Wiley & Sons, Inc., USA, 1985.

Clough, R. W. & J. Penzien :
Dynamics of Structures.
McGraw-Hill Kogakusha, Ltd, 1975.

Conte S. D. & Carl de Boor :
Elementary Numerical Analysis, an Algorithmic Approach.
McGraw-Hill Kogakusha, Ltd, 1972.

Hodge, P. G. :
Plastic Analysis of Structures.
McGraw-Hill Book Company, New York Toronto London, 1959.

Lin, Y. K. :
Probabilistic Theory of Structural Dynamics.
McGraw-Hill International Book Company, 1967.

Langen, I. & R. Sigbjørnsson :
Dynamisk Analyse av Konstruksjoner (in Norwegian).
Tapir Publishers, Trondheim, 1979.

Kuester J. L. & J. H. Mize :
Optimization Techniques with Fortran.
McGraw-Hill Book Company, 1973.

Madsen, H. O., S. Krenk & N. C. Lind :
Methods of Structural Safety.
Prentice-Hall, Inc., Englewood Cliffs, New Jersey, 1986.

Melchers, R. E. :
Structural Reliability.
Ellis Horwood Limited, England, 1987.

Neal, B. G. :
Plastic Methods of Structural Analysis.
Chapman & Hall Ltd, 1970.

Parzen, E. :
Stochastic Process.
Holden-Day, San Francisco, 1962.

Sarpkaya, T. & M. Isaacson :
Mechanics of Wave Forces on Offshore Structures.
van Nostrand Reinhold Co., 1981.

Thoft-Christensen, P. & M. J. Baker :
Structural Reliability Theory and Its Applications.
Springer-Verlag, Berlin Heidelberg New York, 1982.

Thoft-Christensen, P. & Y. Murotsu :
Application of Structural Systems Reliability Theory.
Springer-Verlag, Berlin Heidelberg New York Tokyo, 1986.

Theses

Bjerager, P. :
Reliability Analysis of Structural Systems.
Series R, Report No. 183, January, Department of Structural Engineering, Technical University of Denmark, Lyngby, Denmark, 1984.

Ortiz, K. :
On the Stochastic Modeling of Fatigue Crack Growth.
Ph.D. Dissertation, Stanford University, USA, 1985.

Sørensen, J. D. :
Pålidelighedsanalyse af statisk og dynamisk belastede elasto-plastiske ramme- og gitterkonstruktioner. (In Danish).
Structural Reliability Theory Series, Report No. R8402, March, Institute of Building Technology and Structural Engineering, University of Aalborg, Denmark, 1984.

Papers

Ang. A. H.-S. & H.-F. Ma. :
On the Reliability Analysis of Framed Structures.
Proc. of the ASCE Special Conf. on Probabilistic Mechanics and Structural Reliability, Tucson, January, 1979, pp. 106-111.

ASCE Papers on Fatigue and Fracture Reliability :
Committee on Fatigue and Fracture and Fracture Reliability.
Journal of the Structural Division, ASCE, Vol. 108, 1982, pp. 1-88.

Atalik, T. S. & S. Utku :
Stochastic Linearization of Multi-Degree-of-Freedom Non-Linear System.
Earthquake Engineering and Structural Dynamics, Vol. 4, 1976, pp. 411-420.

Baker, M. J. :
Supplementary Notes on Fatigue and Fracture Reliability of Offshore Structures.
Structural Safety and Reliability: Theory and Practice, Short Course,
September 1985.

Bjerager, P., A. Karamchandani & C. A. Cornell :
Failure Tree Analysis in Structural System Reliability.
Reliability and Risk Analysis in Civil Engineering, Lind, N. C. (ed.)
ICASP5, May, University of Waterloo, Canada, 1987, pp. 985-996.

Bjerager, P. :
Plastic Systems Reliability by LP and FORM.
DCAMM Report No. 368, December, The Technical University of Denmark, Lyngby,
Denmark, 1987.

Bogdanoff, J. L. :
A New Cumulative Damage Model, Part 1.
ASME, Journal of Applied Mechanics, Vol 45, 1978, pp. 246-251.

Bogdanoff, J. L. & W. Krieger :
A New Cumulative Damage Model, Part 2.
ASME, Journal of Applied Mechanics, Vol 45, No. 2, June 1978, pp. 251-257.

Bogdanoff, J. L. :
A New Cumulative Damage Model, Part 3.
ASME, Journal of Applied Mechanics, Vol 45, No. 4, Dec. 1978, pp. 733-739.

Bogdanoff, J. L. & F. Kozin :
A New Cumulative Damage Model, Part 4.
ASME, Journal of Applied Mechanics, Vol 47, No. 1, June 1980, pp. 40-44.

Cronin, D. J., P. S. Godfrey, P. M. Hook & T. A. Wyatt :
Spectral Fatigue Analysis for Offshore Structures.
Numerical Methods in Offshore Engineering, Zienkiewicz, O. C., Lewis, R. W., Stagg,
K. G. (ed.) John Wiley & Sons, Ltd, 1978, pp.281-316.

Dansk Standard DS 449. :
Danish Code of Practice for Pile-Supported Offshore Steel Structures.
Teknisk Forlag, April 1983. ISBN 87-571-0838-2.

Ditlevsen, O. :
Generalized Second Moment Reliability Index.
ASCE, Journal of Structural Mechanics, Vol. 7, No. 4, 1979, pp. 435-451.

Ditlevsen, O. & Bjerager, P. :
Reliability of Highly Redundant Plastic Structures.
ASCE, Journal of Engineering Mechanics, Vol. 110, No. 5, May, 1984, pp. 671-693.

Ditlevsen, O. & P. Bjerager :
Methods of Structural Systems Reliability.
Structural Safety, Vol. 3, Elsevier Science Publishers B.V., Amsterdam, The Netherlands, 1986, pp 195-229.

Ditlevsen, O. :
Reliability Computations for Rigid Plastic Frames with General Yield Conditions.
Proceedings of the First IFIP WG 7.5 Working Conference, Aalborg, Denmark, May 6-8, Thoft-Christensen P. (ed.), Springer-Verlag, 1987, pp. 91-108.

Ditlevsèn, O. & Bjerager, P. :
Plastic Reliability Analysis by Directional Simulation.
DCAMM Report No. 353, June, The Technical University of Denmark, Lyngby, Denmark, 1987.

Ditlevsen, O. :
Probabilistic Statics of Discretized Ideal Plastic Frames.
DCAMM Report No. 358, August, The Technical University of Denmark, Lyngby, Denmark, 1987.

Edwards, G. E., A. Heidweiller, J. Kerstens & A. Vrouwenvelder :
Methodologies for Limit State Reliability Analysis of Offshore Jacket Platforms.
Behaviour of Offshore Structures, Battjes, J. A. (ed.), Proceedings of the 4th BOSS Conference, Delft, The Netherlands, 1985, pp. 315-323.

Haver, S. :
Long-Term Response Analysis - Advantages and Present Limitations.
Paper presented at the "Deep Water Jacket Seminar", Statoil, Trondheim, August 1985.

Haver, S. :
Wave Climate of Northern Norway.
Applied Ocean Research, Vol. 7, No. 2, 1985, pp.85-92

Haver, S. :
On The Prediction of Extreme Sea States.
E & P - Forum, London, November, 1985.

Haver, S. & K. A. Nyhus :
Wave Climate Elevation for Design Purposes.
5th OMAE, Tokyo, April 1986.

Haver, S. & T. Moan :
On Some Uncertainties Related to the Short Term Stochastic Modelling of Ocean Waves
Applied Ocean Research, Vol. 5, No. 2, 1983, pp.93-108.

Hohenbichler, M. :
An Approximation to the Multivariate Normal Distribution.
DIALOG 6-82, Danish Academy of Engineers, Lyngby, 1983, pp.79-100.

Hosseini A: & M. A. Mahmoud : *Evaluation of Stress Intensity Factor and Fatigue Growth of Surface Cracks in Tension Plates.*
Engineering Fracture Mechanics, Vol. 22, No. 6, 1985, pp.957-974.

Kam J. C. P. & W. D. Dover :
Structural Integrity of Welded Tubular Joints in Random Load Fatigue Combined with Size Effect.
Integrity of Offshore Structures-3, Faulkner, D., M. J. Cowling & A. Incecik (ed.).
Elsevier Applied Science Publishers Ltd., England, 1988.

Karadeniz, H. :
Stochastic Analysis Program for Offshore Structures (SAPOS).
Report, Department of Civil Engineering, Delft University of Technology, Delft, The Netherlands, May 1985.

Kozin, F. & Bogdanoff, J. L. :
On The Probabilistic Modeling of Fatigue Crack Growth.
Engineering Fracture Mechanics, Vol 18, No. 3, 1983, pp. 623-632.

Kozin, F. & Bogdanoff, J. L. :
A Critical Analysis of Some Probabilistic Models of Fatigue Crack Growth.
Engineering Fracture Mechanics, Vol 14, 1981, pp. 59-89.

Lange-Hansen, P. :
Plasticitetsteori for ramme med kombineret bøjning og vridning. (In Danish).
Series F, Report No. 63, August, Department of Structural Engineering, Technical University of Denmark, Lyngby, Denmark, 1983.

Lutes, L. D., M. Corazao, S. J. Hu & J. Zimmerman :
Stochastic Fatigue Damage Accumulation. Journal of Structural Engineering, Vol. 110, No. 11, Nov. 1984, pp. 2585-2601.

Madsen, H. O. :
Stochastic Modeling of Fatigue Crack Growth.
Advanced Seminar on Structural Reliability, ISPRA-COURSES, May 11-15, 1987.

Madsen, H. O. :
Stochastic Modeling of Fatigue Crack Growth.
Advances in Structural Reliability, Lucia. A. C. (ed.) 1987.

Madsen, H. O. :
Random Fatigue Crack Growth and Inspection.
Proc. 4th International Conference on Structural Safety and Reliability, ICOSSAR, 1985, pp. I 475-484.

Madsen, H. O. & P. Bjerager :
Reliability of Ideal Plastic Systems Based on Lower-Bound Theorem.
Proceedings of the First IFIP WG 7.5 Working Conference, Aalborg, Denmark, May 6-8, Thoft-Christensen, P. (ed.), Springer-Verlag, 1987, pp. 417-432.

Madsen, H. O., R. Skjong & F. Kirkemo :
Probabilistic Fatigue Analysis of Offshore Structure - Reliability Updating through Inspection Results.
Integrity of Offshore Structures-3, Faulkner, D., M. J. Cowling & A. Incecik (ed.).
Elsevier Applied Science Publishers Ltd., England, 1988.

Madsen, H. O., R. Skjong & M. Masoud-Zadeh :
Experience on Probabilistic Fatigue Analysis of Offshore Structures.
5th OMAE, Tokyo, April 1986.

Nafday, A. M., R. B. Corotis & J. L. Cohon :
System Reliability of Rigid Plastic Frames.
Reliability and Risk Analysis in Civil Engineering, Lind, N. C., (ed.),
ICASP5, May, University of Waterloo, Canada, 1987, pp. 119-126.

Olufsen, A., K. A. Farnes & D. Fergestad :
FAROW - A Computer Program for Dynamic Response Analysis and Fatigue Life Estimation of Offshore Structures Exposed to Ocean Waves - Theoretical Manual.
SINTEF, Report STF71 A86040, ISBN No:82-595-4318-4, 1986.

Ortiz, K. & N. K. Chen :
Fatigue Damage Prediction for Stationary Wideband Random Stresses.
Reliability and Risk Analysis in Civil Engineering, Lind, N. C. (ed.)
ICASP5, May, University of Waterloo, Canada, 1987, pp. 309-316.

Paris, P. C. & F. Erdogan :
A Critical Analysis of Crack Pripagation Laws.
Journal of Basic Engineering, ASME, Vol. 85, 1963, pp. 528-534.

Penzien, J. & S. Tseng :
Three-Dimensional Dynamic Analysis of Fixed Offshore Platforms.
Numerical Methods in Offshore Engineering, Zienkiewicz, O. C., Lewis, R. W., Stagg, K. G. (ed.) John Wiley & Sons, Ltd, 1978, pp. 221-243.

Schittkowski, K. :
NLPQL : A FORTRAN Subroutine Solving Constrained Non-linear Programming Problems.
Annals of Operations Research, 1986.

Sigbjørnsson, R. :
Stochastic Theory of Wave Loading Processes.
Eng. Struct., Vol. 1, January 1979, pp.58-64.

Sigbjørnsson, R. & E. K. Smith :
Wave Induced Vibrations of Gravity Platforms: A Stochastic Theory.
Applied Mathematical Modelling, Vol. 4, June 1980, pp.155-165.

Sigbjørnsson, R., K. Bell & I. Holand :
Dynamic Response of Framed and Gravity Structures to Waves.
Numerical Methods in Offshore Engineering, Zienkiewicz, O. C., Lewis, R. W., Stagg, K. G. (ed.) John Wiley & Sons, Ltd, 1978, pp. 245-280.

Sigurdsson, G. :
Development of Applicable Methods for Evaluating the Safety of Offshore Structures, Part 4.
Structural Reliability Theory Series, Paper No. 24. Institute of Building Technology and Structural Endineering, University of Aalborg, Denmark, 1985.

Sigurdsson, G. :
Probabilistic Fatigue Analysis of Offshore Structures.
Proceedings of the Second IFIP WG 7.5 Working Conference, London, England, September 25-27, Thoft-Christensen, P. (ed.), Springer-Verlag, 1989.

Sigurdsson, G., J. D. Sørensen & P. Thoft-Christensen :
Development of Applicable Methods for Evaluating the Safety of Offshore Structures, Part 1.
Structural Reliability Theory Series, Paper No. 9. Institute of Building Technology and Structural Engineering, University of Aalborg, Denmark, 1985.

Sørensen, J. D. & R. Brincker :
Simulation of Stochastic Loads for Fatigue Experiments
Submitted to Experimental Mechanics 1989.

Sørensen, J. D., P. Thoft-Christensen & G. Sigurdsson :
Development of Applicable Methods for Evaluating the Safety of Offshore Structures, Part 2.
Structural Reliability Theory Series, Paper No. 11. Institute of Building Technology and Structural Engineering, University of Aalborg, Denmark, 1985.

Thoft-Christensen, P. :
Recent Advances in the Application of Structural Systems Reliability Methods.
Reliability and Risk Analysis in Civil Engineering, Lind, N. C. (ed.)
ICASP5, May, University of Waterloo, Canada, 1987.

Thoft-Christensen, P. :
Application of Structural System Reliability Theory in Offshore Engineering, State-of-the-Art.
Integrity of Offshore Structures-3, Faulkner, D., M. J. Cowling & A. Incecik (ed.).
Elsevier Applied Science Publishers Ltd., England, 1988.

Thoft-Christensen, P., G. Sigurdsson & J. D. Sørensen :
Development of Applicable Methods for Evaluating the Safety of Offshore Structures, Part 3.
Structural Reliability Theory Series, Paper No. 17. Institute of Building Technology and Structural Engineering, University of Aalborg, Denmark, 1986.

Tickell R. G. & P. Holmes :
Approaches to Fluid Loading, Probabilistic and Deterministic Analysis.
Numerical Methods in Offshore Engineering, Zienkiewicz, O. C., Lewis, R. W., Stagg, K. G. (ed.) John Wiley & Sons, Ltd, 1978, pp. 43-85.

Vrouwenvelder, A., H. Karadeniz, S. van Manen :
Probabilistic Reliability Analysis for the Fatigue Limit State of Gravity and Jacket-Type Structure.
DIALOG 6-82, Danish Academy of Engineers, Lyngby, 1982, pp. 349-380.

Watwood, V. B. :
Mechanism Generation for Limit Analysis of Frames.
ASCE, Journal of the Structural Division, Vol. 109, No. ST1, January, 1979, pp. 1-15.

Watt, B. J. :
Basic Structural System - A Review of Their Design and Analysis Requirements.
Numerical Methods in Offshore Engineering, Zienkiewicz, O. C., Lewis, R. W., Stagg, K. G. (ed.) John Wiley & Sons, Ltd, 1978, pp. 1-42.

Wilson E. L. :
Numerical Methods for Dynamic Analysis.
Numerical Methods in Offshore Engineering, Zienkiewicz, O. C., Lewis, R. W., Stagg, K. G. (ed.) John Wiley & Sons, Ltd, 1978, pp. 195-220.

Wirsching P. W. :
Fatigue Reliability for Offshore Structure.
Journal of Structural Engineering, Vol. 110, No. 10, Oct. 1984, pp. 2340-2356.

Wirshing P. H. & M. C. Light :
Fatigue Under Wide Band Random Stresses.
Journal of the Structural Division, ASCM, Vol. 106, No ST7, July, 1980, pp. 1593-1607.

Wirsching P. H. & E. B. Haugen :
Probabilistic Design for Random Fatigue Loads.
Journal of the Engineering Mechanics Division, Vol. 99, No. EM6, Dec., 1973, pp. 1165-1179.

Wirsching P. H. & A. M. Shehata. :
Fatigue Under Wide Band Stresses Using the Rain-Flow Method.
Journal of Engineering Materials and Technology, July 1977, pp.205-211.

Yao, J. T. P., F. Kozin, Y. -K. Wen, J. -N- Yang, G. I. Schuëller & O. Ditlevsen :
Stochastic Fatigue, Fracture and Damage Analysis.
Structural Safety, Vol. 3, Elsevier Science Publishers B.V., Amsterdam, The Netherlands, 1986, pp 231-267.

APPENDIX A

In this appendix yield conditions for four different cross-sections are shown.

I-Section

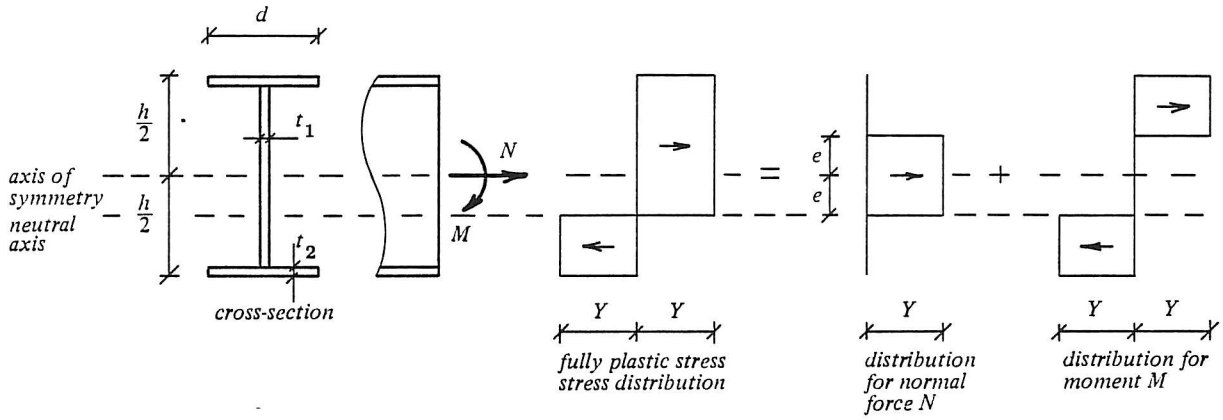

Figure A1. Stress distribution for I-section.

$N/N_F = 2et_1/A$ and $M/M_F = 1 - t_1e^2/W_p$ when $e \leq (h/2 - t_2)$. Therefore,

$$\frac{M}{M_F} = 1 - \left(\frac{N}{N_F}\right)^2 \frac{A^2}{4t_1W_p} \tag{A1}$$

where the plastic modulus W_p is

$$W_p = \frac{1}{2}2t_2d(h - t_2) + \frac{1}{4}(h - 2t_2)(h - 2t_2) \tag{A2}$$

Eq.(A1) can therefore be rewritten for $N/N_F \leq (h - 2t_2)t_1/A = A_W/A$, where A_w is the web area

$$a\left(\frac{N}{N_F}\right)^2 + \frac{M}{M_F} = 1 \tag{A3}$$

where

$$a = \left(2\frac{A_w}{A} - \left(\frac{A_w}{A}\right)^2 + \frac{t_1}{d}\left(\frac{A - A_w}{A}\right)^2\right)^{-1} \tag{A4}$$

Likewise, for $N/N_F > A_w/A$ the yield condition is

$$\frac{N}{N_F} + b\left|\frac{M}{M_F}\right| = 1 \tag{A5}$$

where

$$b = 1 - \frac{A_w}{2A} \qquad (A6)$$

Box-Section

The yield condition for box-section shown in figure A2 can be derived as for I-section by using simple transformation as shown in figure A2.

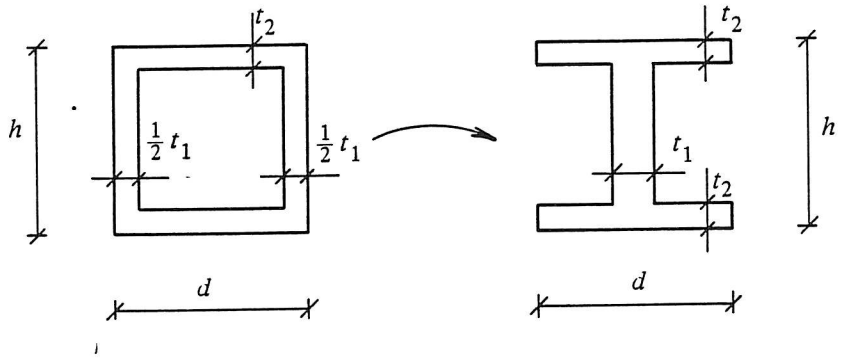

Figure A2. Transformation of box-section to an I-section.

Rectangular Section

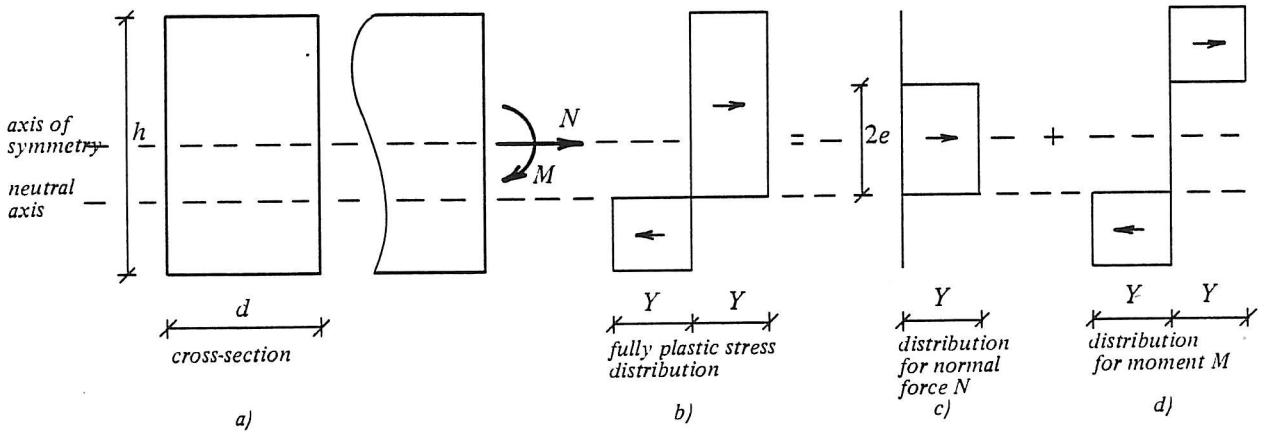

Figure A3. Stress distribution for a rectangular section.

With the notation in figure A3 the following is derived

$$\frac{N}{N_F} = \frac{2ed}{A} = \frac{2e}{h} \qquad (A7)$$

$$\frac{M}{M_F} = 1 - \frac{de^2}{W_p} \tag{A8}$$

where $W_p = dh^2/4$.

The yield condition can therefore be written

$$\frac{M}{M_F} + \left(\frac{N}{N_F}\right)^2 = 1 \tag{A9}$$

Thin-Walled Tubular Section

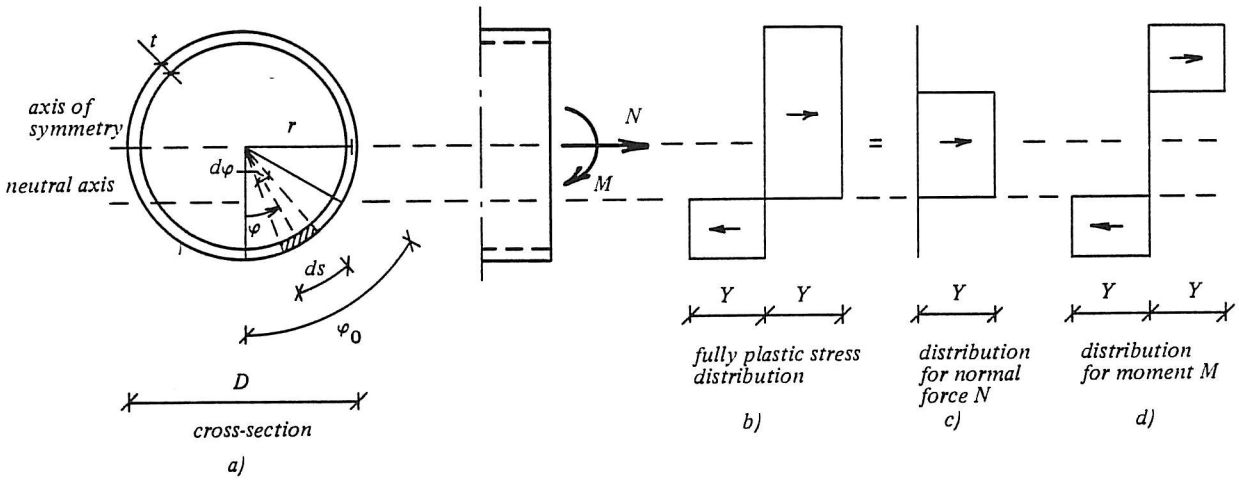

Figure A4. Stress distribution in a thin-walled tubular section.

With the notation shown in figure A4 it is easy to show that ($t \ll D$)

$$M = 4Ytr^2 \sin\varphi_0 \tag{A10}$$

and

$$N = 4Yr(\frac{\pi}{2} - \varphi_0) \tag{A11}$$

The plastic modulus is approximately

$$W_p \approx 4tr^2 \tag{A12}$$

With $M_F = W_pY$ and $N_F = AY$ the yield condition is

$$\frac{M}{M_F} - \cos(\frac{\pi}{2}\frac{N}{N_F}) = 0 \tag{A13}$$

APPENDIX B

This appendix deals with three-dimensional linearization of drag forces by the "minimum mean square error linearization method", Atalik & Utku[p] 1976. A circular cylinder as shown in figure B1 is considered, and it is assumed that Morison's equation may be applied to a cylindrical member in a random manner. The non-linear term in Morison's equation may be written as

$$\overline{f}_D = \begin{bmatrix} f_{Dx} \\ f_{Dy} \\ f_{Dz} \end{bmatrix} = K_D \, |\overline{\dot{u}}_n| \, \overline{\dot{u}}_n = K_D \, (\dot{u}_{nx}^2 + \dot{u}_{ny}^2 + \dot{u}_{nz}^2)^{\frac{1}{2}} \begin{bmatrix} \dot{u}_{nx} \\ \dot{u}_{ny} \\ \dot{u}_{nz} \end{bmatrix} \tag{B1}$$

where

$$\overline{\dot{u}}_n = \begin{bmatrix} \dot{u}_{nx} \\ \dot{u}_{ny} \\ \dot{u}_{nz} \end{bmatrix} = \left(\overline{c} \times (\overline{\dot{u}}^T \times \overline{c}) \right)^T = \begin{bmatrix} 1 - c_x^2 & -c_x c_y & -c_x c_z \\ & 1 - c_y^2 & -c_y c_z \\ \text{sym.} & & 1 - c_z^2 \end{bmatrix} \begin{bmatrix} \dot{u}_x \\ \dot{u}_y \\ \dot{u}_z \end{bmatrix} \tag{B2}$$

$$\overline{c} = (c_x, c_y, c_z)$$

$$\overline{\dot{u}}^T = (\dot{u}_x, \dot{u}_y, \dot{u}_z)$$

$\dot{u}_x$, $\dot{u}_y$ and $\dot{u}_z$ are components of the water particle velocity in the x, y and z-direction, respectively, and $\overline{c}$ is a unit vector along the cylinder axis.

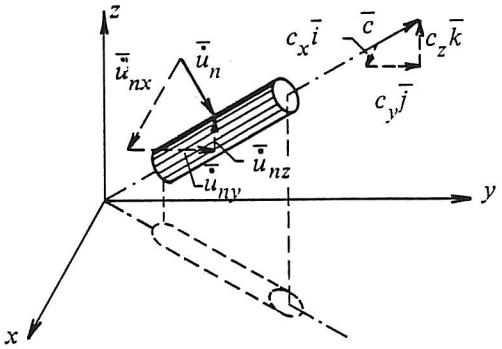

Figure B1. $\overline{i}$, $\overline{j}$ and $\overline{k}$ represent the base vectors in the x, y, z-coordinate system.

The linearized version of equation (B1) is

$$\overline{f}_{DL} = K_D \, \overline{\overline{L}} \, \overline{\dot{u}}_n \tag{B3}$$

where $\overline{\overline{L}}$ is the linearization coefficient matrix, expressed as

$$\overline{\overline{L}} = \begin{bmatrix} l_{xx} & l_{xy} & l_{xz} \\ l_{yx} & l_{yy} & l_{yz} \\ l_{zx} & l_{zy} & l_{zz} \end{bmatrix}$$

The error introduced using equation (B3) instead of equation (B1) is defined as

$$\bar{e} = (\bar{\bar{L}}\,\bar{\dot{u}}_n - \bar{g}(\bar{\dot{u}}_n)) \tag{B4}$$

where

$$\bar{g}(\bar{\dot{u}}_n) = \begin{bmatrix} g_x(\bar{\dot{u}}_n) \\ g_y(\bar{\dot{u}}_n) \\ g_z(\bar{\dot{u}}_n) \end{bmatrix} = (\dot{u}_{nx}^2 + \dot{u}_{ny}^2 + \dot{u}_{nz}^2)^{\frac{1}{2}} \begin{bmatrix} \dot{u}_{nx} \\ \dot{u}_{ny} \\ \dot{u}_{nz} \end{bmatrix}$$

The criterion that the mean square value of the error $\bar{e}$ is at a minimum is expressed as

$$E[\bar{e}\,\bar{e}^T] \rightarrow \text{minimum}$$

where $E[\cdots]$ denotes the expected value.

The coefficients l_{ij} in the linearization matrix $\bar{\bar{L}}$ may be written as, Atalik & Utku[p] 1976

$$l_{ij} = E[\frac{\partial g_i(\bar{\dot{u}}_n)}{\partial \dot{u}_{nj}}] \tag{B5}$$

The matrix $\bar{\bar{L}}$ may now be expressed as

$$\bar{\bar{L}} = E\begin{bmatrix} \frac{2\dot{u}_{nx}^2+\dot{u}_{ny}^2+\dot{u}_{nz}^2}{|\bar{\dot{u}}_n|} & \frac{\dot{u}_{nx}\dot{u}_{ny}}{|\bar{\dot{u}}_n|} & \frac{\dot{u}_{nx}\dot{u}_{nz}}{|\bar{\dot{u}}_n|} \\ & \frac{\dot{u}_{nx}^2+2\dot{u}_{ny}^2+\dot{u}_{nz}^2}{|\bar{\dot{u}}_n|} & \frac{\dot{u}_{nx}\dot{u}_{ny}}{|\bar{\dot{u}}_n|} \\ \text{sym.} & & \frac{\dot{u}_{nx}^2+2\dot{u}_{ny}^2+\dot{u}_{nz}^2}{|\bar{\dot{u}}_n|} \end{bmatrix} = E[\bar{\bar{M}}]$$

where $|\bar{\dot{u}}_n| = (\dot{u}_{nx}^2 + \dot{u}_{ny}^2 + \dot{u}_{nz}^2)^{\frac{1}{2}}$.

When the water particle velocity is assumed to be a zero-mean Gaussian process then the following expression is obtained

$$E[\bar{\bar{M}}] = \int_{-\infty}^{\infty}\int_{-\infty}^{\infty}\int_{-\infty}^{\infty} \bar{\bar{M}}\,\phi_3(\bar{0};\bar{\bar{\Sigma}}_{\dot{u}_x\dot{u}_y\dot{u}_z})d\dot{u}_x d\dot{u}_y d\dot{u}_z \tag{B6}$$

where $\phi_3(\bar{0};\bar{\bar{\Sigma}}_{\dot{u}_x\dot{u}_y\dot{u}_z})$ is a three-dimensional Gaussian density function defined by

$$\phi_3(\bar{0};\bar{\bar{\Sigma}}_{\dot{u}_x\dot{u}_y\dot{u}_z}) = \frac{1}{(2\pi)^{3/2}(det(\bar{\bar{\Sigma}}_{\dot{u}_x\dot{u}_y\dot{u}_z}))^{1/2}} exp(-\frac{1}{2}\bar{\dot{u}}^T\bar{\bar{\Sigma}}^{-1}_{\dot{u}_x\dot{u}_y\dot{u}_z}\,\bar{\dot{u}})$$

where the covariance matrix $\overline{\overline{\Sigma}}_{\dot{u}_x\dot{u}_y\dot{u}_z}$ is defined by

$$\overline{\overline{\Sigma}}_{\dot{u}_x\dot{u}_y\dot{u}_z} = \begin{bmatrix} \int_0^\infty S_{\dot{u}_x\dot{u}_x}(\omega)d\omega & \int_0^\infty S_{\dot{u}_x\dot{u}_y}(\omega)d\omega & \int_0^\infty S_{\dot{u}_x\dot{u}_z}(\omega)d\omega \\ \int_0^\infty S_{\dot{u}_y\dot{u}_x}(\omega)d\omega & \int_0^\infty S_{\dot{u}_y\dot{u}_y}(\omega)d\omega & \int_0^\infty S_{\dot{u}_y\dot{u}_z}(\omega)d\omega \\ \int_0^\infty S_{\dot{u}_z\dot{u}_x}(\omega)d\omega & \int_0^\infty S_{\dot{u}_z\dot{u}_y}(\omega)d\omega & \int_0^\infty S_{\dot{u}_z\dot{u}_z}(\omega)d\omega \end{bmatrix}$$

$S_{\dot{u}_i\dot{u}_j}(\omega)$ is the cross-spectral density of the water particle velocity $\dot{u}_i$ and $\dot{u}_j$ $(i,j = x,y,z)$.

For example,

$$l_{xx} = E[m_{11}] = \int_{-\infty}^{\infty}\int_{-\infty}^{\infty}\int_{-\infty}^{\infty} \frac{2\dot{u}_{nx}^2 + \dot{u}_{ny}^2 + \dot{u}_{nz}^2}{|\bar{\dot{u}}_n|} \frac{1}{(2\pi)^{3/2}(det(\overline{\overline{\Sigma}}_{\dot{u}_x\dot{u}_y\dot{u}_z}))^{1/2}}$$

$$exp(-\frac{1}{2}\bar{\dot{u}}^T\overline{\overline{\Sigma}}^{-1}_{\dot{u}_x\dot{u}_y\dot{u}_z}\bar{\dot{u}})d\dot{u}_x d\dot{u}_y d\dot{u}_z$$

where $\dot{u}_{nx}$, $\dot{u}_{ny}$ and $\dot{u}_{nz}$ can be expressed as functions of $\dot{u}_x$, $\dot{u}_y$ and $\dot{u}_z$ (see eq. (B2)).

APPENDIX C

The density function of the range h between two successive extremes can be estimated by (see eq.(4.5.11))

$$f_H(h) = \int_0^{T_1} \left(\int_{-\infty}^{\infty} f_T(\tau)\, f_{UH|T}(u, h|\tau) du \right) d\tau \qquad (C1)$$

where

$$f_T(\tau) = \begin{cases} \int_0^{\infty} \left(\int_{-\infty}^{0} -\ddot{x}_1 \ddot{x}_2 \; f_{\dot{X}_1 \dot{X}_2 \ddot{X}_1 \ddot{X}_2}(0, 0, \ddot{x}_1, \ddot{x}_2) d\ddot{x}_1 \right) d\ddot{x}_2 & 0 \le \tau \le T_1 \\ 0 & \tau > T_1 \end{cases} \qquad (C2)$$

$$f_{UHT}(u, h, \tau) = \frac{\int_0^{\infty} \left(\int_{-\infty}^{0} -\ddot{x}_1 \ddot{x}_2 \, f_{X_1 X_2 \dot{X}_1 \dot{X}_2 \ddot{X}_1 \ddot{X}_2}(u, u-h, 0, 0, \ddot{x}_1, \ddot{x}_2) d\ddot{x}_1 \right) d\ddot{x}_2}{\int_0^{\infty} \left(\int_{-\infty}^{0} -\ddot{x}_1 \ddot{x}_2 f_{\dot{X}_1 \dot{X}_2 \ddot{X}_1 \ddot{X}_2}(0, 0, \ddot{x}_1, \ddot{x}_2) d\ddot{x}_1 \right) d\ddot{x}_2} \qquad (C3)$$

where $X_1 = X(t)$ and $X_2 = X(t+\tau)$ and where T_1 is determined from the normalisation condition

$$\int_0^{T_1} f_T(\tau) d\tau = 1 \qquad (C4)$$

Using eq.(C1)-eq.(C3), $f_H(h)$ can be written as

$$f_H(h) = \int_0^{T_1} \int_{-\infty}^{\infty} \left(\int_0^{\infty} \int_{-\infty}^{0} -\ddot{x}_1 \ddot{x}_2 \, f_{X_1 X_2 \dot{X}_1 \dot{X}_2 \ddot{X}_1 \ddot{X}_2}(u, u-h, 0, 0, \ddot{x}_1, \ddot{x}_2) d\ddot{x}_1 d\ddot{x}_2 \right) du d\tau$$

$$= \int_0^{T_1} \int_{-\infty}^{\infty} \left(\int_0^{\infty} \int_{-\infty}^{0} -\ddot{x}_1 \ddot{x}_2 \, \phi_6(u, u-h, 0, 0, \ddot{x}_1, \ddot{x}_2 \,; \overline{\overline{\rho}}) d\ddot{x}_1 d\ddot{x}_2 \right) du d\tau \qquad (C5)$$

where $\phi_n(\cdot; \overline{\overline{\rho}})$ is the n-dimensional Gaussian density function of n variables having the correlation coefficient matrix $\overline{\overline{\rho}}$ written as

$$\overline{\overline{\rho}} = \left[\begin{array}{cccc|cc} \rho(0) & \rho(\tau) & 0 & \rho'(\tau) & \rho''(0) & \rho''(\tau) \\ & \rho(0) & -\rho'(\tau) & 0 & \rho''(\tau) & \rho''(0) \\ & & -\rho''(0) & -\rho''(\tau) & 0 & -\rho'''(\tau) \\ & & & -\rho''(0) & \rho'''(\tau) & 0 \\ \hline & & & & \rho''''(0) & \rho''''(\tau) \\ \text{sym.} & & & & & \rho''''(0) \end{array}\right] = \left[\begin{array}{cc} \overline{\overline{\rho}}_{11} & \overline{\overline{\rho}}_{12} \\ \overline{\overline{\rho}}_{12}^T & \overline{\overline{\rho}}_{22} \end{array}\right] \qquad (C6)$$

where

$$\rho(\tau) = \int_0^\infty S_X(\omega)\ cos(\omega\tau)\ d\omega$$

$$\rho'(\tau) = \int_0^\infty -\omega S_X(\omega)\ sin(\omega\tau)\ d\omega$$

$$\rho''(\tau) = \int_0^\infty -\omega^2 S_X(\omega)\ cos(\omega\tau)\ d\omega$$

$$\rho'''(\tau) = \int_0^\infty \omega^3 S_X(\omega)\ sin(\omega\tau)\ d\omega$$

$$\rho''''(\tau) = \int_0^\infty \omega^4 S_X(\omega)\ cos(\omega\tau)\ d\omega$$

Eq.(C5) can then be written

$$f_H(h) = \int_0^{T_1} \int_{-\infty}^{\infty} \phi_4(u, u-h, 0, 0; \overline{\overline{\rho}}_{11}) \int_0^\infty \int_{-\infty}^0 -\ddot{x}_1\ddot{x}_2\phi_2(\ddot{x}_1-\mu_1, \ddot{x}_2-\mu_2\ ; \overline{\overline{R}})d\ddot{x}_1 d\ddot{x}_2 du d\tau$$

$$= -\int_0^{T_1} \int_{-\infty}^{\infty} \phi_4(u, u-h, 0, 0; \overline{\overline{\rho}}_{11})\ \lambda_1\lambda_2(\Psi_2(\frac{-\mu_1}{\lambda_1})\Psi_1(\frac{-\mu_2}{\lambda_2}) + \kappa\ \Phi(\frac{-\mu_1}{\lambda_1})\Phi(\frac{-\mu_2}{\lambda_2})$$

$$+ \lambda_1\lambda_2 \int_0^\kappa (\kappa - k)\ \phi(0,0\ ; \overline{\overline{R}}(k))\ dk\ )\ du d\tau \qquad (C7)$$

where

$$\overline{\mu} = \begin{bmatrix} \mu_1 \\ \mu_2 \end{bmatrix} = \overline{\overline{\rho}}_{12}^T\ \overline{\overline{\rho}}_{11}^{-1} \begin{bmatrix} u \\ u-h \\ 0 \\ 0 \end{bmatrix}$$

$$\overline{\overline{R}}(\kappa) = \overline{\overline{\rho}}_{22} - \overline{\overline{\rho}}_{12}^T\ \overline{\overline{\rho}}_{11}^{-1}\ \overline{\overline{\rho}}_{12} = \begin{bmatrix} \lambda_1^2 & \kappa\lambda_1\lambda_2 \\ \kappa\lambda_1\lambda_2 & \lambda_2^2 \end{bmatrix}$$

$$\Psi_1(x) = -\phi(x) - x\Phi(x)$$

$$\Psi_2(x) = \phi(x) - x\Phi(-x)$$

where $\Phi(\cdot)$ is the standard Gaussian distribution function.

STRUCTURAL RELIABILITY THEORY SERIES

PAPER NO. 26: P. Thoft-Christensen & M. H. Faber: *Deflection and Global Instability Failure Elements for Geometrical Non-Linear Structures.* ISSN 0902-7513 R8706.

PAPER NO. 27: K. J. Mørk, P. Thoft-Christensen & S. R. K. Nielsen: *Simulation Studies of Joint Response Statistics for a One-Degree-of-Freedom Structure.* ISSN 0902-7513 R8707.

PAPER NO. 28: P. Thoft-Christensen, S. R. K. Nielsen & K. J. Mørk: *Simulation Studies of Joint Response Statistics for Two-Storey Hysteretic Frame Structures.* ISSN 0902-7513 R8708.

PAPER NO. 29: J. D. Sørensen & P. Thoft-Christensen: *Integrated Reliability -Based Optimal Design of Structures.* ISSN 0902-7513 R8709.

PAPER NO. 30: S. R. K. Nielsen, K. J. Mørk & P. Thoft-Christensen: *Reliability Analysis of Hysteretic Multi-Storey Frames under Random Excitation.* ISSN 0902-7513 R8711.

PAPER NO. 31: J. D. Sørensen & Rune Brincker: *Simulation of Stochastic Loads for Fatigue Experiments.* ISSN 0902-7513 R8717.

PAPER NO. 32: J. D. Sørensen: *Reliability-Based Optimization of Structural Systems.* ISSN 0902-7513 R8718.

PAPER NO. 33: P. Thoft-Christensen: *Application of Optimization Methods in Structural Systems Reliability Theory.* ISSN 0902-7513 R8719.

PAPER NO. 34: P. Thoft-Christensen: *Recent Advances in the Application of Structural Systems Reliability Methods.* ISSN 0902-7513 R8721.

PAPER NO. 35: P. Thoft-Christensen: *Applications of Structural Systems Reliability Theory in Offshore Engineering. State-of-the-Art.* ISSN 0902-7513 R8722.

PAPER NO. 36: J. D. Sørensen: *PRADSS: Program for Reliability Analysis and Design of Structural Systems.* First Draft. ISSN 0902-7513 R8724.

PAPER NO. 37: Jan Kazimierz Szmidt: *Discrete Analysis of a Plane Initial-Value Problem for an Offshore Structure.* ISSN 0902-7513 R8801.

PAPER NO. 38: M. H. Faber & P. Thoft-Christensen: *Modelling of Floor Loads.* ISSN 0902-7513 R8802.

PAPER NO. 39: S. R. K. Nielsen, K. J. Mørk & P. Thoft-Christensen: *Stochastic Response of Hysteretic Systems.* ISSN 0902-7513 R8803.

PAPER NO. 40: P. Thoft-Christensen & G. B. Pirzada: *Upper-Bound Estimate of the Reliability of Plastic Slabs.* ISSN 0902-7513 R8804.

PAPER NO. 41: S. R. K. Nielsen, K. J. Mørk & P. Thoft-Christensen: *Response Analysis of Hysteretic Multi-Storey Frames under Earthquake Excitation.* ISSN 0902-7513 R8805.

STRUCTURAL RELIABILITY THEORY SERIES

PAPER NO. 42: J. D. Sørensen: *Probabilistic Design of Offshore Structural Systems.* ISSN 0902-7513 R8806.

PAPER NO. 43: S. G. Zhang & P. Thoft-Christensen: *Tool Life Reliability.* ISSN 0902-7513 R8807.

PAPER NO. 44: K. J. Mørk, S. R. K. Nielsen & P. Thoft-Christensen: *Probability Distributions of Damage Indicators in Hysteretic Structures.* ISSN 0902-7513 R8817.

PAPER NO. 45: J. D. Sørensen: *Optimal Design with Reliability Constraints.* ISSN 0902-7513 R8818.

PAPER NO. 46: S. G. Zhang & P. Thoft-Christensen: *Experimental Testing and Monitoring of Tool Wear.* ISSN 0902-7513 R8819.

PAPER NO. 47: P. Thoft-Christensen: *Consequence Modified β-Unzipping of Plastic Structures.* ISSN 0902-7513 R8820.

PAPER NO. 48: J. D. Sørensen & P. Thoft-Chrisstensen: *Inspection Strategies for Concrete Bridges.* ISSN 0902-7512 R8825.

PAPER NO. 49: M. Delmar, J. D. Sørensen & P. Thoft-Christensen: *Collapse Probability of Elasto-Plastic Structures.* ISSN 0902-7513 R8827.

PAPER NO. 50: G. Sigurdsson: *Stochastic Fatigue Analysis of Jacket Type Offshore Structures.* ISSN 0902-7513 R8828.

PAPER NO. 51: S. R. K. Nielsen: *Approximations to the Probability of Failure in Random Vibration by Integral Equation Methods.* ISSN 0902-7513 R8829.

PAPER NO. 52: M. H. Faber: *Excursions of Gaussian Random fields in Structural Reliability.* ISSN 0902-7513 R8905.

PAPER NO. 53: I. Enevoldsen, J. D. Sørensen & P. Thoft-Christensen: *Shape Optimization of Mono-Tower Offshore Platform.* ISSN 0902-7513 R8906.

PAPER NO. 54: P. Thoft-Christensen: *Reliability of Plastic Slabs.* ISSN 0902-7513 R8907.

PAPER NO. 55: G. Sigurdsson: *Some Aspects of Reliability of Offshore Structures.* ISSN 0902-7513 R8909.

PAPER NO. 56: K. J. Mørk: *Stochastic Response and Reliability Analysis of Hysteretic Structures.* ISSN 0902-7513 R8910.

Institute of Building Technology and Structural Engineering
The University of Aalborg, Sohngaardsholmsvej 57. DK 9000 Aalborg
Telephone: Int. +45 8 14 23 33 Telefax: Int. +45 8 14 82 43